

1 **The climate and vegetation of Europe, North Africa and the**
2 **Middle East during the Last Glacial Maximum**
3 **(21,000 years BP) based on pollen data**

4
5
6 Basil A.S. Davis¹, Marc Fasel², Jed O. Kaplan³, Emmanuele Russo⁴, Ariane Burke⁵

7 ¹Institute of Earth Surface Dynamics, University of Lausanne, Lausanne, 1015, Switzerland

8 ²enviroSPACE lab, Institute for Environmental Sciences, University of Geneva, Geneva,
9 1211, Switzerland

10 ³Department of Earth Sciences, The University of Hong Kong, Hong Kong, Peoples Republic
11 of China

12 ⁴Department of Environmental Systems Science, ETH Zurich, Zurich, 8092, Switzerland

13 ⁵Laboratoire d'Ecomorphologie et de Paleoanthropologie, Departement d'Anthropologie,
14 Universite de Montreal, Montreal, Quebec, H3C 3J7, Canada

15
16 *Correspondence to:* Basil A. S. Davis (basil.davis@unil.ch)

17
18 **Abstract.** Pollen data represents one of the most widely available and spatially-resolved
19 sources of information about the past land cover and climate of the Last Glacial Maximum
20 (21,000 years BP). Previous pollen data compilations for Europe, the Mediterranean and the
21 Middle East however have been limited by small numbers of sites and poor dating control.
22 Here we present a new compilation of pollen data from the region that improves on both the
23 number of sites (63) and the quality of the chronological control. Data has been sourced from
24 both public data archives and published (digitized) diagrams. Analysis is presented based on
25 a standardized pollen taxonomy and sum, with maps shown for the major pollen taxa, biomes
26 and total arboreal pollen, as well as quantitative reconstructions of forest cover and winter,
27 summer and annual temperatures and precipitation. The reconstructions are based on the
28 modern analogue technique (MAT) with a modern calibration dataset taken from the latest
29 Eurasian Modern Pollen Database (~8000 samples). A site-by-site comparison of MAT and
30 Inverse Modelling methods shows little or no significant difference between the methods for
31 the LGM, indicating that no-modern-analogue and low CO₂ conditions during the LGM do
32 not appear to have had a major effect on MAT transfer function performance. Previous
33 pollen-based climate reconstructions using modern pollen calibration datasets show a much
34 colder and drier climate for the LGM than both Inverse Modelling and climate model
35 simulations, but our new results suggest much greater agreement. Differences between our
36 latest MAT reconstruction and those in earlier studies can be largely attributed to bias in the
37 small modern calibration dataset previously used. We also find that quantitative forest cover
38 reconstructions show more forest than that previously suggested by biome reconstructions,
39 but less forest than that suggested by simple percentage arboreal pollen, although
40 uncertainties remain large. Overall, we find that LGM climatic cooling/drying was
41 significantly greater in winter than in summer, but with large site to site variance that
42 emphasizes the importance of topography and other local factors in controlling the climate
43 and vegetation of the LGM.
44

45 **1 Introduction**

46

47 During the Last Glacial Maximum (LGM) ~21,000 years BP (Mix et al., 2001), the climate,
48 vegetation and landscape of Europe and its surrounding regions were very different than
49 today. Scandinavia and a large part of the British Isles were covered by a single ice sheet,
50 with separate ice sheets covering the Alps and Pyrenees, while many smaller and lower
51 mountainous areas were also glaciated (Ehlers et al. 2011). As a result of this global build-up
52 of ice on land, sea levels were around 120 meters lower than today, resulting in the retreat of
53 Atlantic and Mediterranean coastlines and the emergence on land of the English Channel and
54 North Sea basin. Falling sea levels also led to the disconnection of the Black Sea from the
55 Mediterranean, and a subsequent drop in Black Sea water levels as evaporation exceeded
56 inflow (Arslanov et al. 2007). On land, permafrost and periglacial processes occurred
57 immediately to the south of the Scandinavian ice sheet, while the massive discharge of glacial
58 clays and sands provided material to be redeposited by the wind as belts of loess across
59 northern France, Benelux, Germany and central Europe (Lehmkuhl et al. 2021). Under these
60 cooler and drier climatic conditions, forests are thought to have retreated to the relative
61 shelter of Southern Europe and the Mediterranean, while relatively unproductive steppe and
62 tundra dominated the region north of the Alps (Grichuk 1992).

63

64 This traditional view of the LGM has been established for many years, but many details
65 concerning the climate and vegetation of the LGM remain debated. Much of this debate
66 concerns information derived from the pollen record, which represents one of the most
67 widely available and spatially-resolved sources of information concerning LGM vegetation
68 and climate, and the primary terrestrial proxy used to evaluate climate models in the
69 Palaeoclimate Modelling Intercomparison Project (PMIP) (Bartlein et al., 2011; Harrison et
70 al., 2014).

71

72 For example, climate model simulations continue to indicate a climate that is less cold and
73 more humid than pollen-based reconstructions (Jost et al., 2005). These results are similar to
74 reconstructions based on glaciological modelling (Allen et al., 2008b). On the other hand, the
75 pollen-based reconstructions that show the greatest disagreement with climate models have
76 themselves been criticized for not considering the possible effect of low atmospheric CO₂ on
77 the physiological relationship between plants and climate (Ramstein et al., 2007). Methods
78 that use modern pollen samples for calibration purposes are based on the assumption that the
79 relationship between vegetation and climate remains the same through time, and that this is
80 independent of change in CO₂ concentration. Studies have shown however that plant growth
81 processes and plant resilience are sensitive to CO₂ concentration, and particularly water-use
82 efficiency which would make plants more drought sensitive in low CO₂ environments
83 (Cowling & Sykes 1999). Atmospheric CO₂ during the LGM was around 190 ppm, some
84 100 ppm lower than the pre-industrial period, and 200 ppm lower than the levels experienced
85 in the last 50 years. Concerns about the effects of lower CO₂ during the LGM has directly led
86 to the development of pollen-climate reconstruction methods that can take account of CO₂
87 effects, either through use of a process-based vegetation model run in inverse mode (Guiot et
88 al. 2000, Guiot et al. 2009), or through the use of a correction algorithm (Prentice et al.
89 2017). Pollen-climate reconstructions based on inverse modelling that account for these low
90 CO₂ effects show less cooling and drying and consequently greater agreement with climate
91 models (Ramstein et al., 2007; Wu et al., 2007).

92

93 Further data-model discrepancies have also been highlighted concerning LGM vegetation
94 cover. Earlier pollen synthesis studies, especially those that applied the biomisation method

95 (Elenga et al., 2000) give the impression that non-glaciated areas of LGM Europe were
96 dominated by treeless steppe, while vegetation models driven by climate model simulations
97 indicate large areas of forest and woodlands (Binney et al., 2017; Kaplan et al., 2016;
98 Velasquez et al., 2021). The apparent data-model discrepancy associated with steppe has led
99 to the suggestion that early humans, which are not included in vegetation models, could have
100 reduced the forest cover with only a relatively moderate use of fire because of the cold
101 climate and slow speed of vegetation recovery (Kaplan et al., 2016). This debate is important
102 because of studies that have shown the sensitivity of the climate system to vegetation
103 boundary conditions during the LGM (Ludwig et al., 2017; Velasquez et al., 2021). This
104 suggests that accurate knowledge of the vegetation cover during the LGM is a necessary
105 prerequisite to understanding the role of other influences on the climate system at this time.
106

107 More recent pollen and macrofossil studies from eastern Central Europe have shown that at
108 least in this region there existed areas of open boreal forest and woodland with some
109 temperate broadleaf species (Kuneš et al., 2008; Willis and Van Andel, 2004). The evidence
110 of forest, and particularly elements of temperate broadleaf forest, north of the Alps has come
111 to represent a challenge to the traditional view that forest species only survived the LGM in
112 sheltered refugia far to the south of the Fenoscandian ice sheet and close to the moderating
113 influence of the Mediterranean Sea. The presence of micro-refugia north of the Alps is
114 important because it would represent a very different baseline for understanding the later rate
115 and route of plant migrations under the rapid warming that occurred during the Late Glacial
116 to Holocene transition (Douda et al., 2014; Giesecke, 2016; Krebs et al., 2019; Nolan et al.,
117 2018), as well as understanding patterns of present-day genetic diversity (Normand et al.,
118 2011; Svenning et al., 2008). Modelling studies have shown difficulty in supporting the very
119 high rates of postglacial expansion that would be necessary for southern refugia (Feurdean et
120 al., 2013, Nogués-Bravo et al. 2018).
121

122 Much of this debate has been informed by an increasing number of LGM pollen studies from
123 an ever-broader geographical area, and especially from an increasing number of studies from
124 north of the Alps. Nevertheless, the synthesis of these studies into a single narrative is made
125 difficult by several factors, for instance: different taxonomic definitions, pollen percentages
126 calculated from non-standardized pollen sums, and quantitative analyses such as climate
127 reconstructions that are based on different training sets and methodologies. This has led to
128 some modelling studies ignoring the pollen record completely, on the basis that data from the
129 LGM is too scarce (Janská et al., 2017). Where standardized methods have been applied to
130 multiple LGM pollen records, poor dating control has resulted in the inclusion of many
131 records that may not actually be from the selected LGM time window. This is particularly
132 important because the 21 ± 2.0 ka time slice commonly used to represent the LGM period in
133 PMIP data-model comparisons and other synthesis studies (MARGO members, 2009;
134 Bartlein et al., 2011) occurs immediately after the glacial maxima in the Alps around 26-23
135 ka (Heiri et al., 2014; Spötl et al., 2021) and Heinrich stadial HS-2 (24.3-26.5), whilst also
136 being closely followed by Heinrich stadial HS-1(15.6-18.0 ka) (Sanchez-Goñi & Harrison,
137 2010). These closely associated time periods can therefore be expected to represent both a
138 different vegetation and climate than the LGM itself.
139

140 For example, of the 18 European pollen records used in the PMIP benchmarking dataset
141 (Bartlein et al., 2011), 10 fall into the worst class ('poor') in the COHMAP chronological
142 quality classification scheme if relative dating such as pollen correlation is excluded. More
143 recent synthesis studies have also relied heavily on records from the European Pollen
144 Database (EPD) which currently has 116 records with samples of LGM age (as of June

145 2022). Many of these records however are based on chronologies that are considered reliable
146 for the Holocene (Giesecke et al., 2014), but have large uncertainties for the LGM as a result
147 of 1) excessive extrapolation back in time from Holocene age dates, 2) the use of pollen
148 correlation or other relative dating despite poorly defined regional biostratigraphy, or 3) the
149 inappropriate use of radiocarbon dates contaminated with old carbon. We found that 104 of
150 these 116 EPD records (Neotoma, 2021) fall into the worst class ('poor') in the COHMAP
151 chronological quality classification.

152

153 Here we address these problems using a new synthesis of LGM pollen records from
154 throughout Europe, the Mediterranean and the Middle East (EurMedMidEst) based on
155 rigorous quality control criteria. Records were compiled from an extensive review of public
156 databases and archives, and the scientific literature. Pollen records were selected according to
157 the robustness of their chronological control around the PMIP LGM time-window (21 ± 2
158 ka), and combined into a single dataset based on a harmonized taxonomy and standardized
159 pollen sum. The dataset was then analysed so that standardised maps could be produced to
160 show the distribution of the major pollen taxa, biomes and total arboreal pollen at the LGM.
161 In addition, quantitative reconstructions of forest cover as well as winter, summer and annual
162 temperatures and precipitation were undertaken using the Modern Analogue Technique
163 (MAT), utilizing the latest Eurasian Modern Pollen Database v2 calibration dataset. These
164 climate reconstructions are compared and evaluated against previous LGM pollen-climate
165 reconstructions, as well as reconstructions based on other proxies. The dataset and results are
166 fully documented and the complete data files are provided in the supplementary information.

167

168 **2 Methods**

169

170 **2.1 Pollen Data**

171

172 LGM fossil pollen data from Europe and bordering regions including North Africa and the
173 Middle East were selected and collated into a single standardized project database. This data
174 was sourced from the EPD/Neotoma database (Williams et al., 2021), the Pangaea data
175 archive, publications in scientific journals, and from the original authors. We selected LGM
176 pollen sites/data according to strict quality control criteria. Where possible, primary raw
177 pollen counts were used where this was available. Where the original electronic data was not
178 available, the data was digitized from the published diagram. Overall we have included 63
179 records in our study, of which 35 were digitized and 28 consisted of the original pollen
180 counts (Table 1).

181

182 The distribution of the 63 sites reflects the distribution of suitable archives, with fewer
183 records available from climatically or environmentally challenging regions (Fig. 1). High
184 rates of erosion and a drier and colder climate during the LGM reduced the number of
185 suitable anoxic sediment sinks for pollen preservation, especially in Central Europe between
186 the Scandinavian and Alpine ice sheets. Nevertheless, our dataset includes sites from this
187 region, as well as North Africa and eastern Central Europe through to Iran, although most
188 sites are located in an arc across eastern Spain, the Alps, and Italy. Lakes sites are the most
189 numerous archive and tend to be located in the more sheltered and topographically favourable
190 regions of Southern Europe and the Mediterranean. Peat is the next most important archive,
191 followed by alluvial and colluvial sediments, as well as cave sites, the later also often being
192 known for their archaeological significance. Sites located at the ice margins that appear to be
193 under the ice reflect uncertainties in the location of the ice margin both in time and space
194 during the LGM, as well as the fact that the selected time window for this study (21 ± 2 ka) is

195 later than the maximum ice advance in some regions (Hughes and Gibbard, 2015). For
196 completeness, we also include 7 marine records which have the advantage of more
197 continuous deposition and often better dating over the LGM period, but which are prone to
198 taphonomic biases compared to terrestrial records. These biases are discussed later in this
199 section.

200

201 LGM pollen records were selected according to a number of quality control criteria, but
202 primary amongst these was the existence of sufficient independent chronological control
203 points to accurately identify samples that would fall within the 21 ± 2 ka BP time-slice of
204 interest. We have used all of the samples within this time frame where the samples have been
205 available in electronic form, else we have used the sample closest to the target time (21 ka
206 BP). For records taken from the EPD we have used the latest Bayesian age-depth models
207 where these were available (Giesecke et al., 2014), otherwise we have used the dates and
208 chronology proposed by the original authors. We classified chronologies according to the
209 COHMAP chronological quality scheme for the LGM period (Anderson et al., 1988; Yu and
210 Harrison, 1995), which classifies record quality from 1-6 depending on whether a date falls
211 within 2000 14C years (or less) of the time being assessed, or whether bracketing dates fall
212 within 6000 and 8000 14C years (or less) about the time being assessed (Table A1).

213 Chronologies based on dates that fall outside of these limits fall into COHMAP class 7, and
214 are regarded as ‘poorly dated’ with respect to the LGM. Importantly, we have only included
215 radiometric and other absolute dates (such as varves) in this assessment, and have excluded
216 dates based on correlation with regional pollen records. These pollen-based stratigraphic
217 dates have been widely used in previous LGM studies, but do not include estimates of
218 uncertainty and are generally regarded as unreliable at this time given the sparsity of well
219 dated pollen sites and samples on which to base any correlation (Giesecke et al., 2014).

220

221 All records that were classified as poorly dated (COHMAP class 7) were subsequently
222 excluded from our analysis. This has meant that many of the pollen records used in previous
223 studies were excluded, including 16 of the 26 LGM records used by PMIP and associated
224 studies in Europe (Bartlein et al., 2011; Elenga et al., 2000; Tarasov et al. 2000, Jost et al.,
225 2005; Peyron et al., 1998; Wu et al., 2007; Cleator et al., 2020). We also excluded 104 of the
226 116 records in the EPD with samples that fall within our LGM time window. Many of these
227 EPD pollen records have been used in more recent studies, although the exact record (EPD
228 Entity number) is often not stated. We estimate that we have excluded 16 of the 17 European
229 sites used by Binney et al. (2017) (this study only included sites above latitude 40N), 5 of the
230 6 European sites used by Allen et al. (2010), 28 of the 33 sites used by Cao et al. (2019) and
231 27 of the 71 sites used by Kaplan et al. (2016).

232

233 Other quality control criteria were also used in the selection of LGM pollen records.
234 Published pollen diagrams that only included a small part of the terrestrial pollen assemblage,
235 or only presented summary taxa, were excluded. Records were also excluded where the
236 dating information was incomplete, for instance where radiocarbon dating uncertainties were
237 not published or where it was not possible to determine if the date shown was in calibrated or
238 uncalibrated radiocarbon years.

239

240 The modern pollen data for the climate and tree cover reconstructions were sourced from the
241 latest version 2 of the Eurasian Modern Pollen Database (Davis et al., 2020), which is
242 managed as part of the EPD. The EMPD2 includes 8133 modern pollen samples from across
243 the Palearctic biogeographic region from Europe to the far East of Asia. The taxa from both
244 the fossil and modern pollen data were consolidated into 120 of the most commonly-

245 occurring terrestrial taxa types. This taxa list was designed to be compatible with the
246 biomisation scheme used in our study (Peyron et al., 1998; Tarasov et al., 2000) and that used
247 in the Holocene mapping study of Brewer et al. (2017). The count of *Larix* was amplified by
248 a factor of 10 due to its low pollen representation (Edwards et al. 2000, Bigelow et al. 2003,
249 Tarasov et al. 1998, 2000, 2013, Binney et al., 2017).

250

251 **2.2 Biomisation**

252

253 We converted pollen assemblages to biomes based on the European biomisation scheme of
254 Peyron et al (1998), which in turn is based on Prentice et al. (1996). The method is described
255 in detail in Collins et al. (2012). We expanded the number of taxa included in the biomisation
256 procedure proposed by Peyron et al (1998) to include taxa from the Northern Eurasian
257 biomisation procedure of Tarasov et al. (1998). The inclusion of additional Northern Eurasian
258 taxa reflects recent evidence that modern analogues of LGM vegetation occur in parts of
259 Siberia (Magyari et al., 2014a). The biomisation procedure (Prentice et al. 1996) assigns each
260 taxa to a plant functional type (PFT) and calculates a score for each of these PFT's based on
261 the sum of the square root of the percentage of each of the taxa included in that PFT. To
262 reduce the influence of long-distance transport, taxa below 0.5% are removed at the start of
263 the procedure. Each biome is then assigned one or more PFT's and a score for each biome is
264 calculated as the sum of the associated PFT scores. The biome with the highest score is then
265 viewed as the dominant biome. Where the highest score is the same for more than one biome,
266 the dominant biome is decided based on a hierarchy of unique PFT's. Peyron et al. (1998)
267 also included a procedure for distinguishing warm and cold steppe biomes based on re-
268 assigning certain steppe PFT's according to the presence or otherwise of PFT's indicative of
269 cold or warm conditions. Following the Biome6000 project (Elenga et al., 2000) and Allen et
270 al. (2010), we did not apply this additional procedure and present only the merged steppe
271 biome. In summary, the biomisation procedure categorised 39 arboreal pollen taxa and 39
272 non-arboreal taxa into 22 plant functional types (PFT's), which were then combined into 12
273 biomes.

274

275 **2.3 Quantitative climate reconstruction**

276

277 We reconstructed climate from pollen data based on a standard Modern Analogue Technique
278 (MAT) that used PFT scores to match fossil samples with modern calibration pollen samples
279 (as used by Davis et al., 2003). This is a similar approach to that used by Peyron et al. (1998)
280 and Jost et al. (2005) who also applied pollen PFT scores to reconstruct LGM climate from
281 pollen data, but who used an artificial neural network technique (ANN) (Chevalier et al.,
282 2020). PFT scores have been used in previous large-scale European pollen-based climate
283 reconstructions for the Holocene (Davis et al., 2003; Mauri et al., 2014, 2015), where
284 performance was found to be better than the conventional approach based on individual taxa
285 (eg Marsicek et al., 2018). A particular advantage of the PFT approach for the LGM is that it
286 can help overcome problems associated with vegetation (pollen) assemblages that may have
287 no modern analogue (Davis et al. 2003). This can be a problem during the LGM when the
288 climate and environment could be expected to be very different from today, and when many
289 taxa formed unusual vegetation assemblages as a result of their forced retreat to sheltered
290 refugia locations. The problem of modern analogues is also addressed in our reconstruction
291 by using the latest EMPD2 modern pollen dataset for calibration purposes. The EMPD2
292 provides a large number of potential modern analogues for many different LGM vegetation
293 types and climates found today across the Palearctic region. PFT scores were calculated

294 according to the methods outlined already in the Biomisation section, then normalized so that
295 each sample was proportional to every other sample (Juggins and Birks, 2012).

296
297 The MAT method was applied using the Rioja program for R (Juggins, 2020). The modern
298 calibration data was taken from the latest version 2 of the EMPD (as detailed earlier). The
299 EMPD2 includes 8133 samples, which is considerably larger than the modern datasets used
300 in previous LGM pollen-based reconstructions. For instance, Peyron et al. (1998) used a
301 calibration dataset of 683 samples, which was updated by Jost et al (2005) to include an
302 additional 185 samples. These datasets were also mainly taken from the steppes of Kazakstan
303 and Mongolia, while the EMPD2 covers a much wider area, spanning most of the Eurasian
304 Palearctic region (Davis et al., 2020). The size and distribution of the modern training set in
305 climate and vegetation space is important because in order for the method to work
306 effectively, it is necessary to have samples representative of the likely vegetation and climate
307 space that could be occupied by the fossil assemblage (Turner et al. 2021, Chevalier et al.,
308 2020; Salonen et al. 2012, Juggins, 2013).

309
310 A known problem with MAT is the role of spatial auto-correlation in providing
311 unrealistically low estimates of uncertainty (Chevalier et al., 2020; Telford and Birks, 2009).
312 This results from the fact that closely analogous modern pollen samples can also be located
313 closely in physical space, and therefore in climate space. To reduce this problem it is possible
314 to exclude closely located samples from the analogue matching process using a filter based
315 on a set distance (h-block filter) (Telford and Birks, 2009). While this approach can help,
316 there are also three main problems associated with it. The first is error substitution, since
317 removing samples also reduces the number of potential analogues, creating a different source
318 of error that is not easy to categorise. Secondly, multiple samples taken from the same
319 location are actually a strength of pollen training sets, since they are more likely to capture
320 the full range of the assemblage diversity associated with a given climate. Thirdly, current
321 methods that limit spatial range such as the h-block filter only do so on the horizontal axis,
322 and do not consider the fact that samples can also be found at different elevations. In hilly or
323 mountainous regions samples can therefore be excluded because they are closely located in
324 horizontal space, but in fact they actually occupy very different climates and vegetation
325 associations, contradicting the logical premise of the h-block filter. It was therefore decided
326 not to apply this filter.

327
328 Uncertainties for the pollen-climate reconstructions were calculated using a standard method
329 for MAT (Juggins 2020) based on the spread of the climates associated with the best modern
330 pollen analogues used for each fossil sample. The closer the climates of the best modern
331 pollen analogues (6 in the case of this study) then the smaller are the calculated uncertainties
332 assigned to the reconstructed climate of the fossil pollen sample.

333
334 Climate reconstructions are presented as anomalies. These have been calculated with respect
335 to modern climate (1970-2000 average) at each core site location using WorldClim 2 (Fick
336 and Hijmans, 2017) (Table A2), which was also used to assign the modern climate for the
337 modern pollen samples in the transfer function (Davis et al., 2020).

338 339 **2.4 Quantitative tree cover reconstruction**

340
341 It has long been recognized that the proportional representation of individual pollen taxa in a
342 pollen assemblage does not necessarily reflect the proportion of land area covered by that
343 taxa in the pollen source area surrounding the sample site (Davis 1963, Gaillard et al. 2010,

344 Zanon et al. 2018). These differences can be caused by variations in pollen productivity,
345 differential transport, deposition and preservation of pollen grains, and even the ease or
346 otherwise of the identification of pollen grains themselves. This can make the interpretation
347 of pollen taxa percentages difficult, even for relatively simple questions such as the
348 proportion of forest to non-forest in the landscape.

349
350 There have been two main methods developed to account for this quantification problem, one
351 using a physical modelling technique (PMT) based on estimates of pollen production for
352 individual taxa (Gaillard et al., 2010), and the other using a MAT very similar to that used in
353 pollen-climate reconstructions (Williams and Jackson, 2003). Both approaches have been
354 widely applied during the Holocene in Europe (Zanon et al., 2018), but we know of no
355 previous study that has applied either of these approaches to the LGM. The LGM presents a
356 number of challenges, not least the problem of potential missing vegetation analogues, as
357 well as low atmospheric CO₂, which has been shown to influence pollen productivity (Leroy
358 and Arpe, 2007).

359
360 Here we use the MAT to provide quantitative estimates of forest cover, following the
361 approach of Zanon et al. (2018) who applied this method to the Holocene pollen record of
362 Europe. We apply MAT in exactly the same way as for the climate reconstructions described
363 earlier, including the use of PFT scores to match fossil and modern pollen samples. Instead of
364 modern climate values, we assigned an estimate of modern forest cover to each of our
365 modern pollen sites. To do this we use a high resolution (~100m) remote sensing dataset
366 derived from satellite observations (Hansen et al., 2013). Zanon et al. (2018) have shown that
367 the MAT calibrated in this way gives comparable results to the PMT approach in Europe, at
368 least for the Holocene. One of the main differences however is that the PMT is designed to
369 provide estimates of the proportions of different taxa, whereas the MAT (as applied here) is
370 designed to provide estimates of the proportion of forest cover. Where the PMT can only
371 reconstruct the proportion of forest forming trees, irrespective of their size, the MAT
372 (following Zanon et al. 2018) is calibrated specifically to reconstruct forest composed of trees
373 over 5m tall. This follows the FAO definition of forest as “land spanning more than 0.5
374 hectares with trees higher than 5 meters and a canopy cover of more than 10 percent, or trees
375 able to reach these thresholds in situ” (FAO Terms and definitions 2020
376 <http://www.fao.org/3/I8661EN/i8661en.pdf>).

377

378 **2.5 Maps**

379

380 We present our results in the form of maps that include the main physiographic features of
381 the LGM in the study area. The maps are based on the WGS84 projection. Coastlines reflect
382 LGM sea level at 120m below present, while ice sheets are based on Ehlers et al. (2011).
383 Modern national country boundaries are also included for reference.

384

385 **2.6 Marine pollen records**

386

387 We have included marine pollen records in our analysis for reasons explained below, but it is
388 important that these records should be viewed with caution, particularly when used for biome
389 and quantitative MAT reconstructions, and when compared with terrestrial records from
390 different archives. Biomisation methods have been applied to individual marine pollen
391 records (Combourieu Nebout et al., 2009), as well as multi-site synthesis studies such as the
392 ACER project (ACER project members et al., 2017). However, marine records were
393 specifically excluded from the Biome6000 project (Elenga et al., 2000). Similarly,

394 quantitative climate methods have been applied to individual marine pollen records
395 (Combourieu Nebout et al., 2009; Fletcher et al., 2010), as well as multi-site synthesis studies
396 (Sánchez Goñi et al., 2005; Brewer et al., 2008; Salonen et al., 2021). However, marine
397 records have also been specifically excluded from other major pollen-climate studies
398 (Cheddadi et al., 1996; Davis et al., 2003; Marsicek et al., 2018), as well as quantitative forest
399 cover reconstructions (Zanon et al. 2018).

400

401 Discussion on the advantages and problems associated with marine records can be found
402 elsewhere (Chevalier et al., 2020; Danianu et al., 2019), but are reviewed briefly here where
403 relevant to the methodologies applied in this study. Marine sedimentary records provide
404 continuous and well dated pollen records for the LGM that are often lacking from many
405 terrestrial regions, especially in arid areas with few alternative anaerobic sediment sinks.
406 Conversely however, pollen source areas for marine sites may be many hundreds of
407 kilometers from the coring site and may be liable to change through time in response to
408 changes in distance to the coastline, rates of river discharge and ocean and atmospheric
409 dynamics. This can theoretically give rise to changes in the vegetation shown in the pollen
410 assemblage recorded at the marine site without any actual change in climate or other
411 environmental pressure. The large and indeterminable source area of marine records also
412 mean that it is difficult to apply quantitative MAT reconstruction methods, not least because
413 the mean climate or forest cover of the source area is almost impossible to determine. In
414 addition, the pollen record and the calibration dataset to which it is being compared are
415 composed largely of terrestrial lakes and bog sites with much smaller and more homogeneous
416 source areas. This creates a series of problems, the more obvious of which is the calculation
417 of anomalies, since we cannot assume that the modern climate at the (marine) coring site
418 location is representative of the (terrestrial) source area. In this study we have taken the
419 closest point on land as the modern climate for the calculation of anomalies, but provide the
420 absolute values for all sites so that these can be recalculated if necessary (Table A2). The
421 next problem is that the large source area may capture a combination of different vegetation
422 types that is not going to be represented in a calibration dataset based on samples from
423 terrestrial sites with much smaller source areas, for instance a mixture of coastal and
424 mountain vegetation, or even vegetation from different continents (Magri and Parra, 2002).
425 However, in our analysis we did not find any sample from a marine record (or terrestrial
426 record) that did not have a reasonable modern analogue in our training set (chord distance
427 <0.3) (Huntley, 1990), even though we did not adjust the pollen assemblage for the over-
428 representation of *Pinus* in the marine pollen samples.

429

430 Typically, the Pine component is excluded from the terrestrial pollen sum when calculating
431 percentages for marine pollen samples, and in some cases Pine has been excluded entirely
432 from the samples used in marine pollen-climate reconstructions (Combourieu Nebout et al.,
433 2009). The problem with excluding *Pinus* is two-fold, the first is that *Pinus* often represents
434 the main forest forming tree in the Koeppen Csb climate zone on the Atlantic coast where
435 many marine sites are located (García-Amorena et al., 2007), as well as representing the most
436 abundant tree taxa in Europe during the LGM (Figure A3c). Removing *Pinus* from the
437 assemblage would almost certainly create an artificially arid assemblage in these
438 circumstances, undermining the ability of the transfer function to reconstruct precipitation,
439 although temperature would likely be less affected since *Pinus* is a generalist found in both
440 hot and cold temperature regions. The second problem is that the remaining terrestrial taxa
441 often constitute a very small number of pollen grains in a typical marine pollen sample (<100
442 grains), which can result in pollen assemblages that are not based on a statistically stable
443 count of the pollen sample (Chevalier et al., 2020).

444

445 3. Results

446

447 3.1 Vegetation & Biomes

448

449 Results of the biomisation analysis shows that steppe (STEP) was the most common biome at
450 the LGM across the study area, occurring at 36 out of 63 sites, indicating that the landscape
451 was largely dominated by cool temperate grasslands across much of western Central Europe,
452 central and eastern Mediterranean, as well as North Africa and the Middle East (Fig. 2).

453 However, at the same time we also find that there were a significant number of sites where
454 we find that woody and forest biomes occur, more particularly in southern and eastern Iberia,
455 northern Italy and central eastern Europe. The most dominant of these forest and woody
456 biomes are taiga (TAIG) in the north, and cool-mixed forest (COMX) and xerophytic
457 woodlands (XERO) in the south.

458

459 As would be expected, the dominance of STEP biomes is generally reflected in low arboreal
460 pollen percentages across the same areas/sites (Fig. 3 & 4). Exceptions to this rule can be
461 found at marine sites such as [MD99-2331 site #3] and [MD01-2430 site #58] where STEP is
462 reconstructed despite arboreal pollen percentages of 71 and 80 percent respectively. This
463 apparent contradiction illustrates some of the idiosyncrasies of the biomisation method,
464 especially when applying the method to marine pollen samples. In this case it is important to
465 remember that the AP% is calculated from the sum of the percentages of each relevant taxa,
466 but the score for each biome is the sum of the square root of the percentages of each of its
467 constituent taxa. This results in biomes with taxa with large percentage values scoring
468 proportionally smaller, and biomes with taxa with small percentage values scoring
469 proportionally larger. For example, a single taxa at 50% has a square root of 7.07, but the
470 sum of the square roots of 10 taxa each at 5% is 22.36 even though the sum of the
471 percentages is the same 50%. This effect can be particularly pronounced in marine pollen
472 samples because they are usually dominated by a single taxa (*Pinus*) that forms a high
473 percentage of the total assemblage. Since there are often more non-arboreal taxa than
474 arboreal taxa in a pollen assemblage, the non-arboreal taxa can dominate in the biomisation
475 process even if collectively their percentage of the assemblage is a lot less than the arboreal
476 taxa, resulting in a non-arboreal biome such as STEP having the highest biome score.

477

478 Of the main arboreal biomes, Taiga (TAIG) is the dominant biome at 3 sites at the eastern
479 end of the Alpine ice sheet, as well as at a site just to the north in northern Germany and a
480 site in Slovakia, while Cool Conifer Forest (COCO) is found at 1 site close to the
481 Scandinavian ice sheet in Lithuania. Cool Mixed Forest (COMX) is found much more widely
482 at 8 sites south of the Alps from south-west Iberia to Romania, with Xerophytic Scrub
483 (XERO) occurring at 8 sites with a similar distribution but not as far east or west. Cold
484 Mixed Forest (CLMX) occurs at just two sites in Georgia and the Alboran Sea at the far east
485 and west of the study area, while Warm Mixed Forest (WAMX) is the dominant biome at just
486 1 site in Southern Spain. We do not record Temperate Deciduous Forest (TEDE), Tundra
487 (TUND) or Desert (DESE) as the dominant biome at any site at the LGM, although they do
488 occur as sub-dominant biomes.

489

490 An alternative picture of LGM tree-cover is provided by the MAT reconstructions (Fig. 4).
491 MAT performance statistics for tree cover are shown in table 2, based on an evaluation using
492 the modern training set. This shows a relatively large root mean square error (RMSE) of
493 21.03. and an R2 of 0.52 that is not as good as for the MAT climate analysis, but overall the

494 results are comparable with previous MAT tree cover studies (Zanon et al., 2018). In general,
495 the MAT values (site average 34%) show forest-cover around 16% less than that suggested
496 from AP% (site average 50%) (Fig. A1), although sites with very low AP% also show higher
497 values based on MAT. These differences are consistent with comparisons between MAT and
498 AP% in Zanon et al (2018), although it should be noted that uncertainties related to the MAT
499 reconstructions are large ($\pm 23\%$). Zanon et al (2018) found that the differences between
500 MAT and AP% were greatest over Northern Europe and in Arctic and sub-Arctic climate
501 regions that are likely to be comparable to many areas of Europe during the LGM. These
502 regions today are associated with tree-forming taxa such as Birch that fail to grow to a height
503 of 5m or more, developing only as shrubs or krummholz forms.

504
505 Pollen taxa percentages are shown in supplementary figure A2, and distribution maps of the
506 33 most common taxa are shown in the supplementary figures A3a-f. Of the 21 arboreal taxa,
507 *Pinus* generally has the highest values and is the most widespread, being present at all 63
508 sites. Other acicular arboreal taxa include *Juniperus*, which also has a wide distribution
509 across EurMedMidEst although at lower values. The rest of the acicular arboreal taxa have
510 more regional distributions. *Picea* is found mainly to the north of the study region, away from
511 the Mediterranean, whilst *Abies* is generally found more to the south. *Larix* occurs only in the
512 central European area including the northern edge of the Po plain just south of the Alps,
513 whilst *Cedrus* is found mainly across south and west Europe in locations much further north
514 than its Holocene and modern distribution which is confined mainly to Morocco and Lebanon
515 (Collins et al., 2012). Temperate broadleaf arboreal taxa which also include cold-tolerant
516 species such as *Betula* and *Salix* are relatively widely spread across the EurMedMidEst
517 during the LGM, while less drought tolerant taxa such as *Alnus*, *Carpinus* and *Corylus* are
518 found more to the south-west through to the north-east. Other temperate broadleaf arboreal
519 taxa such as *Quercus* (deciduous) and *Ulmus* have a much more southern distribution, with
520 *Fraxinus*, *Olea*, and *Quercus* (evergreen) being more prevalent in the south-west. In contrast,
521 *Fagus* occurs more to centre and the east, while *Tilia* is found even in more northern
522 locations of central Europe. The remaining arboreal taxa are more shrubby and drought
523 adapted, with *Ephedra* and particularly *Ephedra fragilis* having a southern distribution,
524 whilst the more cold adapted *Hippophae* being found even in the north of central Europe
525 (similar to *Tilia*).

526
527 The main non-arboreal taxa generally indicate cool, dry and environmentally disturbed
528 conditions across much of the EurMedMidEst. The most widely distributed taxon is Poaceae,
529 which like *Pinus*, is found in all records. Other non-arboreal taxa with a widespread
530 distribution include Rubiaceae, Apiaceae and Asteraceae (Asteroideae), while *Plantago*,
531 Cayophyllaceae, Brassicaceae and Asteraceae (Cichorioideae) have a more southern and
532 western distribution. *Thalictrum* can be found mostly at sites in the centre of the
533 EurMedMidEst, along with *Helianthemum* which also extends to sites in the south-west.
534 Other taxa such as *Chenopodiaceae* and *Artemisia* have a more southern distribution,
535 reflecting their preference for drier and less cold climates.

536 537 **3.2 Climate reconstruction evaluation**

538
539 Evaluation of transfer function performance based on the modern training set is presented in
540 table 2. This shows that root mean square error predicted (RMSEP) values were smallest for
541 summer temperatures (2.21C), and largest for winter temperature (3.35C), with mean annual
542 temperatures in between (2.28C). The weaker performance for winter temperatures largely
543 reflects the much greater range of winter temperatures in the training set. In turn, this

544 contributes to a better R2 performance for winter temperatures (0.91) than annual
545 temperatures (0.9) and summer temperatures (0.81). Overall R2 performance for precipitation
546 is weaker than for temperature, which is typical because of the higher spatial variability of
547 precipitation compared to temperature. Summer precipitation has the strongest R2
548 performance (0.75) compared to winter and annual precipitation (both 0.69), as well as
549 smaller RMSE values (52mm) than winter (78mm).

550
551 Given the widespread occurrence of steppe during the LGM, we also undertook a separate
552 evaluation of transfer function performance in this type of environment. For this we used a
553 subset of 1588 pollen samples from the EMPD2 that are classified with the steppe pollen-
554 biome (Davis et al. 2020). The results indicate (Table A3) little difference in performance
555 compared to the full dataset, with a small decrease in performance in annual and summer
556 seasons in both precipitation and temperature, and a slight increase in performance in winter.

557
558 The results overall indicate good transfer function performance especially for temperature,
559 and are comparable with those found in other continental scale pollen-climate studies
560 (Bartlein et al., 2011). It is important to remember though that comparisons between studies
561 can only be made with caution because results are often heavily dependent on the nature of
562 the modern pollen dataset used as the training set, which is not the same in all studies
563 (Juggins, 2013).

564
565

566 **3.3 Climate reconstruction**

567
568 Reconstructed LGM temperatures indicate an overall mean annual cooling of $-7.2 \pm 3.3\text{C}$,
569 with a greater cooling of around $-9.3 \pm 4.5\text{C}$ in winter and $-5.0 \pm 3.2\text{C}$ in summer (Fig. 5). All
570 sites apart from Lake Van [site #62] in eastern Turkey show cooler temperatures at the LGM
571 compared to modern (Fig. 6), and even at this site cooler conditions fall within the
572 uncertainties. With greater cooling in winter compared to summer, the difference in
573 temperature between winter and summer also increased (shown by positive anomalies) at
574 most (but not all) sites (Fig. 6). This increase in continentality was around $+4.2\text{C}$ on average
575 across all sites (Fig. 5).

576
577 We reconstruct an overall decline in mean annual precipitation of around $-91 \pm 270\text{mm}$ (-
578 13%) at the LGM. Most of this decline is in winter ($-38 \pm 90\text{mm}$) (-21%), while in summer a
579 small increase is shown ($10 \pm 57\text{mm}$) (6%), although uncertainties are large (Fig. 7).
580 Compared to temperature there is significant seasonal and spatial variability in positive and
581 negative precipitation anomalies (Fig. 8). Positive anomalies appear more predominant in
582 eastern and southern Spain and in central eastern Europe in both summer and winter, while
583 positive anomalies are found more generally in summer across sites in Southern Europe and
584 the Mediterranean. These more positive summer anomalies also reflect a relative shift from
585 winter to summer in the seasonality of precipitation in this region.

586
587

587 **4.0 Discussion**

588
589 Before we consider the results of our analysis it is important to provide some context in terms
590 of European LGM geography and environment, which was very different from today (Fig. 1).
591 Major ice sheets covered Scandinavia and much of the UK, the Alps, and the Pyrenees. Sea
592 level was 120m lower, resulting in much of the North Sea and English Channel becoming dry
593 land, and the European coastline extending over 100 km out into the Atlantic and

594 Mediterranean, especially around the Bay of Biscay and Adriatic. The Black Sea was no
595 longer connected to the Mediterranean, and was smaller with a water level around 100m
596 lower than today (Genov, 2016). These changes in sea or water level had two main
597 consequences, the first being that the marine sites were closer to land, and therefore closer to
598 (low lying) terrestrial vegetation and (pollen carrying) river discharge points than they are
599 today. The second consequence of lower seas levels is that terrestrial pollen sites were
600 located further from the moderating effect of the ocean than they are today, resulting in a
601 localised modification of the climate experienced by the site irrespective of regional or global
602 changes (Geiger, 1960).

603
604 The maps used in our analysis shows the maximum ice sheet at $21k \pm 2k$ (Ehlers et al., 2011).
605 The precise geographical location of the ice sheet is difficult to resolve at a fine spatial scale,
606 however, which explains why some sites close to the ice margin appear to be actually located
607 under the ice (for example sites Kersdorf-Briesen site #46 & Mickunai site #54). The
608 resolution of the map also shows the occurrence of permanent ice not only to the north and
609 over the Alps, but also on many subsidiary areas of high ground across central and southern
610 Europe, including areas such as the Pyrenees, Massif Central, Vosges and Carpathian
611 Mountains. While global ice volume may have peaked ~ 21 ka individual ice sheets in Europe
612 and other areas are known to have reached their maximum extent at different times (Hughes
613 et al., 2016). The larger ice sheets are likely to have had a significant influence on regional
614 climate and environmental conditions across Europe, but the smaller ice sheets had similar if
615 more localized impacts as well. Surrounding each ice sheet would have been an unglaciated
616 area of active peri-glacial processes and newly created and unstable ground. This would
617 include outwash plains, impounded lakes and recently drained lake beds, seasonally and
618 sporadically flooded areas, moraines, kettle holes and other glaciological and peri-glacial
619 features. Soils in these areas would be non-existent or skeletal, and vegetation would find it
620 difficult to obtain nutrients and water for survival, irrespective of the prevailing climatic
621 conditions. Outside of these areas, permafrost is also likely to have been present, particularly
622 north of the Alps (Vandenbergh et al., 2014), which would also act as an impediment to
623 vegetation growth.

624
625 In terms of regional climate, the major ice sheets would have provided significant barriers to
626 westerly atmospheric circulation, or even north-south circulation in the case of the Alps and
627 Pyrenees. As well as representing a physical obstruction, the thermodynamic response of the
628 atmosphere to these high, cold obstructions would have been to encourage the formation of
629 areas of semi-permanent high pressure, similar to those found today for instance over the
630 Greenland ice sheet. In addition, the Laurentide ice sheet located over North America would
631 have generated downstream effects over Europe (COHMAP, 1988). These physical and
632 thermodynamic effects would have affected the direction of storm tracks, as well as more
633 local climatic effects commonly associated with ice sheets such as strong katabatic winds
634 (Kageyama, et al. 2021, Velasquez et al. 2021, Luetscher et al. 2015, Lefort et al. 2019)

635 636 **4.1 Vegetation Cover**

637
638 The nature and extent of forest cover during the LGM remains a matter of considerable
639 debate. Vegetation models driven by LGM climate model simulations generally indicate
640 extensive areas of boreal forest north of the Alps, and a mix of temperate and warm-
641 temperate woodland to the south across southern Europe and much of the Mediterranean.
642 Treeless areas such as steppe are mainly confined to those areas where it is also found today,
643 namely inland Iberia, Ukraine, southern Russia and Turkey, while Tundra is found to the

644 north close to the Scandinavian Ice Sheet (Allen et al., 2010; Cao et al., 2019; Prentice et al.,
645 2011; Velasquez et al., 2021).

646
647 Evaluation of these vegetation-model simulations against data has been largely based on
648 comparison with compilations of pollen-biome reconstructions (Prentice et al., 2011; Allen et
649 al., 2010; Cao et al., 2019; Velasquez et al., 2021). Early studies were based on only a limited
650 number of sites from southern Europe, and showed steppe at all sites in contradiction with
651 model simulations (Elenga et al. 2000). More recent pollen compilations have included more
652 sites especially to the north that have revealed a more mixed picture of vegetation cover, with
653 forest biomes at some sites both south and north of the Alps that appear more consistent with
654 model simulations (Binney et al., 2017; Cao et al., 2019). However, many of these pollen
655 sites used in these studies were assigned an LGM age based on poor or incorrect dating
656 control, and likely date to MIS3, the Late-Glacial or even the Holocene. Nevertheless, based
657 on our compilation of more securely dated LGM pollen sites, we also show a wider
658 distribution of forest biomes particularly in Iberia, northern Italy and Central Europe,
659 although with greater areas of steppe than suggested by the models over the remaining
660 regions.

661
662 However, the interpretation of biome reconstructions requires care since the forest cover and
663 vegetation composition may not be as clear as the dominant biome suggests. For instance, we
664 find that steppe is still reconstructed as the dominant biome at some sites despite arboreal
665 pollen forming 70-80% of the pollen assemblage. In addition, it is important to remember
666 that pollen-biomes are based only on the proportion of taxa that can form forest and
667 woodland, while these taxa may in fact exist only as shrubs or stunted krummholz forms in
668 the challenging climate and environment of the LGM. Alternatively, similar conditions may
669 favour low-lying non-arboreal taxa forms with poor pollen dispersion or even insect
670 pollinated taxa forms that may be poorly represented in the pollen assemblage, giving greater
671 prominence to arboreal taxa whose pollen may be the result of long-distance transport
672 particularly *Pinus*. However there also appear to be plenty of samples with low or even very
673 low (<20%) arboreal percentages, so not all sites in open areas may be affected by long-
674 distance transport of *Pinus* in the same way.

675
676 Quantitative MAT based reconstructions of forest cover can overcome some of these
677 problems, where they can be detected, based on the composition of the pollen assemblage
678 when compared with the modern land-cover. Chord-distance measurements of the match
679 between fossil and modern pollen assemblages indicate good LGM analogues exist in our
680 large Eurasian modern pollen dataset. The results of the MAT forest cover reconstruction
681 indicates that forest cover was low but not entirely devoid of woodland in most areas, similar
682 to the modern boreal forests of Siberia and consistent with a steppe-tundra-woodland mosaic
683 proposed by many authors (e.g. Birks and Willis, 2008; Willis and Van Andel, 2004). This is
684 confirmed in an analysis of the most commonly found modern analogue ecoregions for LGM
685 pollen samples at each site (Table A4). Uncertainties are large, but for comparison the MAT
686 site-average of 33% forest cover is slightly less than the average today over the Boreal region
687 of Europe (43%) and slightly more than the average today over Mediterranean region (27%)
688 (Zanon et al. 2018).

689
690 By calculating the percentage of each of the taxa in each LGM pollen sample using a
691 standardized pollen sum, we are able to make direct comparisons between different LGM
692 pollen records and their taxa percentages (Figure A2, A3). The results show a preponderance
693 of boreal forest taxa to the north of the Alps, consistent with biome results mentioned earlier.

694 *Pinus* is the most common forest forming taxa in this boreal zone, together with *Picea*, and
695 including *Larix* to the east and *Abies* to the west. The occurrence of *Betula* and *Juniperus*
696 also suggests shrubby elements consistent with arctic shrub-tundra, although high Poaceae
697 and other herbaceous taxa such as *Artemisia* and *Chenopodiaceae* indicate more steppe than
698 tundra. Other deciduous taxa found north of the Alps include cold tolerant generalists such as
699 *Corylus* and *Alnus*, as well as low percentages of relatively thermophilous taxa in the east,
700 such as *Carpinus* and *Tilia*.

701
702 These results are consistent with charcoal (Magyari et al., 2014a; Willis and Van Andel,
703 2004), malacological (Juříčková et al., 2014), biomarkers (Zech et al., 2010) and genetic
704 evidence (Stivrians et al., 2016; Willis and Van Andel, 2004) that the main forest region north
705 of the Alps was in the eastern region of Central Europe around the Carpathian basin. This
706 was also an area where cold and moisture sensitive deciduous taxa were also able to survive
707 (Magyari et al., 2014), although evidence of temperate taxa found in the pollen record has yet
708 to be supported by charcoal and macrofossil records (Feurdean et al., 2014). Our pollen
709 evidence indicates an open taiga or cool mixed forest that extended in central and eastern
710 Europe to areas close to the Scandinavian and Alpine ice caps, as proposed by Willis and Van
711 Andel (2004) and Huntley and Allen (2003), although whether this represents isolated
712 pockets of forest or an extended open steppe-forest is difficult to determine (Kuneš et al.,
713 2008). Even steppe or tundra areas in western Europe show a low but significant presence of
714 the pollen of tree taxa at sites close to the ice sheets that are unlikely to be solely the result of
715 long distance transport or reworking (Kelly et al., 2010). The presence of woodland in these
716 areas is also supported by mammalian remains, for instance at Kents Cavern in SW England
717 (Stewart and Lister, 2001).

718
719 Overall however, our results clearly show a much greater predominance of thermophilous
720 and moisture sensitive deciduous taxa south of the Alps, particularly in Iberia and Northern
721 Italy, where temperate broadleaf forests survived in sheltered refugia (Kaltenrieder et al.,
722 2009). Most of these appear to be in hilly areas with the ability to generate orographic rainfall
723 (Monegato et al., 2015), on south facing slopes to make the most of the sun's radiant energy
724 and located above the valley floor to escape frost and flooding. We might also expect these
725 areas to be sheltered from cold northerly winds, and benefit from relatively mild and moisture
726 laden winds coming from the Mediterranean Sea. For instance, the presence of woodland and
727 low glacier altitudes along the southern slopes of the Alps around the Po Valley and Trentino
728 region is consistent with strong orographic rains generated by southerly and easterly winds
729 that today can be generated by low pressure located south of the Alps in the Gulf of Genoa,
730 and consistent with a southerly storm track around the Alps (Kehrwald et al., 2010; Luetscher
731 et al., 2015). Generally, as might be expected, areas of forest reconstruct similar or increased
732 precipitation compared to today, and areas of steppe indicate decreased precipitation (see next
733 section).

734
735 Independent evidence of LGM vegetation is provided by archaeozoological data. This data
736 supports the palynological evidence for the existence of forest and woodland refugia across
737 the ice-free areas of Europe at latitudes north of the Alps. For instance, large vertebrates in
738 these areas show patterns of extirpation and extinction in response to shifts in climate and
739 vegetation cover that is different for different species, indicating a variety of environments
740 and niches (Lister and Stuart, 2008; Stewart and Lister, 2001). As with the pollen record, the
741 presence of temperate adapted large vertebrate taxa within the glacial landscape of Western
742 Europe also suggests the existence of temperate "micro-refugia" (Stewart and Lister, 2001),
743 consistent with suggestions that temperate arboreal taxa were not entirely extirpated from the

744 region during the LGM (Magri, 2010). Further east, mammal assemblages indicate
745 generalized loss of forest components in the East European Plain (Demay et al. 2021,
746 Puzachenko et al., 2021) which is consistent with our data indicating low forest cover in this
747 region. In other areas, evidence of the prevailing land cover at the LGM comes from studies
748 of small vertebrate communities, which have a closer affinity to the prevailing environment
749 than large vertebrates (López-García and Blain, 2020) that have the propensity to migrate
750 large distances, often on a seasonal basis. These studies of small vertebrate assemblages also
751 support the existence of temperate “micro-refugia” in France (Royer et al., 2016) and the
752 existence of woodland components in many regions across Southern Europe including parts
753 of Iberia (Bañuls-Cardona et al., 2014) Italy (Berto et al., 2019) and the Balkan Peninsula
754 (Mauch Lenardić et al., 2018).

755
756 Other paleobotanical evidence also supports our land cover reconstruction. Schafer et al.
757 (2016) suggest leaf wax patterns from palaeosols in Spain may indicate the presence of
758 drought intolerant deciduous trees and more humid conditions during the LGM. Significantly,
759 none of the pollen sites indicate that temperate broadleaf forests were dominant, and
760 broadleaf temperate taxa always appear part of a mixed woodland together with cold or
761 aridity adapted evergreen and needleleaf taxa, including typical Mediterranean taxa. This type
762 of mixed vegetation probably extended to the Balkans where the hilly terrain and proximity
763 to the Mediterranean would appear to have provided favourable climatic conditions, although
764 we still lack LGM sites from this region. At sites in central and southern Italy and east
765 through Greece and Turkey to the Middle East (and including North Africa), the vegetation
766 appears drier with a greater prevalence of steppe. Only a site in Georgia at the edge of the
767 Caucasian mountains indicates the presence of significant amounts of forest (mainly *Pinus*), a
768 result that was also found by Tarasov et al. (2000), and probably linked to favourable
769 orographic precipitation and proximity to the Black Sea.

770
771 Comparison with LGM land cover from vegetation modelling studies driven by climate
772 model simulations indicate a much wider presence of forest than that shown by the pollen
773 data (Kaplan et al., 2016). Data-model agreement appears to be closest over eastern-central
774 Europe where pollen indicates the presence of open Boreal forest, and over south-west
775 Europe with the presence of cool mixed temperate forest, including broadleaf deciduous and
776 thermophilous elements (Prentice et al., 2011; Allen et al., 2010; Cao et al., 2019; Velasquez
777 et al., 2021). Nevertheless, agreement still appears to be weak over western-central Europe
778 and Southern and Eastern Europe through to the Middle East, where pollen data continues to
779 indicate widespread steppe. One proposed explanation for this data-model discrepancy has
780 been the role of fire (including man-made fire) in maintaining forest openness, a factor
781 influencing forest cover that is not included in most vegetation models (Kaplan et al., 2016).
782 In the Carpathian basin Magyari et al. (2014a) noted that charcoal increased as forest cover
783 declined, suggesting that wildfires played a role in decreasing forest cover during the LGM.
784 Other studies have noted low levels of charcoal and therefore fires during the LGM, although
785 these tend to be from steppe areas with low biomass and fuel availability (Connor et al.,
786 2013; Kaltenrieder et al., 2009). Recent LGM vegetation simulations that include fire indicate
787 much lower values of forest cover than those without fire over western central Europe, while
788 forest remains in central eastern Europe (see figure 6 in Velasquez et al., 2021). This appears
789 closer to the data, but the values are perhaps too low compared with our MAT
790 reconstructions here (Figure 4).

791 792 **4.2 Climate** 793

794 **4.2.1 Comparison with previous pollen-based reconstructions**

795

796 The climate of the LGM is generally considered to have been cooler and drier than today, but
797 data-model comparisons continue to highlight important discrepancies, not only in the degree
798 of cooling and drying but also in their seasonal and spatial distribution. Data-model
799 comparisons over Europe have mainly used pollen-based climate reconstructions, especially
800 the Paleoclimate Modelling Intercomparison Project (PMIP/CMIP) (Kageyama et al., 2021,
801 Bartlein et al., 2011; Harrison et al., 2015; Kageyama et al., 2006). The most commonly used
802 reconstructions have been based on two main methods, a neural-network methodology
803 (ANN) of Peyron et al. (1998) and Jost et al. (2005), and an Inverse Modelling approach
804 (INV) applied by Wu et al. (2007). The ANN method uses modern pollen samples for
805 calibration and does not include any correction for CO₂ effects, being similar in these
806 respects with the MAT method used in this study. In contrast the INV method does not use
807 modern pollen samples for calibration, but instead uses a process-based vegetation model run
808 in inverse mode. Ordinarily, a vegetation model will use climate as an input to generate a
809 vegetation as an output, but in inverse mode the model is reconfigured to generate climate as
810 an output given a particular vegetation (pollen) assemblage as an input. One of the
811 advantages of the INV method is that CO₂ can also be varied as an input, and therefore the
812 effect of changes in CO₂ on the vegetation, and therefore reconstructed climate, can be
813 investigated. Comparison of these ANN and INV reconstructions have shown important
814 differences, with the INV reconstruction generally not as cold and somewhat drier than ANN
815 (Wu et al. 2007). These differences between pollen-climate methods have often been
816 attributed to CO₂ effects (Wu et al. 2007) but this is not clear since there may be other
817 factors, such as the size and location of the training set used in the ANN reconstruction.

818

819 We make a comparison with these earlier reconstructions based on 10 sites/records in our
820 dataset which we identified as also being included in these earlier studies (Fig. 9). While we
821 were able to identify the site and data source, as well as the time window, we were unable to
822 establish if the the data represented a single sample or the mean of multiple samples within a
823 time-window or the exact depth of those samples, or the actual sediment core in the case of
824 multiple cores from the same site. While these aspects are unknown, it seems likely that the
825 pollen data we used in our analysis was very similar if not identical in most cases, and
826 reconstructed biomes for these sites from our pollen dataset are identical to the biomes
827 reconstructed using the earlier pollen dataset (Elenaga et al., 2000).

828

829 We compare our MAT with the ANN and INV reconstructions in figure 9. On average across
830 all 10 records, the MAT and INV methods give almost identical results for both anomalies of
831 mean annual temperature (MAT -6.6C, INV -7.2C) and precipitation (MAT 158mm, INV
832 165mm). Uncertainties are also similar for both methods. In contrast, the ANN method gives
833 much cooler mean annual temperature anomalies (ANN -13.9C) and drier precipitation
834 anomalies (ANN -474mm). On a site by site basis the MAT and INV methods show closer
835 agreement for temperatures than precipitation, although precipitation has proportionally
836 larger uncertainties. The reconstructions based on these two methods are close enough that
837 the uncertainties overlap at all sites for both temperature and precipitation, except the
838 precipitation reconstruction at Lac de Bouchet (site #25). The reason for this is not clear, but
839 there could easily be minor differences with the pollen data analysed by Wu et al. (2007) in
840 their INV reconstruction since the pollen record (Reille and de Beaulieu, 1988) includes
841 multiple cores each with many different samples covering the LGM period.

842

843 This comparison shows that our MAT reconstructions are very similar to the INV method,
844 but not as cold or dry as the ANN method. This has two main implications. The first is that
845 our reconstructions indicate greater agreement with the results of climate model simulations
846 since climate models indicate temperatures closer to the INV reconstructions (Latombe et al.,
847 2018) than the ANN reconstructions (Jost et al., 2005; Kageyama et al., 2006). The difference
848 between our MAT and earlier ANN reconstructions is likely the result of the modern
849 calibration datasets used, since the ANN reconstruction was based on a considerably smaller
850 number of samples taken mainly from the cold dry steppes of Kazakstan and Mongolia.

851
852 The second implication is that the MAT method may not be significantly impacted by the
853 effects of lower CO₂ (Cowling and Sykes, 1999; Prentice and Harrison, 2009; Williams et
854 al., 2000) or indeed insolation changes during the LGM, since the MAT results are similar to
855 those based on the INV method which specifically takes account of these non-climatic factors
856 (Wu et al., 2007). This would suggest that MAT could also work well for pollen-based
857 climate reconstructions on longer glacial-interglacial timescales where insolation and CO₂
858 vary significantly from their modern values. This is consistent with the findings of Pini et al.
859 (2021) who applied a correction algorithm developed by Prentice et al. (2017) and Cleator et
860 al. (2020) to a MAT reconstruction of mean annual precipitation at Lake Fimon in Northern
861 Italy. This shows a very small correction of 0mm to 30mm for samples across the LGM time-
862 window, which indicates that CO₂ is not a very significant factor in influencing this type of
863 reconstruction, at least compared to the overall uncertainties (+/- 200mm) of the
864 reconstruction itself. The uncertainties associated with the correction algorithm are not
865 discussed, but given that inputs include estimates of both LGM temperature and cloud cover,
866 it seems likely that these could be significant. Importantly, both Pini et al (2021) and Cleator
867 et al (2020) specifically exclude the necessity of applying a correction algorithm to
868 temperature reconstructions, since they consider only hydrological variables to be affected by
869 changes in atmospheric CO₂.

870

871

872 **4.2.2 Comparison with climate reconstructions based on other proxies**

873

874 **4.2.2.1 Temperature**

875

876 Proxies that are not based on plants should remain unaffected by the CO₂ problem during the
877 LGM, and provide an alternative basis for evaluating pollen-based reconstructions. Samartin
878 et al. (2016) reconstructed LGM summer temperatures based on chironomid remains from
879 Lago della Costa (site #34) in Northern Italy. They also undertook pollen analysis on the
880 same samples down the core, allowing us to make a sample-by-sample comparison between
881 the chironomid temperature record and our MAT reconstruction (Fig. 10). Our pollen-climate
882 reconstruction is for JJA mean temperature, while the chironomid reconstruction is for July
883 mean temperature, with the anomalies based on the modern equivalent JJA and July mean
884 temperatures respectively. The average anomaly values for all 8 samples reconstructed by the
885 pollen-climate MAT are $-10.2 \pm 3.5^{\circ}\text{C}$, and for the chironomids $-9.5 \pm 3.0^{\circ}\text{C}$. This indicates
886 that pollen and chironomid average summer temperature reconstructions are very similar on
887 average, taking into account the overlapping uncertainties, while also showing a strong
888 similarity on a sample-by-sample basis throughout the time-series.

889

890 Other reconstructions based on other proxies provide a basis for more general regional
891 comparisons (Figure A4, A5). We reconstruct both summer and winter temperatures and
892 show that cooling in winter was greater than in summer at most sites, associated with an

893 increase in continentality (increased temperature difference between summer and winter). A
894 similar seasonal pattern of temperature change has also been shown in other studies that
895 reconstruct both summer and winter LGM temperatures, including Prud'homme et al. (2016)
896 using $\delta^{18}\text{O}$ analysis of earthworm calcite granules at Nussloch near the French-German
897 border, Bañuls-Cardona et al. (2014) using faunal remains of small mammals at 4 locations in
898 western Spain, and Ferguson et al. (2011) who examined seasonal temperature change using
899 $\delta^{18}\text{O}$ and Mg/Ca analysis of limpet shells at Gibraltar in southern Spain. The increase in
900 continentality at Nussloch (Prud'homme et al., 2016) was reconstructed at between 11.6 to
901 15.6 °C, comparable at the lower end with nearby pollen sites [La Grotte Walou site #28]
902 10.4 ± 5.8 °C and [Bergsee site #29] 7.9 ± 5.7 °C. The faunal sites in western Spain studied
903 by Bañuls-Cardona et al. (2014) gave much reduced increases in continentality, but
904 nevertheless similar to nearby pollen sites. For instance at Valdavara 5.1 °C [MD99-2331 site
905 #3] 5.2 ± 3.1 °C, El Miron 1.2 °C [Tourbiere de l'Estarres site #19] 5.1 ± 6.2 °C, El Portalon
906 0.9C [Torrecilla de Valmadrid site #16] 2.8 ± 1.8 °C and Cueva de Maltrvieso 6.1C [SU81-18
907 site #2] 4.8 ± 3.4 °C. Further south at Gibraltar the limpet-based study of Ferguson et al.
908 (2011) also shows a relatively small increase of 2 °C. The nearest pollen site [Gorham Cave
909 site #5] however shows a larger increase of 4.7 ± 2.3 °C, although differences could be
910 expected given the different temporal resolution of annual laminae on mollusk shells
911 compared to pollen assemblages that reflecting much slower changes in trees and other long-
912 lived flora.

913

914 Summer temperatures were warm enough during the LGM over the Alpine areas that Swiss
915 lakes were largely ice free in summer, while glacier ELA's around the time of the LGM
916 suggest summers were -6.5 to -7.7 °C cooler compared to the LIA (Heiri et al., 2014). This
917 cooling was similar to that found at Nussloch some 200km north of the Swiss border by
918 Prud'homme et al. (2016), who reconstructed anomalies of -6 to -8 ± 4 °C from $\delta^{18}\text{O}$
919 analysis of earthworm calcite granules (representing warm season May-September
920 temperatures). Slightly less cooling was found close by at the nearby site of Achenheim
921 where analysis of Mollusc assemblages gave summer (August) cooling estimates of -3.5 to -
922 6.5 °C based on MAT (Rousseau, 1991), and -5.5 to -9.5 °C based on the Mutual Climatic
923 Range method (Moine et al., 2002). These reconstructions appear somewhat cooler than
924 nearby pollen sites [La Grotte Walou site #28] -1.4 ± 3.6 °C and [Bergsee site #29] -2.7 ± 5.1
925 °C, although comparable with the pollen site [Pilsensee site #32] -7.3 ± 5.0 °C 200 km further
926 east. Similar differences also occur at the site of Les Echets on the western edge of the Alps
927 where a diatom based reconstruction of summer (July) temperatures (Ampel et al., 2010)
928 indicated a greater cooling (-10.5 to -11.5 °C) than our pollen reconstruction [Les Echets G
929 site #27] (-4 ± 2.7 °C). However, the authors caution that the results were based on poor
930 analogues and rare taxa, as well as a small training set of only 90 lakes in Switzerland.

931

932 South of the Alps, other proxies show the opposite relationship with the pollen
933 reconstructions. For instance, at Lago della Costa in the Po valley, a summer (July)
934 temperature chironomid reconstruction by Samartin et al. (2016) is around 1-2 °C less cool
935 than the pollen reconstruction (JJA) for the same site [Lago della Costa site #34] $-11.4 \pm$
936 2.7 °C, although both reconstructions fall within their respective uncertainty ranges (Figure 8).
937 In the Pindus Mountains in Greece, Hughes et al. (2006) estimated LGM summer
938 temperature anomalies of - 7 °C based on glacier modelling, which is comparable with that
939 reconstructed at the nearest pollen site [Ioannina site #51] -7.7 ± 2.8 °C. In Spain the analysis
940 of small mammal remains by Bañuls-Cardona et al. (2014) shows similarly less cooling in
941 summer or even warmer than present positive anomalies compared to the nearest pollen sites,
942 such as Valdavara 1.4 °C [MD99-2331 site #3] -2.3 ± 2.8 °C, El Miron -2.3 °C [Tourbiere de

943 l'Estarres site #19] -5.7 ± 5.4 °C, El Portalon 0.8 °C [Torrecilla de Valmadrid site #16] $-2.6 \pm$
944 1.1 °C and Cueva de Maltrvieso -1.1 C [SU81-18 site #2] -10.4 ± 2.8 °C. Further south at
945 Gibraltar, the limpet-based study of Ferguson et al. (2012) suggests an anomaly of around -7
946 °C, which is a greater cooling than the pollen reconstruction from this location [Gorham Cave
947 site #5] -1.3 ± 2.2 °C, although comparable with other pollen sites slightly further east.
948

949 Winter temperature reconstructions from non-pollen proxies show a similar pattern in relation
950 to pollen reconstructions as for summer temperatures. North of the Alps at Achenheim,
951 Prud'homme et al. (2016) use $\delta^{18}O$ on earthworm remains to reconstruct particularly cold
952 winter anomalies of -17.6 to -23.6 °C compared to nearby pollen sites [La Grotte Walou site
953 #28] -11.8 ± 8.0 °C and [Bergsee site #29] -10.6 ± 6.3 °C. South of the Alps in Spain, the
954 analysis by Bañuls-Cardona et al (2014) based on the remains of small mammals shows less
955 cooling in winter compared to the nearest pollen sites, in particular Valdavara -3.7 °C
956 [MD99-2331 site #3] -7.5 ± 3.4 °C, El Miron -3.5 °C [Tourbiere de l'Estarres site #19] -10.8
957 ± 7.0 °C, El Portalon -0.1 °C [Torrecilla de Valmadrid #16] -5.4 ± 2.5 °C and Cueva de
958 Maltrvieso -7.2 C [SU81-18 site #2] -15.2 ± 4.0 °C. And again, in southern Spain at Gibraltar,
959 analysis of limpet shells by Ferguson et al (2011) suggests winter cooling of around -9 °C
960 while the pollen reconstruction suggests [Gorham Cave site #5] -6.0 ± 2.5 °C, although sites
961 further east indicate cooler conditions.
962

963 A number of additional proxies have also been used to reconstruct LGM mean annual
964 temperature. Heyman et al. (2013) applied glacier mass balance modelling at sites located in
965 the smaller mountain regions north of the Alps. These are generally slightly cooler than our
966 pollen-based reconstructions at sites close to the Vosge Mountains -12.7 ± 2.0 °C and Black
967 Forest -11.4 ± 2.3 °C [Bergsee site #29] -8.2 ± 3.3 °C, Bavarian Forest -10.7 ± 2.2 [Pilsensee
968 site #32] -9.2 ± 1.2 °C and Giant Mountains -8.5 ± 1.8 [Kersdorf-Briesen site #46] -7.3 ± 0.3
969 °C. These values obtained by Heyman et al. (2013) are warmer than Pud'homme et al. (2016)
970 who estimated annual mean temperature anomalies of -15.1 to -19.1 °C based on $\delta^{18}O$ of
971 earthworm calcite at the Nussloch site just north of the Vosge and Black Forest. The annual
972 temperatures reconstructed by Heyman et al. (2013) are also around 2C warmer than Allen et
973 al. (2008) who applied a similar, although simpler method to over 29 different mountainous
974 regions across Europe that had been glaciated during the LGM. Since glacier mass balance is
975 a function of both snowfall and temperature, these estimated temperatures vary according to
976 estimated changes in precipitation. For instance, mean annual temperature estimates by Allen
977 et al. (2008a) are much cooler than reconstructed by pollen, with an average anomaly of -13.2
978 °C for the 29 sites assuming a 40% reduction in precipitation, but this is reduced to -11.8 °C
979 assuming the same precipitation as modern. This compares with -7.2 °C for our 63 pollen
980 sites. The glacier mass balance modelling by Allen et al. (2008a) assumes a seasonal
981 distribution of precipitation that is similar to the present day, and does not consider increases
982 in winter precipitation or mean annual precipitation above present day levels. Both of these
983 are suggested by the pollen data in some regions, and both could explain glacier extent found
984 during the LGM based on less extreme temperature anomalies more comparable with the
985 pollen data.
986

987 To the east of the Alps in the Panonian basin, mean annual temperature anomaly estimates
988 have been made from noble gas measurements on groundwater ranging from -2 to -4 °C
989 (Stute and Deak, 1990) up to -9 °C (Varsányi et al., 2011). These are similar to estimates
990 ranging from -2 to -9 °C from oxygen isotope ratios from mammoth tooth enamel (Kovács et
991 al., 2012) and are comparable with nearby pollen sites [Feher Lake site #50] -8.2 ± 3.3 °C and
992 [Kokad site #52] -4.5 ± 2.3 °C. On a broader scale, Sanchi et al (2014) estimated LGM

993 cooling in the Danube and Dneiper basins based on Lipid biomarkers in a core from the
994 Black Sea and came up with similar mean annual temperature anomalies between -6 to -10
995 °C, which again are comparable with pollen sites from the region that range from
996 [Nagymohos site #48] -10.5 ± 4.1 °C to [Straldzha site #57] -4.3 ± 5.8 °C.

997
998 Further south and west, García-Amorena et al. (2007) reported mean annual temperature
999 anomalies of -2.0 to -11.3 °C at LGM sites along the Portuguese coast, based on an indicator
1000 species method using plant macrofossils. This is similar to the closest marine pollen sites off
1001 the coast, which recorded values of [MD95-2039 site #1] -10.5 ± 4.6 °C and [MD99-2331 site
1002 #3] -5.3 ± 2.9 °C. Meanwhile, in the far east of the study area, Zaarur et al. (2016) estimated a
1003 mean annual temperature anomaly of around -3 °C based on clumped isotope analysis of
1004 *Melanopsis* shells from LGM sediments in the Sea of Galilee. This limited cooling appears
1005 similar to the nearest pollen site [Lake Zeribar site #63] where we reconstruct a cooling of -
1006 2.2 ± 4.6 °C.

1007
1008 Reconstructions of LGM sea surface temperatures (SST's) provide yet another source of
1009 comparison with our terrestrial pollen-based reconstructions, although many of the physical
1010 processes controlling surface sea temperatures such as upwelling, surface mixing, surface
1011 currents, stratification and thermal inertia through the seasonal cycle, represent quite different
1012 processes to those controlling surface temperatures over land, particularly at the sub-regional
1013 scale. Nevertheless, the Atlantic coastal waters of Iberia and the waters throughout the
1014 Mediterranean Sea include many SST sites that lie in relative proximity to our terrestrial
1015 pollen-sites, allowing us to make a comparison at the largest scale. Within this area the
1016 MARGO database (MARGO Members, 2009) includes 13 Alkenone, 2 Mg/Ca and 41
1017 Foraminifera based SST records of mean annual temperature, with the Foraminifera records
1018 also providing an additional 41 winter (JFM) and summer (JAS) SST estimates. We compare
1019 the SST records with the 36 closest terrestrial pollen records which fall within a box of -11 to
1020 35 degrees longitude and 32 to 43 degrees latitude containing all of the SST records. A
1021 simple site average indicates a mean annual SST anomaly of -5.5 ± 1.0 °C which is relatively
1022 close to the value of -7.2 ± 3.4 °C obtained from the terrestrial pollen sites [sites #1-4, 5, 7-
1023 24, 25, 26, 30, 35-38, 41, 47, 51, 53, 56-59]. Interestingly the inter-site variance (standard
1024 deviation of the reconstructed temperatures across all sites) is almost identical for the two
1025 datasets, 2.57 °C for the SST sites and 2.63 °C for the pollen sites, despite representing very
1026 different environments, proxies and uncertainties. However, when we look at the seasonal
1027 temperature anomalies, we find very different results. Site averaged winter SST anomalies
1028 are -3.7 ± 1.1 °C compared to -9.3 ± 4.2 °C for winter temperatures from terrestrial pollen
1029 sites, while in summer the values are reversed, -7.0 ± 0.8 °C compared to -5.38 ± 3.3 °C
1030 respectively. This suggests that SST's experienced greater cooling in summer compared to
1031 winter, which is the opposite to that generally found in terrestrial seasonal temperature
1032 reconstructions throughout the region, although this is consistent with model simulations
1033 (Mikolajewicz, 2011).

1034 1035 **4.2.2.2 Precipitation**

1036
1037 Few proxies apart from pollen provide quantitative reconstructions of precipitation during the
1038 LGM. Glacier mass balance modelling includes assumptions about precipitation in order to
1039 derive temperatures (Allen et al., 2008a), but neither is independent of the other. Hughes et
1040 al. (2006) estimate from glacier modelling that mean annual precipitation during the LGM at
1041 sites in the Pindus mountains in Greece was around 2300 ± 200 mm, which they consider to
1042 be similar to the present day (>2000 mm). A small change in precipitation compared to

1043 modern values is also indicated by the nearest pollen site, which is around 47 km to the south
1044 [Ioannina #51], and indicates a mean annual precipitation anomaly of -152 ± 294 mm,
1045 representing just 15% of the modern value. A larger reduction in mean annual precipitation of
1046 -45% (maximum) is reconstructed by García-Amorena et al. (2007) based on plant
1047 macrofossil remains from sites on the Portuguese coast. In comparison, the closest pollen
1048 sites record values which are a little lower, ranging from [MD95-2039 site #1] -22% to
1049 [MD99-2331 site #3] -34%. Further north in south-west Germany, Prud'homme et al. (2018)
1050 reconstructed mean annual precipitation from the delta ^{13}C of earthworm calcite granules at
1051 Fussloch. They estimate a field site average of 333 (159-574) mm/yr at the LGM, which
1052 represents an anomaly of -503 mm/yr (-60%) relative to the modern precipitation of 836
1053 mm/yr. This is comparable with the closest pollen site [Bergsee #29] with an anomaly of -
1054 540 mm/yr.

1055
1056 As with glaciers, lake levels reflect changes in moisture balance that includes the effects of
1057 both temperature (via evapotranspiration) and precipitation, rather than just precipitation.
1058 They also represent semi-quantitative data at best, with changes often described relative to
1059 the modern or other baseline. There are few lake level records available north of the Alps, but
1060 to the south, many records indicate high lake levels in areas such as Spain (Lacey et al., 2016;
1061 Moreno et al., 2012; Vegas et al., 2010), Italy (Belis et al., 1999; Giraudi, 2017), Greece and
1062 Turkey (Harrison et al., 1996; Reimer et al., 2009) and the Middle East (Kolodny et al., 2005;
1063 Lev et al., 2019). These lake records are also supported by evidence of higher river levels in
1064 Morocco (El Amrani et al., 2008). The cause of the higher lake levels has been the subject of
1065 some debate, since many pollen records (and especially early biome reconstructions) show
1066 steppe vegetation that would suggest aridity that appears incompatible with higher lake
1067 levels. Prentice et al. (1992) proposed that the co-existence of steppe vegetation and high lake
1068 levels could be possible if precipitation increased outside of the summer growing season,
1069 while summers themselves were drier and cooler with decreased evaporation. However, the
1070 results of our analysis tend to indicate the opposite in regions with higher lake levels, with
1071 increased summer rainfall and decreased winter rainfall. In addition, the increase in summer
1072 precipitation was enough to compensate for the decrease in winter rainfall, leading to an
1073 overall increase in mean annual precipitation at many pollen sites in Spain and Greece for
1074 instance. This together with depressed temperatures and consequently decreased evaporation
1075 could explain the higher lake levels, whilst also limiting the growth of trees as a result of
1076 cooler temperatures and prolonged aridity outside of the summer season. Davis & Stevenson
1077 (2007) also note a differential hydrological response between summer and winter rainfall in
1078 the Mediterranean during the Holocene that may also provide an explanation. In this case
1079 sporadic summer storms may result in high rates of runoff that may fill run-off fed lakes, but
1080 low rates of soil moisture recharge that fails to benefit vegetation in the same way winter
1081 rainfall does.

1082
1083 Overall, we reconstruct only a small reduction in precipitation during the LGM of around
1084 91mm (13%) averaged over all sites, which is less than the ~200mm reduction based on the
1085 sites in the pollen-climate compilation used by PMIP (Bartlein et al., 2011). Since our
1086 precipitation reconstruction on average matches that of the INV reconstruction by Wu et al
1087 (2007), we can attribute much of the difference to the greater aridity shown in the ANN
1088 reconstruction by Peyron et al and Jost et al (2005) (see figure 9). As with temperature, this is
1089 probably a reflection of the modern training set used in the ANN reconstruction which is
1090 much smaller than our training set and is largely taken from the arid steppes of Kazakhstan
1091 and Mongolia. However, it is also important to recognize the significant spatial variability in
1092 precipitation, which means that a simple average of different sets of sites from different

1093 regions may not accurately reflect the change in LGM precipitation at the European scale.
1094 Nevertheless, one of the most consistent signals in our dataset is for an increase in summer
1095 precipitation over many areas of Southern Europe and the Mediterranean. This is also found
1096 in climate models, where it has been attributed to an increase in convection-driven
1097 precipitation, although the amount of precipitation generated by this mechanism varies
1098 significantly between models (Beghin et al., 2016). It may seem counter-intuitive to see an
1099 increase in reconstructed precipitation in the same regions where we also find a
1100 preponderance of steppe or xerophytic biomes and taxa, including *Artemisia* and
1101 *Chenopodiaceae*. This is attributable to the fact that climate can change quite markedly with
1102 necessarily invoking a major change in vegetation, and especially the pollen biome. For
1103 instance, a semi-arid climate ranges from 250-500mm rainfall a year, so we could expect a
1104 semi-arid vegetation to be dominant even if the rainfall increases 250mm (100%).
1105

1106 A more consistent response in models is for an increase in winter precipitation across
1107 Southern Europe and the Mediterranean related to a stronger and more southerly displaced jet
1108 stream, with winter precipitation also accounting for much of the change in mean annual
1109 precipitation (Beghin et al., 2016). Our reconstruction of winter precipitation however shows
1110 less support for this scenario with a more general decrease in winter precipitation apart from
1111 southern and eastern Iberia, and with summer precipitation generally more important in those
1112 sites that show an overall increase in mean annual precipitation. This may not necessarily
1113 contradict the models in terms of the strength and position of the winter jet stream, but may
1114 instead indicate that models over-estimate the amount of moisture being carried westward
1115 from the cold North Atlantic along the storm track, especially across the far northern
1116 Mediterranean. The increase in winter precipitation across southern and eastern Iberia is
1117 however entirely consistent with a strengthened and more southerly jet stream, which also
1118 brings increased winter precipitation to the region today as a result of blocking over northern
1119 Europe/Atlantic and a negative NAO (Vicente-Serrano et al., 2011).
1120

1121 Other areas that show an increase in winter precipitation include pollen sites around the
1122 eastern end of the Alps. This is consistent with a recent study by Spötl et al (2021) who
1123 argued, on the basis of cryogenic carbonates preserved in a cave in Austria, that heavy winter
1124 (and autumn) precipitation was a significant factor in driving LGM glaciation in the region.
1125 The seasonally specific nature of this precipitation is also supported by the same pollen sites,
1126 which do not show any increase in summer precipitation at this time.
1127

1128 **5.0 Conclusions**

1129

1130 We have reconstructed the climate and vegetation cover across Europe, North Africa and the
1131 Middle East at the time of the LGM based on 63 pollen records. These records were selected
1132 using strict quality control criteria, with particular attention paid to dating control, which led
1133 to the exclusion of many records that have been used in previous studies. This fully
1134 documented dataset represents the most chronologically precise and spatially resolved view
1135 of LGM climate and vegetation during the PMIP benchmarking time window at 21 ± 2 ka.
1136 Nevertheless, it is important to recognize that there are still significant spatial gaps in pollen
1137 sites especially north of the Alps, the Balkans, Turkey and the Middle East, and we continue
1138 to have only a partial understanding of the LGM over these areas.
1139

1140 One of the key questions concerning the vegetation landscape of the LGM in Europe has
1141 been the extent to which forest rather than steppe covered the continent, and to what extent
1142 temperate elements could be found north of the classical refugia areas of Southern Europe

1143 and the Mediterranean. Our results show that although steppe and tundra was extensive at the
1144 time of the LGM, areas of open forest also occurred in many regions, particularly (but not
1145 exclusively) in Iberia, northern Italy and Central Europe. These forest or woodland stands are
1146 likely to have been located in environmentally favourable areas, with good soils, elevated
1147 rainfall and shelter from cold, desiccating winds. In those areas where woodland existed,
1148 Boreal taxa generally dominated north and east of the Alps, while temperate and
1149 thermophilous (mainly drought adapted) taxa were generally confined to areas south of the
1150 Alps and around the Mediterranean. The temperate deciduous forests that compose the
1151 climax community in many areas of Europe today were displaced to the south and reduced to
1152 a partnership role with Boreal elements. Overall our new reconstruction indicates greater
1153 agreement with model land cover simulations, but models still appear to over-estimate the
1154 amount of forest and woodland over areas such as France and the Benelux, Greece, Turkey
1155 and the Far East.

1156
1157 Another key question about the LGM concerns the ability of climate models to simulate the
1158 climate of this period and whether pollen-based climate reconstructions which show
1159 disagreement with models have been biased by the effects of low CO₂ on plant physiology.
1160 We find that our new pollen-climate reconstruction shows much closer agreement with
1161 climate models than previous reconstructions that did not take account of low CO₂ effects.
1162 We also find close agreement with previous reconstructions that did take account of CO₂
1163 effects. Since our MAT method itself does not specifically take account of low CO₂ effects,
1164 this would suggest that this problem is not a significant hindrance to MAT performance at the
1165 time of the LGM, at least not compared to other uncertainties. Instead, we suggest that the
1166 main factor in the performance of pollen-climate transfer functions that use modern analogue
1167 methods is the provision of a large enough modern pollen dataset with suitable LGM
1168 analogues.

1169
1170 This conclusion is supported by comparison with climate reconstructions based on other
1171 proxies. We found little difference between our MAT reconstruction and a Chironomid-based
1172 summer temperature record based on a downcore sample by sample comparison, as well as
1173 comparisons with records from a variety of other proxies at a regional scale. However, it is
1174 notable that some studies using glacier mass balance modelling methods indicate LGM
1175 temperatures that are much cooler than our pollen-based reconstruction. The reasons behind
1176 this are not clear, but our pollen-based results indicate higher than present precipitation in
1177 some areas that could potentially explain low elevation glacier ELA's without the need for
1178 such cold temperatures.

1179
1180 We also find that although our pollen-based reconstruction and those of SST's generally
1181 agree in terms of mean annual temperatures, SST's indicate greater cooling in summer
1182 compared to winter, while terrestrial records indicate greater cooling in winter compared to
1183 summer. These seasonal differences are also reproduced in climate models, and probably
1184 reflect the different processes driving seasonal temperature change in the terrestrial and
1185 marine domain.

1186
1187 Our reconstructions of precipitation show large spatial and seasonal variability, but generally
1188 indicate less overall aridity than previously suggested from smaller scale studies which
1189 sampled less of the spatial domain. We find that in some regions of Southern Europe
1190 precipitation may actually have been greater than present, especially in summer, but also in
1191 winter in southern and eastern Iberia and around the southern slopes of the Alps. This may
1192 have important implications in understanding the development of LGM glaciation, which

1193 may be less a function of temperature than previously supposed. This could also help better
1194 explain the observed asynchronous nature of glaciation even within relatively small regions
1195 such as Europe, as a result of more localized controls on ice sheet development such as
1196 precipitation.

1197
1198 We hope that this new continental-scale dataset of climate and vegetation reconstructions will
1199 provide an improved baseline for data-model comparisons and other studies that will allow us
1200 to better understand the complex LGM environment.

1201

1202

1203 **Code/Data availability**

1204

1205 All of the data shown in the figures together with the fossil and modern pollen datasets will
1206 be made available on pangaea.de once the review process has been completed and these
1207 datasets are therefore no longer subject to change.

1208

1209 **Author contribution**

1210

1211 BASD designed the study, undertook the analysis and wrote the manuscript. MF and ER
1212 designed and prepared the maps. JOK and AB reviewed the manuscript and provided
1213 additional input.

1214

1215 **Competing interests**

1216

1217 The authors declare that they have no conflict of interest.

1218

1219 **Acknowledgements**

1220

1221 This work was supported by a grant from the Fonds de Recherche du Québec Société et
1222 Culture (2019-SE3-254686) to AB. Data were obtained from the European Pollen Database
1223 (EPD), based within the Neotoma Paleoecology Database (<http://www.neotomadb.org>). The
1224 work of data contributors, data stewards, and the Neotoma and EPD community is gratefully
1225 acknowledged. We dedicate this paper in memory of Eric Grimm, whose tireless work for the
1226 EPD and Neotoma helped make this study possible.

1227

1228

1229

1230 **References**

1231

1232 ACER project members, Goñi, M. F. S., Desprat, S., Daniau, A. L., Bassinot, F. C., Polanco-
1233 Martínez, J. M., Harrison, S. P., Allen, J. R. M., Scott Anderson, R., Behling, H., Bonnefille,
1234 R., Burjachs, F., Carrión, J. S., Cheddadi, R., Clark, J. S., Combourieu-Nebout, N., Mustaphi,
1235 C. J. C., Debusk, G. H., Dupont, L. M., Finch, J. M., Fletcher, W. J., Giardini, M., González,
1236 C., Gosling, W. D., Grigg, L. D., Grimm, E. C., Hayashi, R., Helmens, K., Heusser, L. E.,
1237 Hill, T., Hope, G., Huntley, B., Igarashi, Y., Irino, T., Jacobs, B., Jiménez-Moreno, G.,
1238 Kawai, S., Peter Kershaw, A., Kumon, F., Lawson, I. T., Ledru, M. P., Lézine, A. M., Mei
1239 Liew, P., Magri, D., Marchant, R., Margari, V., Mayle, F. E., Merna Mckenzie, G., Moss, P.,
1240 Müller, S., Müller, U. C., Naughton, F., Newnham, R. M., Oba, T., Pérez-Obiol, R., Pini, R.,
1241 Ravazzi, C., Roucoux, K. H., Rucina, S. M., Scott, L., Takahara, H., Tzedakis, P. C., Urrego,
1242 D. H., Van Geel, B., Guido Valencia, B., Vandergoes, M. J., Vincens, A., Whitlock, C. L.,
1243 Willard, D. A. and Yamamoto, M.: The ACER pollen and charcoal database: A global
1244 resource to document vegetation and fire response to abrupt climate changes during the last
1245 glacial period, *Earth Syst. Sci. Data*, 9(2), 679–695, doi:10.5194/essd-9-679-2017, 2017.

1246

1247 Allen, J. R. M., Hickler, T., Singarayer, J. S., Sykes, M. T., Valdes, P. J. and Huntley, B.:
1248 Last glacial vegetation of northern Eurasia, *Quat. Sci. Rev.*, 29(19–20), 2604–2618,
1249 doi:10.1016/j.quascirev.2010.05.031, 2010.

1250

1251 Allen, R., Siegert, M. J. and Payne, A. J.: Reconstructing glacier-based climates of LGM
1252 Europe and Russia – Part 2 : A dataset of LGM precipitation / temperature relations derived
1253 from degree-day modelling of palaeo glaciers, , 249–263, 2008a.

1254

1255 Allen, R., Siegert, M. J. and Payne, A. J.: Reconstructing glacier-based climates of LGM
1256 Europe and Russia – Part 3 : Comparison with previous climate reconstructions, , (1999),
1257 265–280, 2008b.

1258

1259 Ampel, L., Bigler, C., Wohlfarth, B., Risberg, J., Lotter, A. F. and Veres, D.: Modest summer
1260 temperature variability during DO cycles in western Europe, *Quat. Sci. Rev.*, 29(11–12),
1261 1322–1327, doi:10.1016/j.quascirev.2010.03.002, 2010.

1262

1263 El Amrani, M., Macaire, J. J., Zarki, H., Bréhéret, J. G. and Fontugne, M.: Contrasted
1264 morphosedimentary activity of the lower Kert River (northeastern Morocco) during the Late
1265 Pleistocene and the Holocene. Possible impact of bioclimatic variations and human action,
1266 *Comptes Rendus - Geosci.*, 340(8), 533–542, doi:10.1016/j.crte.2008.05.004, 2008.

1267

1268 Anderson, P. M., Barnosky, C. W., Bartlein, P. J., Behling, P. J., Brubaker, L., Cushing, E. J.,
1269 Dodson, J., Dworetsky, B., Guetter, P. J., Harrison, S. P., Huntley, B., Kutzbach, J. E.,
1270 Markgraf, V., Marvel, R., McGlone, M. S., Mix, A., Moar, N. T., Morley, J., Perrott, R. A.,
1271 Peterson, G. M., Prell, W. L., Prentice, I. C., Ritchie, J. C., Roberts, N., Ruddiman, W. F.,
1272 Salinger, M. J., Spaulding, W. G., Street-Perrott, F. A., Thompson, R. S., Wang, P. K., Webb,
1273 T., Winkler, M. G. and Wright, H. E.: Climatic changes of the last 18,000 years:
1274 Observations and model simulations, *Science* (80-), 241(4869), 1043–1052,
1275 doi:10.1126/science.241.4869.1043, 1988.

1276

1277 Arpe, K., Leroy, S. A. G. and Mikolajewicz, U.: A comparison of climate simulations for the
1278 last glacial maximum with three different versions of the ECHAM model and implications
1279 for summer-green tree refugia, *Clim. Past*, 91–114, doi:10.5194/cp-7-91-2011, 2011.
1280

1281 Arslanov, K. A., Dolukhanov, P. M. and Gei, N. A.: Climate, Black Sea levels and human
1282 settlements in Caucasus Littoral 50,000-9000 BP, *Quat. Int.*, 167–168, 121–127,
1283 doi:10.1016/j.quaint.2007.02.013, 2007.
1284

1285 Bañuls-Cardona, S., López-García, J. M., Blain, H. A., Lozano-Fernández, I. and Cuenca-
1286 Bescós, G.: The end of the Last Glacial Maximum in the Iberian Peninsula characterized by
1287 the small-mammal assemblages, *J. Iber. Geol.*, 40(1), 19–27,
1288 doi:10.5209/rev_JIGE.2014.v40.n1.44085, 2014.
1289

1290 Bartlein, P. J., Harrison, S. P., Brewer, S., Connor, S., Davis, B. A. S., Gajewski, K., Guiot,
1291 J., Harrison-Prentice, T. I., Henderson, A., Peyron, O., Prentice, I. C., Scholze, M., Seppä, H.,
1292 Shuman, B., Sugita, S., Thompson, R. S., Viau, A. E., Williams, J. and Wu, H.: Pollen-based
1293 continental climate reconstructions at 6 and 21 ka: A global synthesis, *Clim. Dyn.*, 37(3),
1294 775–802, doi:10.1007/s00382-010-0904-1, 2011.
1295

1296 de Beaulieu, J.-L. and Reille, M.: Pollen analysis of a long upper Pleistocene continental
1297 sequence in a Velay maar (Massif Central, France), *Palaeogeogr. Palaeoclimatol. Palaeoecol.*,
1298 80(1), 35–48, 1990.
1299

1300 Beghin, P., Charbit, S., Kageyama, M., Combourieu-Nebout, N., Hatté, C., Dumas, C. and
1301 Peterschmitt, J. Y.: What drives LGM precipitation over the western Mediterranean? A study
1302 focused on the Iberian Peninsula and northern Morocco, *Clim. Dyn.*, 46(7–8), 2611–2631,
1303 doi:10.1007/s00382-015-2720-0, 2016.
1304

1305 Belis, C. A., Lami, A., Guilizzoni, P., Ariztegui, D. and Geiger, W.: The late Pleistocene
1306 ostracod record of the crater lake sediments from Lago di Albano (Central Italy): Changes in
1307 trophic status, water level and climate, *J. Paleolimnol.*, 21(2), 151–169,
1308 doi:10.1023/A:1008095805748, 1999.
1309

1310 Berto, C., López-García, J. M. and Luzi, E.: Changes in the Late Pleistocene small-mammal
1311 distribution in the Italian Peninsula, *Quat. Sci. Rev.*, 225,
1312 doi:10.1016/j.quascirev.2019.106019, 2019.
1313

1314 Bigelow, N.H., Brubaker, L.B., Edwards, M.E., Harrison, S.P., Prentice, I.C., Anderson,
1315 P.M., Andreev, A.A., Bartlein, P.J., Christiansen, T.R., Cramer, W., Kaplan, J.O., Lozhkin,
1316 A.V., Matveyeva, N.V., Murray, D.F., McGuire, A.D., Razzhivin, V.Y., Ritchie, J.C., Smith,
1317 B., Walker, D.A., Gajewski, K., Wolf, V., Holmqvist, B.H., Igarashi, Y., Kremenetskii, K.,
1318 Paus, A., Pisaric, M.F.J., Volkova, V.S.: Climate change and arctic ecosystems: 1. Vegetation
1319 changes north of 55 N between the last glacial maximum, mid-Holocene, and present. *J.*
1320 *Geophys. Res.* 108 (D19), 8170. doi.org/10.1029/2002JD002558, 2013.
1321

1322 Binney, H., Edwards, M., Macias-Fauria, M., Lozhkin, A., Anderson, P., Kaplan, J. O.,
1323 Andreev, A., Bezrukova, E., Blyakharchuk, T., Jankovska, V., Khazina, I., Krivonogov, S.,
1324 Kremenetski, K., Nield, J., Novenko, E., Ryabogina, N., Solovieva, N., Willis, K. and
1325 Zernitskaya, V.: Vegetation of Eurasia from the last glacial maximum to present: Key
1326 biogeographic patterns, *Quat. Sci. Rev.*, 157, 80–97, doi:10.1016/j.quascirev.2016.11.022,
2017.

1327
1328 Birks, H. J. B. and Willis, K. J.: Alpines, trees, and refugia in Europe, *Plant Ecol. Divers.*,
1329 1(2), 147–160, doi:10.1080/17550870802349146, 2008.
1330
1331 Bonatti, E.: Pollen sequence in the lake sediments. In: *Ianula: an account of the history and*
1332 *development of the Lago di Monterosi, Latium, Italy*, in *Trans. Am. phil. Soc.*, vol. 60, edited
1333 by G. E. Hutchinson, pp. 26–31., 1970.
1334
1335 Brewer, S., Guiot, J., Sánchez-Goñi, M. F. and Klotz, S.: The climate in Europe during the
1336 Eemian: a multi-method approach using pollen data, *Quat. Sci. Rev.*, 27(25–26), 2303–2315,
1337 doi:10.1016/j.quascirev.2008.08.029, 2008.
1338
1339 Brewer, S., Giesecke, T., Davis, B. A. S., Finsinger, W., Wolters, S., Binney, H., de
1340 Beaulieu, J. L., Fyfe, R., Gil-Romera, G., Köhl, N., Kuneš, P., Leydet, M. and Bradshaw, R.
1341 H.: Mapping Lateglacial and Holocene European pollen data: The maps, *J. Maps*, 13(2), 921–
1342 928, doi:10.1080/17445647.2016.1197613, 2017.
1343
1344 Camuera, J., Jiménez-Moreno, G., Ramos-Román, M. J., García-Alix, A., Toney, J. L.,
1345 Anderson, R. S., Jiménez-Espejo, F., Bright, J., Webster, C., Yanes, Y. and Carrión, J. S.:
1346 Vegetation and climate changes during the last two glacial-interglacial cycles in the western
1347 Mediterranean: A new long pollen record from Padul (southern Iberian Peninsula), *Quat. Sci.*
1348 *Rev.*, 205, 86–105, doi:10.1016/j.quascirev.2018.12.013, 2019.
1349
1350 Cao, X., Tian, F., Dallmeyer, A. and Herzschuh, U.: Northern Hemisphere biome changes
1351 (>30°N) since 40 cal ka BP and their driving factors inferred from model-data comparisons,
1352 *Quat. Sci. Rev.*, 220, 291–309, doi:10.1016/j.quascirev.2019.07.034, 2019.
1353
1354 Carrión, J. S.: Late quaternary pollen sequence from Carihuela Cave, southern Spain, *Rev.*
1355 *Palaeobot. Palynol.*, 71(1–4), doi:10.1016/0034-6667(92)90157-C, 1992.
1356
1357 Carrión, J. S.: Patterns and processes of Late Quaternary environmental change in a montane
1358 region of southwestern Europe, *Quat. Sci. Rev.*, 21, 2047–2066, 2002.
1359
1360 Carrión, J. S., Finlayson, C., Fernández, S., Finlayson, G., Allué, E., López-Sáez, J. A.,
1361 López-García, P., Gil-Romera, G., Bailey, G. and González-Sampériz, P.: A coastal reservoir
1362 of biodiversity for Upper Pleistocene human populations: palaeoecological investigations in
1363 Gorham’s Cave (Gibraltar) in the context of the Iberian Peninsula, *Quat. Sci. Rev.*, 27(23–
1364 24), 2118–2135, doi:10.1016/j.quascirev.2008.08.016, 2008.
1365
1366 Cheddadi, R., Yu, G., Guiot, J., Harrison, S. P. and Colin Prentice, I.: The climate of Europe
1367 6000 years ago, *Clim. Dyn.*, 13(1), 1–9, 1996.
1368
1369 Chevalier, M., Davis, B. A. S., Heiri, O., Seppä, H., Chase, B. M., Gajewski, K., Lacourse,
1370 T., Telford, R. J., Finsinger, W., Guiot, J., Köhl, N., Maezumi, S. Y., Tipton, J. R., Carter, V.
1371 A., Brussel, T., Phelps, L. N., Dawson, A., Zanon, M., Vallé, F., Nolan, C., Mauri, A., de
1372 Vernal, A., Izumi, K., Holmström, L., Marsicek, J., Goring, S., Sommer, P. S., Chaput, M.
1373 and Kupriyanov, D.: Pollen-based climate reconstruction techniques for late Quaternary
1374 studies, *Earth-Science Rev.*, 210, doi:10.1016/j.earscirev.2020.103384, 2020.
1375

1376 Cleator, S. F., Harrison, S. P., Nichols, N. K., Colin Prentice, I. and Roulstone, I.: A new
1377 multivariable benchmark for Last Glacial Maximum climate simulations, *Clim. Past*, 16(2),
1378 699–712, doi:10.5194/cp-16-699-2020, 2020.

1379
1380 COHMAP,: Climatic changes of the last 18,000 years: observations and model
1381 simulations. *Science*, 241, 1043-1052, 1988.

1382
1383 Collins, P. M., Davis, B. A. S. and Kaplan, J. O.: The mid-Holocene vegetation of the
1384 Mediterranean region and southern Europe, and comparison with the present day, *J.*
1385 *Biogeogr.*, 39(10), doi:10.1111/j.1365-2699.2012.02738.x, 2012.

1386
1387 Combourieu Nebout, N., Peyron, O., Dormoy, I., Desprat, S., Beaudouin, C., Kotthoff, U.
1388 and Marret, F.: Rapid climatic variability in the west Mediterranean during the last 25 000
1389 years from high resolution pollen data, *Clim. Past*, 5(3), 503–521, doi:10.5194/cp-5-503-
1390 2009, 2009.

1391
1392 Connor, S. E., Ross, S. A., Sobotkova, A., Herries, A. I. R., Mooney, S. D., Longford, C. and
1393 Iliev, I.: Environmental conditions in the SE Balkans since the Last Glacial Maximum and
1394 their influence on the spread of agriculture into Europe, *Quat. Sci. Rev.*, 68, 200–215,
1395 doi:10.1016/j.quascirev.2013.02.011, 2013.

1396
1397 Cowling, S. A. and Sykes, M. T.: Physiological significance of low atmospheric CO₂ for
1398 plant-climate interactions, *Quat. Res.*, 52(2), 237–242, doi:10.1006/qres.1999.2065, 1999.

1399
1400 Damblon, F.: L'enregistrement palynologique de la sequence pléistocène et holocène de la
1401 grotte Walou, in *La grotte Walou à Trooz (Belgique)*, edited by C. Draily, S. Pirson, and M.
1402 Toussaint, pp. 84–129, Service public de Wallonie (Etudes et Documents, Archéologie, 21).,
1403 2011.

1404
1405 Daniau, A.-L., Desprat, S., Aleman, J. C., Bremond, L., Davis, B., Fletcher, W., Marlon, J.
1406 R., Marquer, L., Montade, V., Morales-Molino, C., Naughton, F., Rius, D. and Urrego, D. H.:
1407 Terrestrial plant microfossils in palaeoenvironmental studies, pollen, microcharcoal and
1408 phytolith. Towards a comprehensive understanding of vegetation, fire and climate changes
1409 over the past one million years, *Rev. Micropaleontol.*, 63, doi:10.1016/j.revmic.2019.02.001,
1410 2019.

1411
1412 Davis, B. A. S. and Stevenson, A. C.: The 8.2 ka event and Early-Mid Holocene forests, fires
1413 and flooding in the Central Ebro Desert, NE Spain, *Quat. Sci. Rev.*, 26(13–14),
1414 doi:10.1016/j.quascirev.2007.04.007, 2007.

1415
1416 Davis, B. A. S., Brewer, S., Stevenson, A. C., Guiot, J., Allen, J., Almqvist-Jacobson, H.,
1417 Ammann, B., Andreev, A. A., Argant, J., Atanassova, J., Balwierz, Z., Barnosky, C. D.,
1418 Bartley, D. D., De Beaulieu, J. L., Beckett, S. C., Behre, K. E., Bennett, K. D., Berglund, B.
1419 E. B., Beug, H.-J., Bezusko, L., Binka, K., Birks, H. H., Birks, H. J. B., Björck, S.,
1420 Bliakhartchouk, T., Bogdel, I., Bonatti, E., Bottema, S., Bozilova, E. D. B., Bradshaw, R.,
1421 Brown, A. P., Brugiapaglia, E., Carrion, J., Chernavskaya, M., Clerc, J., Clet, M., Coûteaux,
1422 M., Craig, A. J., Cserny, T., Cwynar, L. C., Dambach, K., De Valk, E. J., Digerfeldt, G.,
1423 Diot, M. F., Eastwood, W., Elina, G., Filimonova, L., Filipovitch, L., Gaillard-Lemdhal, M.
1424 J., Gauthier, A., Göransson, H., Guenet, P., Gunova, V., Hall, V. A. H., Harmata, K., Hicks,
1425 S., Huckerby, E., Huntley, B., Huttunen, A., Hyvärinen, H., Ilves, E., Jacobson, G. L., Jahns,

1426 S., Jankovská, V., Jóhansen, J., Kabailiene, M., Kelly, M. G., Khomutova, V. I., Königsson,
 1427 L. K., Kremenetski, C., Kremenetskii, K. V., Krisai, I., Krisai, R., Kvavadze, E., Lamb, H.,
 1428 Lazarova, M. A., Litt, T., Lotter, A. F., Lowe, J. J., Magyari, E., Makohonienko, M.,
 1429 Mamakowa, K., Mangerud, J., Mariscal, B., Markgraf, V., McKeever, Mitchell, F. J. G.,
 1430 Munuera, M., Nicol-Pichard, S., Noryskiewicz, B., Odgaard, B. V., Panova, N. K.,
 1431 Pantaleon-Cano, J., Paus, A. A., Pavel, T., Peglar, S. M., Penalba, M. C., Pennington, W.,
 1432 Perez-Obiol, R., et al.: The temperature of Europe during the Holocene reconstructed from
 1433 pollen data, *Quat. Sci. Rev.*, 22(15–17), doi:10.1016/S0277-3791(03)00173-2, 2003.
 1434
 1435 Davis, B. A. S., Chevalier, M., Sommer, P., Carter, V. A., Finsinger, W., Mauri, A., Phelps,
 1436 L. N., Zanon, M., Abegglen, R., Åkesson, C. M., Alba-Sánchez, F., Scott Anderson, R.,
 1437 Antipina, T. G., Atanassova, J. R., Beer, R., Belyanina, N. I., Blyakharchuk, T. A., Borisova,
 1438 O. K., Bozilova, E., Bukreeva, G., Jane Bunting, M., Clò, E., Colombaroli, D., Combourieu-
 1439 Nebout, N., Desprat, S., Di Rita, F., Djamali, M., Edwards, K. J., Fall, P. L., Feurdean, A.,
 1440 Fletcher, W., Florenzano, A., Furlanetto, G., Gaceur, E., Galimov, A. T., Galka, M., García-
 1441 Moreiras, I., Giesecke, T., Grindean, R., Guido, M. A., Gvozdeva, I. G., Herzsuh, U.,
 1442 Hjelle, K. L., Ivanov, S., Jahns, S., Jankovska, V., Jiménez-Moreno, G., Karpińska-Kołaczek,
 1443 M., Kitaba, I., Kołaczek, P., Lapteva, E. G., Latałowa, M., Lebreton, V., Leroy, S., Leydet,
 1444 M., Lopatina, D. A., López-Sáez, J. A., Lotter, A. F., Magri, D., Marinova, E., Matthias, I.,
 1445 Mavridou, A., Mercuri, A. M., Mesa-Fernández, J. M., Mikishin, Y. A., Milecka, K.,
 1446 Montanari, C., Morales-Molino, C., Mrotzek, A., Sobrino, C. M., Naidina, O. D., Nakagawa,
 1447 T., Nielsen, A. B., Novenko, E. Y., Panajiotidis, S., Panova, N. K., Papadopoulou, M.,
 1448 Pardoe, H. S., Pędziszewska, A., Petrenko, T. I., Ramos-Román, M. J., Ravazzi, C., Rösch,
 1449 M., Ryabogina, N., Ruiz, S. S., Sakari Salonen, J., Sapelko, T. V., Schofield, J. E., Seppä, H.,
 1450 Shumilovskikh, L., Stivrins, N., Stojakowits, P., Svitavska, H. S., Święta-Musznicka, J.,
 1451 Tantau, I., Tinner, W., Tobolski, K., Tonkov, S., Tsakiridou, M., et al.: The Eurasian Modern
 1452 Pollen Database (EMPD), version 2, *Earth Syst. Sci. Data*, 12(4), 2423–2445,
 1453 doi:10.5194/essd-12-2423-2020, 2020.
 1454
 1455 Davis M.B.: On the theory of pollen analysis. *American Journal of Sciences*, 26, 897–912,
 1456 1963.
 1457
 1458 Demay, L., Julien, M.A., Anghelinu, M., Shydlovskiy, P.S., Koulakovska, L.V., P'ean, S.,
 1459 Stupak, D.V., Vasyliiev, P.M., Obřada, T., Wojtal, P., Belyaeva, V.I.: Study of human
 1460 behaviors during the Late Pleniglacial in the East European Plain through their relation to the
 1461 animal world. *Quat. Int.* <https://doi.org/10.1016/j.quaint.2020.10.047>, 2021.
 1462
 1463 Douada, J., Doudová, J., Drařnarová, A., Kuneř, P., Hadincová, V., Krak, K., Zákřavský, P.
 1464 and Mandák, B.: Migration patterns of subgenus *Alnus* in Europe since the last glacial
 1465 maximum: A systematic review, *PLoS One*, 9(2), doi:10.1371/journal.pone.0088709, 2014.
 1466
 1467 Duprat-Oualid, F., Rius, D., Bégeot, C., Magny, M., Millet, L., Wulf, S. and Appelt, O.:
 1468 Vegetation response to abrupt climate changes in Western Europe from 45 to 14.7k cal a BP:
 1469 the Bergsee lacustrine record (Black Forest, Germany), *J. Quat. Sci.*, 32(7), 1008–1021,
 1470 doi:10.1002/jqs.2972, 2017.
 1471
 1472 Dupre Ollivier, M.: *Palinología y paleoambiente- nuevos datos españoles referencias*,
 1473 Universidad de Valencia., 1988.
 1474

1475 Edwards, M. E., Anderson, P. M., Brubaker, L. B., Ager, T., Andreev, A. A., Bigelow, N. H.,
1476 Cwynar, L. C., Eisner, W. R., Harrison, S. P., Hu, F.-S., Jolly, D., Lozhkin, A. V.,
1477 MacDonald, G. M., Mock, C. J., Ritchie, J. C., Sher, A. V., Spear, R. W., Williams, J. & Yu,
1478 G.: Pollen-based biomes for Beringia 18,000, 6000 and 0 14C yr bp. *Journal of*
1479 *Biogeography*, **27**, 521– 554, doi: [10.1046/j.1365-2699.2000.00426.x](https://doi.org/10.1046/j.1365-2699.2000.00426.x), 2000.
1480
1481 Ehlers, J., Gibbard, P. L. and Hughes, P. D.: Quaternary Glaciations - Extent and Chronology
1482 A Closer Look, edited by J. Ehlers, P. L. Gibbard, and P. D. Hughes, Elsevier., 2011.
1483
1484 Elenga, H., Peyron, O., Bonnefille, R., Jolly, D., Cheddadi, R., Guiot, J., Andrieu, V.,
1485 Bottema, S., Buchet, G., De Beaulieu, J. L., Hamilton, A. C., Maley, J., Marchant, R., Perez-
1486 Obiol, R., Reille, M., Riollet, G., Scott, L., Straka, H., Taylor, D., Van Campo, E., Vincens,
1487 A., Laarif, F. and Jonson, H.: Pollen-based biome reconstruction for southern Europe and
1488 Africa 18,000 yr BP, *J. Biogeogr.*, **27**(3), 621–634, doi:10.1046/j.1365-2699.2000.00430.x,
1489 2000.
1490
1491 Ferguson, J. E., Henderson, G. M., Fa, D. A., Finlayson, J. C. and Charnley, N. R.: Increased
1492 seasonality in the Western Mediterranean during the last glacial from limpet shell
1493 geochemistry, *Earth Planet. Sci. Lett.*, **308**(3–4), 325–333, doi:10.1016/j.epsl.2011.05.054,
1494 2011.
1495
1496 Feurdean A, Bhagwat SA, Willis KJ, Birks HJB, Lischke H, Hickler T.: Tree migration-rates:
1497 narrowing the gap between inferred post-glacial rates and projected rates. *PLoS ONE* **8**:
1498 e71797, 2013.
1499
1500 Feurdean, A., Perşoiu, A., Tanţău, I., Stevens, T., Magyari, E. K., Onac, B. P., Marković, S.,
1501 Andrić, M., Connor, S., Fărcaş, S., Gałka, M., Gaudeny, T., Hoek, W., Kolaczek, P., Kuneš,
1502 P., Lamentowicz, M., Marinova, E., Michezyńska, D. J., Perşoiu, I., Płóciennik, M.,
1503 Słowiński, M., Stancikaite, M., Sumegi, P., Svensson, A., Tămaş, T., Timar, A., Tonkov, S.,
1504 Toth, M., Veski, S., Willis, K. J. and Zernitskaya, V.: Climate variability and associated
1505 vegetation response throughout Central and Eastern Europe (CEE) between 60 and 8ka, *Quat.*
1506 *Sci. Rev.*, **106**, 206–224, doi:10.1016/j.quascirev.2014.06.003, 2014.
1507
1508 Fick, S. E. and Hijmans, R. J.: WorldClim 2: new 1-km spatial resolution climate surfaces for
1509 global land areas, *Int. J. Climatol.*, **37**(12), 4302–4315, doi:10.1002/joc.5086, 2017.
1510
1511 Fletcher, W. J., Goni, M. F. S., Peyron, O. and Dormoy, I.: Abrupt climate changes of the last
1512 deglaciation detected in a Western Mediterranean forest record, *Clim. Past*, **6**(2), 245–264,
1513 doi:10.5194/cp-6-245-2010, 2010.
1514
1515 Gaillard, M. J., Sugita, S., Mazier, F., Trondman, A. K., Broström, A., Hickler, T., Kaplan, J.
1516 O., Kjellström, E., Kokfelt, U., Kuneš, P., Lemmen, C., Miller, P., Olofsson, J., Poska, A.,
1517 Rundgren, M., Smith, B., Strandberg, G., Fyfe, R., Nielsen, A. B., Alenius, T., Balakauskas,
1518 L., Barnekow, L., Birks, H. J. B., Bjune, A., Björkman, L., Giesecke, T., Hjelle, K., Kalnina,
1519 L., Kangur, M., Van Der Knaap, W. O., Koff, T., Lageras, P., Latałowa, M., Leydet, M.,
1520 Lechterbeck, J., Lindbladh, M., Odgaard, B., Peglar, S., Segerström, U., Von Stedingk, H.
1521 and Seppä, H.: Holocene land-cover reconstructions for studies on land cover-climate
1522 feedbacks, *Clim. Past*, **6**(4), 483–499, doi:10.5194/cp-6-483-2010, 2010.
1523

1524 García-Amorena, I., Gómez Manzaneque, F., Rubiales, J. M., Granja, H. M., Soares de
1525 Carvalho, G. and Morla, C.: The Late Quaternary coastal forests of western Iberia: A study of
1526 their macroremains, *Palaeogeogr. Palaeoclimatol. Palaeoecol.*, 254(3–4), 448–461,
1527 doi:10.1016/j.palaeo.2007.07.003, 2007.

1528
1529 Genov, I.: The Black Sea level from the Last Glacial Maximum to the present time, *Geol.*
1530 *Balc.*, 45(1–3), 3–19, 2016.

1531
1532 Giesecke, T.: Did thermophilous trees spread into central Europe during the Late Glacial?,
1533 *New Phytol.*, 212(1), 15–18, doi:10.1111/nph.14149, 2016.

1534
1535 Giesecke, T., Davis, B., Brewer, S., Finsinger, W., Wolters, S., Blaauw, M., de Beaulieu, J.-
1536 L., Binney, H., Fyfe, R. M., Gaillard, M.-J., Gil-Romera, G., van der Knaap, W. O., Kuneš,
1537 P., Köhl, N., van Leeuwen, J. F. N., Leydet, M., Lotter, A. F., Ortu, E., Semmler, M. and
1538 Bradshaw, R. H. W.: Towards mapping the late Quaternary vegetation change of Europe,
1539 *Veg. Hist. Archaeobot.*, 23(1), doi:10.1007/s00334-012-0390-y, 2014.

1540
1541 Geiger, R.: *The climate near the ground*. Cambridge: Blue Hill Met. Observ. Harvard
1542 University 1960

1543
1544 Giraudi, C.: Lake levels and climate for the last 30,000 years in the fucino area (Abruzzo-
1545 Central Italy) - A review, *Palaeogeogr. Palaeoclimatol. Palaeoecol.*, 70(1–3), 249–260,
1546 doi:10.1016/0031-0182(89)90094-1, 1989.

1547
1548 Giraudi, C.: Climate evolution and forcing during the last 40 ka from the oscillations in
1549 Apennine glaciers and high mountain lakes, Italy, *J. Quat. Sci.*, 32(8), 1085–1098,
1550 doi:10.1002/jqs.2985, 2017.

1551
1552 Guido, M. A., Molinari, C., Moneta, V., Branch, N., Black, S., Simmonds, M., Stastney, P.
1553 and Montanari, C.: Climate and vegetation dynamics of the Northern Apennines (Italy)
1554 during the Late Pleistocene and Holocene, *Quat. Sci. Rev.*, 231,
1555 doi:10.1016/j.quascirev.2020.106206, 2020.

1556 Hansen, M. C., Potapov, P. V., Moore, R., Hancher, M., Turubanova, S. A., Tyukavina, A.,
1557 Thau, D., Stehman, S. V., Goetz, S. J., Loveland, T. R., Kommareddy, A., Egorov, A., Chini,
1558 L., Justice, C. O. and Townshend, J. R. G.: High-resolution global maps of 21st-century
1559 forest cover change, *Science (80-.)*, 342(6160), 850–853, doi:10.1126/science.1244693,
1560 2013.

1561
1562 Grichuk, V. P.: Main types of vegetation (ecosystems) for the maximum cooling of the last
1563 glaciation. B. Frenzel, B. Pecs, A.A. Velichko (Eds.), *Atlas of Palaeoclimates and*
1564 *Palaeoenvironments of the Northern Hemisphere*, NQUA/Hungarian Academy of
1565 Sciences, Budapest, pp. 123-124, doi: [10.2307/1551555](https://doi.org/10.2307/1551555), 1992.

1566
1567 Guiot, J., Torre, F., Jolly, D., Peyron, O., Boreux, J.J., Cheddadi, R.: Inverse vegetation
1568 modeling by Monte Carlo sampling to reconstruct palaeoclimates under changed precipitation

1569 seasonality and CO2 conditions: application to glacial climate in Mediterranean region. *Ecol.*
1570 *Model.* 127, 119–140. doi: 10.1016/
1571 S0304-3800(99)00219-7, 2000.
1572
1573 Harrison, S. P., Yu, G. E. and Tarasov, P. E.: Late Quaternary Lake-Level Record from
1574 Northern Eurasia, *Quat. Res.*, 45(2), 138–159, doi:10.1006/qres.1996.0016, 1996.
1575
1576 Harrison, S. P., Bartlein, P. J., Brewer, S., Prentice, I. C., Boyd, M., Hessler, I., Holmgren,
1577 K., Izumi, K. and Willis, K.: Climate model benchmarking with glacial and mid-Holocene
1578 climates, *Clim. Dyn.*, 43(3–4), 671–688, doi:10.1007/s00382-013-1922-6, 2014.
1579
1580 Harrison, S. P., Bartlein, P. J., Izumi, K., Li, G., Annan, J., Hargreaves, J., Braconnot, P. and
1581 Kageyama, M.: Evaluation of CMIP5 palaeo-simulations to improve climate projections, *Nat.*
1582 *Clim. Chang.*, 5(8), 735–743, doi:10.1038/nclimate2649, 2015.
1583
1584 Heiri, O., Koinig, K. A., Spötl, C., Barrett, S., Brauer, A., Drescher-Schneider, R., Gaar, D.,
1585 Ivy-Ochs, S., Kerschner, H., Luetscher, M., Moran, A., Nicolussi, K., Preusser, F., Schmidt,
1586 R., Schoeneich, P., Schwörer, C., Sprafke, T., Terhorst, B. and Tinner, W.: Palaeoclimate
1587 records 60–8 ka in the Austrian and Swiss Alps and their forelands, *Quat. Sci. Rev.*, 106,
1588 186–205, doi:10.1016/j.quascirev.2014.05.021, 2014.
1589
1590 Heyman, B. M., Heyman, J., Fickert, T., Harbor, J. M. and Forest, B.: Paleo-climate of the
1591 central European uplands during the last glacial maximum based on glacier mass-balance
1592 modeling Bavarian Forest Republic, *Quat. Res.*, 79(1), 49–54,
1593 doi:10.1016/j.yqres.2012.09.005, 2013.
1594
1595 Hughes, A. L. C., Gyllencreutz, R., Lohne, Ø. S., Mangerud, J. and Svendsen, J. I.: The last
1596 Eurasian ice sheets - a chronological database and time-slice reconstruction, *DATED-1,*
1597 *Boreas*, 45(1), 1–45, doi:10.1111/bor.12142, 2016.
1598
1599 Hughes, P. D. and Gibbard, P. L.: A stratigraphical basis for the Last Glacial Maximum
1600 (LGM), *Quat. Int.*, 383(June 2014), 174–185, doi:10.1016/j.quaint.2014.06.006, 2015.
1601
1602 Hughes, P. D., Woodward, J. C. and Gibbard, P. L.: Late Pleistocene glaciers and climate in
1603 the Mediterranean, *Glob. Planet. Change*, 50(1–2), 83–98,
1604 doi:10.1016/j.gloplacha.2005.07.005, 2006.
1605 Huntley, B.: Dissimilarity mapping between fossil and contemporary pollen spectra in
1606 Europe for the past 13,000 years, *Quat. Res.*, 33(3), 360–376, doi:10.1016/0033-
1607 5894(90)90062-P, 1990.
1608
1609 Huntley B.: Dissimilarity mapping between fossil and contemporary pollen spectra in Europe
1610 for the past 13,000 years. *Quaternary Research* 33:360–376, 1990.
1611
1612 Huntley, B. and Allen, J. R. M.: Glacial environments III. Palaeovegetation patterns in late
1613 glacial Europe, in Neanderthals and modern humans in the European landscape during the
1614 last glaciation, edited by T. H. Van Andel and H. C. Davies, pp. 79–102, McDonald Institute
1615 for Archaeological Research, Cambridge., 2003.
1616

- 1617 Huntley, B. and Birks, H. J. B.: An Atlas of Past and Present Pollen Maps for Europe: 0–
1618 13,000 B.P. years ago, Cambridge University Press, Cambridge., 1983.
1619
- 1620 Jalut, G., Andrieu, V., Delibrias, G., Fontaugne, M. and Pages, P.: Palaeoenvironment of the
1621 valley of Ossau (Western French Pyrenees) during the last 27 000 year, *Pollen et Spores*,
1622 30(3–4), 357–393, 1988.
1623
- 1624 Jalut, G., Marti, J. M., Fontugne, M., Delibrias, G., Vilaplana, J. M. and Julia, R.: Glacial to
1625 interglacial vegetation changes in the northern and southern Pyrénées: Deglaciation,
1626 vegetation cover and chronology, *Quat. Sci. Rev.*, 11(4), 449–480, doi:10.1016/0277-
1627 3791(92)90027-6, 1992.
1628
- 1629 Jankovska, V.: Vegetation cover in West Carpathians during the Last Glacial period -
1630 analogy of present day siberian forest-tundra nad taiga, *Palynol. Stratigr. geoecology*,
1631 (SEPTEMBER 2008), 282–289, 2008.
1632
- 1633 Janská, V., Jiménez-Alfaro, B., Chytrý, M., Divíšek, J., Anenkhonov, O., Korolyuk, A.,
1634 Lashchinskyi, N. and Culek, M.: Palaeodistribution modelling of European vegetation types
1635 at the Last Glacial Maximum using modern analogues from Siberia: Prospects and
1636 limitations, *Quat. Sci. Rev.*, 159, 103–115, doi:10.1016/j.quascirev.2017.01.011, 2017.
1637
- 1638 Jost, A., Lunt, D., Abe-Ouchi, A., Abe-Ouchi, A., Peyron, O., Valdes, P. J. and Ramstein, G.:
1639 High-resolution simulations of the last glacial maximum climate over Europe: A solution to
1640 discrepancies with continental palaeoclimatic reconstructions?, *Clim. Dyn.*, 24(6), 577–590,
1641 doi:10.1007/s00382-005-0009-4, 2005.
1642
- 1643 Juggins, S.: Quantitative reconstructions in palaeolimnology : new paradigm or sick
1644 science ?, *Quat. Sci. Rev.*, 64, 20–32, doi:10.1016/j.quascirev.2012.12.014, 2013.
1645
- 1646 Juggins, S.: Rioja: Analysis of Quaternary Science Data, [online] Available from:
1647 <https://cran.r-project.org/package=rioja>, 2020.
1648
- 1649 Juggins, S. and Birks, H. J. B.: Quantitative Environmental Reconstructions from Biological
1650 Data, in *Developments in Paleoenvironmental Research 5*, edited by H. J. B. Birks, pp. 431–
1651 494, Springer ScienceCBusiness Media B.V., 2012.
1652
- 1653 Juříčková, L., Horáčková, J. and Ložek, V.: Direct evidence of central European forest
1654 refugia during the last glacial period based on mollusc fossils, *Quat. Res. (United States)*,
1655 82(1), 222–228, doi:10.1016/j.yqres.2014.01.015, 2014.
1656
- 1657 Kageyama, M., Laine, A., Abe-Ouchi, A., Braconnot, P., Cortijo, E., Crucifix, M., de Vernal,
1658 A., Guiot, J., Hewitt, C. D., Kitoh, A., Kucera, M., Marti, O., Ohgaito, R., Otto-Bliesner, B.,
1659 Peltier, W. R., Rosell-Melé, A., Vettoretti, G., Weber, S. L. and Yu, Y.: Last Glacial
1660 Maximum temperatures over the North Atlantic, Europe and western Siberia: a comparison
1661 between PMIP models, MARGO sea-surface temperatures and pollen-based reconstructions,
1662 *Quat. Sci. Rev.*, 25(17–18), 2082–2102, doi:10.1016/j.quascirev.2006.02.010, 2006.
1663
- 1664 Kageyama, M., Harrison, S. P., Kapsch, M. L., Lofverstrom, M., Lora, J. M., Mikolajewicz,
1665 U., ... & Zhu, J. The PMIP4 Last Glacial Maximum experiments: preliminary results and
1666 comparison with the PMIP3 simulations. *Climate of the Past*, 17(3), 1065–1089, 2021.

1667
1668 Kaltenrieder, P., Belis, C. A., Hofstetter, S., Ammann, B., Ravazzi, C. and Tinner, W.:
1669 Environmental and climatic conditions at a potential Glacial refugial site of tree species near
1670 the Southern Alpine glaciers. New insights from multiproxy sedimentary studies at Lago
1671 della Costa (Euganean Hills, Northeastern Italy), *Quat. Sci. Rev.*, 28(25–26), 2647–2662,
1672 doi:10.1016/j.quascirev.2009.05.025, 2009.
1673
1674 Kaplan, J. O., Pfeiffer, M., Kolen, J. C. A. and Davis, B. A. S.: Large scale anthropogenic
1675 reduction of forest cover in last glacial maximum Europe, *PLoS One*, 11(11),
1676 doi:10.1371/journal.pone.0166726, 2016.
1677
1678 Kehrwald, N. M., McCoy, W. D., Thibeault, J., Burns, S. J. and Oches, E. A.: Paleoclimatic
1679 implications of the spatial patterns of modern and LGM European land-snail shell $\delta^{18}\text{O}$,
1680 *Quat. Res.*, 74(1), 166–176, doi:10.1016/j.yqres.2010.03.001, 2010.
1681
1682 Kelly, A., Charman, D. J. and Newnham, R. M.: A last glacial maximum pollen record from
1683 bodmin moor showing a possible cryptic Northern refugium in Southwest England, *J. Quat.*
1684 *Sci.*, 25(3), 296–308, doi:10.1002/jqs.1309, 2010.
1685
1686 Kolodny, Y., Stein, M. and Machlus, M.: Sea-rain-lake relation in the Last Glacial East
1687 Mediterranean revealed by $\delta^{18}\text{O}$ - $\delta^{13}\text{C}$ in Lake Lisan aragonites, *Geochim. Cosmochim.*
1688 *Acta*, 69(16), 4045–4060, doi:10.1016/j.gca.2004.11.022, 2005.
1689
1690 Kovács, J., Moravcová, M., Újvári, G. and Pintér, A. G.: Reconstructing the
1691 paleoenvironment of East Central Europe in the Late Pleistocene using the oxygen and
1692 carbon isotopic signal of tooth in large mammal remains, *Quat. Int.*, 276–277, 145–154,
1693 doi:10.1016/j.quaint.2012.04.009, 2012.
1694
1695 Krebs, P., Pezzatti, G. B., Beffa, G., Tinner, W. and Conedera, M.: Revising the sweet
1696 chestnut (*Castanea sativa* Mill.) refugia history of the last glacial period with extended pollen
1697 and macrofossil evidence, *Quat. Sci. Rev.*, 206, 111–128,
1698 doi:10.1016/j.quascirev.2019.01.002, 2019.
1699
1700 Kuneš, P., Pelánková, B., Chytrý, M., Jankovská, V., Pokorný, P. and Petr, L.: Interpretation
1701 of the last-glacial vegetation of eastern-central Europe using modern analogues from southern
1702 Siberia, *J. Biogeogr.*, 35(12), 2223–2236, doi:10.1111/j.1365-2699.2008.01974.x, 2008.
1703
1704 Küster, H.: Postglaziale Vegetationsgeschichte Südbayerns. Geobotanische Studien zur
1705 Prähistorischen Landschaftskunde, Akademie Verlag, Berlin., 1995.
1706
1707 Lacey, J. H., Leng, M. J., Höbig, N., Reed, J. M., Valero-Garcés, B. and Reicherter, K.:
1708 Western Mediterranean climate and environment since Marine Isotope Stage 3: a 50,000-year
1709 record from Lake Banyoles, Spain, *J. Paleolimnol.*, 55(2), 113–128, doi:10.1007/s10933-015-
1710 9868-9, 2016.
1711
1712 Latombe, G., Burke, A., Vrac, M., Levavasseur, G. and Dumas, C.: Comparison of spatial
1713 downscaling methods of general circulation model results to study climate variability during
1714 the Last Glacial Maximum, , 2563–2579, 2018.
1715

- 1716 Lefort J.P., Monnier J.L., Danukalova G.: Transport of Late Pleistocene loess particles by
 1717 katabatic winds during the lowstands of the English Channel. *Journal of the Geological*
 1718 *Society* 176: 1169–1181, doi: [10.1144/jgs2019-07](https://doi.org/10.1144/jgs2019-07), 2019.
- 1719
 1720 Lehmkuhl, F., Nett, J.J., Pöfner, S., Schulte, P., Sprafke, T., Jary, Z., Antoine, P., Wacha, L.,
 1721 Wolf, D., Zerboni, A., Hoesek, J., Marković, S.B., Obrecht, I., Sümege, P., Veres, D.,
 1722 Zeeden, C., Boemke, B., Schaubert, V., Viehweger, J., Hambach, U.: Loess landscapes of
 1723 Europe re-mapping, geomorphology, and zonal differentiation. *Earth Sci. Rev.* 215, 103496.
 1724 <https://doi.org/10.1016/j.earscirev.2020.103496>, 2021.
- 1725
 1726 Leroy, S. A. G. and Arpe, K.: Glacial refugia for summer-green trees in Europe and south-
 1727 west Asia as proposed by ECHAM3 time-slice atmospheric model simulations, *J. Biogeogr.*,
 1728 34(12), 2115–2128, doi:10.1111/j.1365-2699.2007.01754.x, 2007.
- 1729
 1730 Lev, L., Stein, M., Ito, E., Fruchter, N., Ben-Avraham, Z. and Almogi-Labin, A.:
 1731 Sedimentary, geochemical and hydrological history of Lake Kinneret during the past 28,000
 1732 years, *Quat. Sci. Rev.*, 209, 114–128, doi:10.1016/j.quascirev.2019.02.015, 2019.
- 1733
 1734 Lister, A. M. and Stuart, A. J.: The impact of climate change on large mammal distribution
 1735 and extinction: Evidence from the last glacial/interglacial transition, *Comptes Rendus -*
 1736 *Geosci.*, 340(9–10), 615–620, doi:10.1016/j.crte.2008.04.001, 2008.
- 1737
 1738 López-García, J. M. and Blain, H. A.: Quaternary small vertebrates: State of the art and new
 1739 insights, *Quat. Sci. Rev.*, 233, doi:10.1016/j.quascirev.2020.106242, 2020.
- 1740
 1741 Ludwig, P., Pinto, J. G., Raible, C. C. and Shao, Y.: Impacts of surface boundary conditions
 1742 on regional climate model simulations of European climate during the Last Glacial
 1743 Maximum, *Geophys. Res. Lett.*, 44(10), 5086–5095, doi:10.1002/2017GL073622, 2017.
- 1744
 1745
 1746 Luetscher, M., Boch, R., Sodemann, H., Spötl, C., Cheng, H., Edwards, R. L., Frisia, S., Hof,
 1747 F. and Müller, W.: North Atlantic storm track changes during the Last Glacial Maximum
 1748 recorded by Alpine speleothems, *Nat. Commun.*, 6, 27–32, doi:10.1038/ncomms7344, 2015.
- 1749
 1750 Magri, D.: Persistence of tree taxa in Europe and Quaternary climate changes, *Quat. Int.*,
 1751 219(1–2), 145–151, doi:10.1016/j.quaint.2009.10.032, 2010.
- 1752
 1753 Magri, D. and Parra, I.: Late Quaternary western Mediterranean pollen records and African
 1754 winds, *Earth Planet. Sci. Lett.*, 200(3–4), 401–408, doi:10.1016/S0012-821X(02)00619-2,
 1755 2002.
- 1756
 1757 Magri, D. and Sadori, L.: Late Pleistocene and Holocene pollen stratigraphy at Lago di Vico,
 1758 central Italy, *Veg. Hist. Archaeobot.*, 8(4), 247–260, doi:10.1007/BF01291777, 1999.
- 1759
 1760 Magyari, E., Jakab, G., Rudner, E. and Sümege, P.: Palynological and plant macrofossil data
 1761 on Late Pleistocene short-term climatic oscillations in NE-Hungary, *Acta Palaeobot. Suppl.*,
 1762 2(January), 491–502, 1999.
- 1763
 1764 Magyari, E. K., Kuneš, P., Jakab, G., Sümege, P., Pelánková, B., Schäbitz, F., Braun, M. and
 1765 Chytrý, M.: Late Pleniglacial vegetation in eastern-central Europe: Are there modern

1766 analogues in Siberia?, *Quat. Sci. Rev.*, 95, 60–79, doi:10.1016/j.quascirev.2014.04.020,
1767 2014a.

1768

1769 Magyari, E. K., Veres, D., Wennrich, V., Wagner, B., Braun, M., Jakab, G., Karátson, D.,
1770 Pál, Z., Ferenczy, G., St-Onge, G., Rethemeyer, J., Francois, J. P., von Reumont, F. and
1771 Schäbitz, F.: Vegetation and environmental responses to climate forcing during the Last
1772 Glacial Maximum and deglaciation in the East Carpathians: Attenuated response to
1773 maximum cooling and increased biomass burning, *Quat. Sci. Rev.*, 106, 278–298,
1774 doi:10.1016/j.quascirev.2014.09.015, 2014b.

1775

1776 Magyari, E. K., Pál, I., Vincze, I., Veres, D., Jakab, G., Braun, M., Szalai, Z., Szabó, Z. and
1777 Korponai, J.: Warm Younger Dryas summers and early late glacial spread of temperate
1778 deciduous trees in the Pannonian Basin during the last glacial termination (20-9 kyr cal BP),
1779 *Quat. Sci. Rev.*, 225, doi:10.1016/j.quascirev.2019.105980, 2019.

1780

1781 Margari, V., Gibbard, P. L., Bryant, C. L. and Tzedakis, P. C.: Character of vegetational and
1782 environmental changes in southern Europe during the last glacial period; evidence from
1783 Lesvos Island, Greece, *Quat. Sci. Rev.*, 28(13–14), 1317–1339,
1784 doi:10.1016/j.quascirev.2009.01.008, 2009.

1785

1786 Marsicek, J., Shuman, B. N., Bartlein, P. J., Shafer, S. L. and Brewer, S.: Reconciling
1787 divergent trends and millennial variations in Holocene temperatures, *Nature*, 554(7690), 92–
1788 96, doi:10.1038/nature25464, 2018.

1789

1790 Mauch Lenardić, J., Oros Sršen, A. and Radović, S.: Quaternary fauna of the Eastern Adriatic
1791 (Croatia) with the special review on the Late Pleistocene sites, *Quat. Int.*, 494, 130–151,
1792 doi:10.1016/j.quaint.2017.11.028, 2018.

1793

1794 Mauri, A., Davis, B. A. S., Collins, P. M. and Kaplan, J. O.: The influence of atmospheric
1795 circulation on the mid-Holocene climate of Europe: A data-model comparison, *Clim. Past*,
1796 10(5), 1925–1938, doi:10.5194/cp-10-1925-2014, 2014.

1797

1798 Mauri, A., Davis, B. A. S., Collins, P. M. and Kaplan, J. O.: The climate of Europe during the
1799 Holocene: A gridded pollen-based reconstruction and its multi-proxy evaluation, *Quat. Sci.*
1800 *Rev.*, 112, doi:10.1016/j.quascirev.2015.01.013, 2015.

1801

1802 MARGE Project Members.: Constraints on the magnitude and patterns of ocean cooling at
1803 the Last Glacial Maximum, , (January), 1–6, doi:10.1038/ngeo411, 2009.

1804

1805 Mikolajewicz, U.: Modeling mediterranean ocean climate of the last glacial maximum, *Clim.*
1806 *Past*, 7(1), 161–180, doi:10.5194/cp-7-161-2011, 2011.

1807

1808 Miola, A., Bondesan, A., Corain, L., Favaretto, S., Mozzi, P., Piovan, S. and Sostizzo, I.:
1809 Wetlands in the Venetian Po Plain (northeastern Italy) during the Last Glacial Maximum:
1810 Interplay between vegetation, hydrology and sedimentary environment, *Rev. Palaeobot.*
1811 *Palynol.*, 141(1–2), 53–81, doi:10.1016/j.revpalbo.2006.03.016, 2006.

1812

1813 Mix, A. C., Bard, E. and Schneider, R.: Environmental processes of the ice age: Land,
1814 oceans, glaciers (EPILOG), *Quat. Sci. Rev.*, 20(4), 627–657, doi:10.1016/S0277-
1815 3791(00)00145-1, 2001.

- 1816 Moine, O., Rousseau, D. D., Jolly, D. and Vianey-Liaud, M.: Paleoclimatic reconstruction
 1817 using mutual climatic range on terrestrial mollusks, *Quat. Res.*, 57(1), 162–172,
 1818 doi:10.1006/qres.2001.2286, 2002.
- 1819
- 1820 Monegato, G., Ravazzi, C., Donegana, M., Pini, R., Calderoni, G. and Wick, L.: Evidence of
 1821 a two-fold glacial advance during the last glacial maximum in the Tagliamento end moraine
 1822 system (eastern Alps), *Quat. Res.*, 68(2), 284–302, doi:10.1016/j.yqres.2007.07.002, 2007.
- 1823
- 1824 Monegato, G., Ravazzi, C., Culiberg, M., Pini, R., Bavec, M., Calderoni, G., Jež, J. and
 1825 Perego, R.: Sedimentary evolution and persistence of open forests between the south-eastern
 1826 Alpine fringe and the Northern Dinarides during the Last Glacial Maximum, *Palaeogeogr.*
 1827 *Palaeoclimatol. Palaeoecol.*, 436, 23–40, doi:10.1016/j.palaeo.2015.06.025, 2015.
- 1828
- 1829 Moreno, A., González-Sampériz, P., Morellón, M., Valero-Garcés, B. L. and Fletcher, W. J.:
 1830 Northern Iberian abrupt climate change dynamics during the last glacial cycle: A view from
 1831 lacustrine sediments, *Quat. Sci. Rev.*, 36, 139–153, doi:10.1016/j.quascirev.2010.06.031,
 1832 2012.
- 1833
- 1834 Nogues-Bravo D, Rodríguez-Sánchez F, Orsini L, de Boer E, Jansson R, Morlon, H.,
 1835 Fordham, D.A., Jackson, S.T.: Cracking the code of biodiversity responses to past climate
 1836 change. *Trends Ecol. Evol.* 33:765–76, 2018.
- 1837
- 1838
- 1839 Nolan, C., Overpeck, J. T., Allen, J. R. M., Anderson, P. M., Betancourt, J. L., Binney, H. A.,
 1840 Brewer, S., Bush, M. B., Chase, B. M., Cheddadi, R., Djamali, M., Dodson, J., Edwards, M.
 1841 E., Gosling, W. D., Haberle, S., Hotchkiss, S. C., Huntley, B., Ivory, S. J., Kershaw, A. P.,
 1842 Kim, S. H., Latorre, C., Leydet, M., Lézine, A. M., Liu, K. B., Liu, Y., Lozhkin, A. V.,
 1843 McGlone, M. S., Marchant, R. A., Momohara, A., Moreno, P. I., Müller, S., Otto-Bliesner, B.
 1844 L., Shen, C., Stevenson, J., Takahara, H., Tarasov, P. E., Tipton, J., Vincens, A., Weng, C.,
 1845 Xu, Q., Zheng, Z. and Jackson, S. T.: Past and future global transformation of terrestrial
 1846 ecosystems under climate change, *Science* (80-.), 361(6405), 920–923,
 1847 doi:10.1126/science.aan5360, 2018.
- 1848
- 1849 Normand, S., Treier, U. A. and Odgaard, B. V.: Tree refugia and slow forest development in
 1850 response to post - LGM warming in North - Eastern European Russia, , 2(4), 2–5, 2011.
- 1851
- 1852 Paganelli, A.: Evolution of vegetation and climate in the Veneto-Po Plain during the Late-
 1853 Glacial and Early Holocene using pollen-stratigraphical data, *Alp. Mediterr. Quat.*, 9(2),
 1854 581–589, 1996.
- 1855
- 1856 Peyron, O., Guiot, J., Cheddadi, R., Tarasov, P., Reille, M., De Beaulieu, J. L., Bottema, S.
 1857 and Andrieu, V.: Climatic Reconstruction in Europe for 18,000 YR B.P. from Pollen Data,
 1858 *Quat. Res.*, 49(2), 183–196, doi:10.1006/qres.1997.1961, 1998a.
- 1859
- 1860 Pons, A. and Reille, M.: The Holocene- and upper Pleistocene pollen record from Padul
 1861 (Granada, Spain): A new study, *Palaeogeogr. Palaeoclimatol. Palaeoecol.*, 66(3–4),
 1862 doi:10.1016/0031-0182(88)90202-7, 1988.
- 1863
- 1864 Potì, A., Kehl, M., Broich, M., Carrión Marco, Y., Hutterer, R., Jentke, T., Linstädter, J.,
 1865 López-Sáez, J. A., Mikdad, A., Morales, J., Pérez-Díaz, S., Portillo, M., Schmid, C., Vidal-

1866 Matutano, P. and Weniger, G. C.: Human occupation and environmental change in the
1867 western Maghreb during the Last Glacial Maximum (LGM) and the Late Glacial. New
1868 evidence from the Iberomaurusian site Ifri El Baroud (northeast Morocco), *Quat. Sci. Rev.*,
1869 220, 87–110, doi:10.1016/j.quascirev.2019.07.013, 2019.

1870
1871 Prentice, I. C., Cleator, S. F., Huang, Y. H., Harrison, S. P., and Roulstone, I.: Reconstructing
1872 ice-age palaeoclimates: Quantifying low-CO₂ effects on plants, *Global Planet. Change*, 149,
1873 166–176, <https://doi.org/10.1016/j.gloplacha.2016.12.012>, 2017.

1874
1875 Prentice, I. C. and Harrison, S. P.: Ecosystem effects of CO₂ concentration: Evidence from
1876 past climates, *Clim. Past*, 5(3), 297–307, doi:10.5194/cp-5-297-2009, 2009.

1877
1878 Prentice, I. C., Guiot, J. and Harrison, S. P.: Mediterranean vegetation, lake levels and
1879 palaeoclimate at the Last Glacial Maximum, *Nature*, 360(6405), 658–660,
1880 doi:10.1038/360658a0, 1992.

1881
1882 Prentice, I. C., Guiot, J., Huntley, B., Jolly, D. and Cheddadi, R.: Reconstructing biomes
1883 from palaeoecological data: A general method and its application to European pollen data at
1884 0 and 6 ka, *Clim. Dyn.*, 12(3), 185–194, doi:10.1007/BF00211617, 1996.

1885
1886 Prentice, I. C., Harrison, S. P. and Bartlein, P. J.: Global vegetation and terrestrial carbon
1887 cycle changes after the last ice age, *New Phytol.*, 189(4), 988–998, doi:10.1111/j.1469-
1888 8137.2010.03620.x, 2011.

1889
1890 Prud'homme, C., Lécuyer, C., Antoine, P., Moine, O., Hatté, C., Fourel, F., Martineau, F. and
1891 Rousseau, D. D.: Palaeotemperature reconstruction during the Last Glacial from $\delta^{18}\text{O}$ of
1892 earthworm calcite granules from Nussloch loess sequence, Germany, *Earth Planet. Sci. Lett.*,
1893 442, 13–20, doi:10.1016/j.epsl.2016.02.045, 2016.

1894
1895 Prud'homme, C., Lécuyer, C., Antoine, P., Hatté, C., Moine, O., Fourel, F., Amiot, R.,
1896 Martineau, F. and Rousseau, D. D.: $\delta^{13}\text{C}$ signal of earthworm calcite granules: A new proxy
1897 for palaeoprecipitation reconstructions during the Last Glacial in western Europe, *Quat. Sci.*
1898 *Rev.*, 179, 158–166, doi:10.1016/j.quascirev.2017.11.017, 2018.

1899
1900 Puzachenko, A. Y., Markova, A. K. and Pawłowska, K.: Evolution of Central European
1901 regional mammal assemblages between the late Middle Pleistocene and the Holocene (MIS7–
1902 MIS1), *Quat. Int.*, (November), doi:10.1016/j.quaint.2021.11.009, 2021.

1903
1904 Ramstein, G., Kageyama, M., Guiot, J. and Wu, H.: How cold was Europe at the Last Glacial
1905 Maximum ? A synthesis of the progress achieved since the first PMIP model-data
1906 comparison, , 331–339, 2007.

1907
1908 Reille, M. and Andrieu, V.: The late Pleistocene and Holocene in the Lourdes Basin, Western
1909 Pyrénées, France: new pollen analytical and chronological data, *Veg. Hist. Archaeobot.*, 4(1),
1910 1–21, doi:10.1007/BF00198611, 1995.

1911
1912 Reille, M. and de Beaulieu, J. L.: History of the Würm and Holocene vegetation in western
1913 velay (Massif Central, France): A comparison of pollen analysis from three corings at Lac du
1914 Bouchet, *Rev. Palaeobot. Palynol.*, 54(3–4), 233–248, doi:10.1016/0034-6667(88)90016-4,
1915 1988.

1916

1917 Reimer, A., Landmann, G. and Kempe, S.: Lake Van, Eastern Anatolia, hydrochemistry and
1918 history, *Aquat. Geochemistry*, 15(1–2), 195–222, doi:10.1007/s10498-008-9049-9, 2009.

1919

1920 Rousseau, D. D.: Climatic transfer function from quaternary molluscs in European loess
1921 deposits, *Quat. Res.*, 36(2), 195–209, doi:10.1016/0033-5894(91)90025-Z, 1991.

1922

1923 Royer, A., Montuire, S., Legendre, S., Discamps, E., Jeannet, M. and Lécuyer, C.:
1924 Investigating the influence of climate changes on rodent communities at a regional-scale
1925 (MIS 1-3, Southwestern France), *PLoS One*, 11(1), 1–25, doi:10.1371/journal.pone.0145600,
1926 2016.

1927

1928 Ruiz-Zapata, M. B., Vegas, J., Garcia-Cortes, A., Gil Garcia, M. J., Torres, T., Ortiz, J. E.
1929 and Perez-Gonzalez, A.: Vegetation evolution during the Last Maximum Glacial Period in
1930 FU-1 sequence (Fuentillejo Lacustrin Maar, Campo de Calatrava, Ciudad Real), *Polen*, 18,
1931 37–49, 2008.

1932

1933 Salonen, J., Sanchez Goñi, M.F., Renssen, H. and Plikk, A.: Contrasting northern and
1934 southern European winter climate trends during the Last Interglacial. *Geology* 49.
1935 10.1130/G49007.1. 2021

1936

1937 Salonen, J.S., Ilvonen, L., Seppä, H., Holmström, L., Telford, R.J., Gaidamavicius, A.,
1938 Stancikaite, M., Subetto, D. Comparing different calibration methods (WA/WA-PLS
1939 regression and Bayesian modelling) and different-sized calibration sets in pollen-based
1940 quantitative climate reconstruction. *The Holocene* 22, 413–424, 2012.

1941

1942 Samartin, S., Heiri, O., Kaltenrieder, P., Köhl, N. and Tinner, W.: Reconstruction of full
1943 glacial environments and summer temperatures from Lago della Costa, a refugial site in
1944 Northern Italy, *Quat. Sci. Rev.*, 143, 107–119, doi:10.1016/j.quascirev.2016.04.005, 2016.

1945

1946 Sánchez Goñi, M.F., Loutre, M.F., Crucifix, M., Peyron, O., Santos, L., Duprat, J., Malaizé,
1947 B., Turon, J.-L., and Peypouquet, J.-P.: Increasing vegetation and climate gradient in western
1948 Europe over the Last Glacial inception (122–110 ka): Data–model comparison. *Earth and
1949 Planetary Science Letters*, 231, 111–130, doi: 10.1016/j.epsl.2004.12.010, 2005.

1950

1951 Sanchez Goñi, M.F., Harrison, S.P.: Millennial-scale climate variability and vegetation
1952 changes during the Last Glacial: concepts and terminology. *Quaternary Science
1953 Reviews* 29, 2823–2827, doi: [10.1016/j.quascirev.2009.11.014](https://doi.org/10.1016/j.quascirev.2009.11.014), 2010.

1954

1955 Sanchi, L., Ménot, G. and Bard, E.: Insights into continental temperatures in the northwestern
1956 Black Sea area during the Last Glacial period using branched tetraether lipids, *Quat. Sci.
1957 Rev.*, 84, 98–108, doi:10.1016/j.quascirev.2013.11.013, 2014.

1958

1959 Satkūnas, J. and Grigienė, A.: Eemian-Weichselian palaeoenvironmental record from the
1960 Mickūnai glacial depression (Eastern Lithuania), *Geologija*, 54(2), 35–51,
1961 doi:10.6001/geologija.v54i2.2482, 2012.

1962 Schäfer, I. K., Bliedtner, M., Wolf, D., Faust, D. and Zech, R.: Evidence for humid
1963 conditions during the last glacial from leaf wax patterns in the loess-paleosol sequence El
1964 Paraíso, Central Spain, *Quat. Int.*, 407, 64–73, doi:10.1016/j.quaint.2016.01.061, 2016.

1965

- 1966 Scourse, J. D.: Late Pleistocene stratigraphy and palaeobotany of the Isles of Scilly, *Philos.*
1967 *Trans. - R. Soc. London, B*, 334(1271), 405–448, doi:10.1098/rstb.1991.0125, 1991.
- 1968
- 1969 Spötl, C., Koltai, G., Jarosch, A. H. and Cheng, H.: Increased autumn and winter
1970 precipitation during the Last Glacial Maximum in the European Alps, *Nat. Commun.*, 12(1),
1971 doi:10.1038/s41467-021-22090-7, 2021.
- 1972
- 1973 Stewart, J. R. and Lister, A. M.: Cryptic northern refugia and the origins of the modern biota,
1974 *Trends Ecol. Evol.*, 16(11), 608–613, doi:10.1016/S0169-5347(01)02338-2, 2001.
- 1975
- 1976 Stivrins, N., Soininen, J., Amon, L., Fontana, S. L., Gryguc, G., Heikkilä, M., Heiri, O.,
1977 Kisielienė, D., Reitalu, T., Stančikaitė, M., Veski, S. and Seppä, H.: Biotic turnover rates
1978 during the Pleistocene-Holocene transition, *Quat. Sci. Rev.*, 151, 100–110,
1979 doi:10.1016/j.quascirev.2016.09.008, 2016.
- 1980
- 1981 Strahl, J.: Zur Pollenstratigraphie des Weichselspätglazials von Berlin-Brandenburg [On the
1982 palynostratigraphy of the Late Weichselian in Berlin-Brandenburg], *Brand.*
1983 *Geowissenschaftliche Beiträge*, 12, 87–112, 2005.
- 1984
- 1985 Stute, M. and Deak, J.: Environmental isotope study (^{14}C , ^{13}C , ^{18}O , D, noble gases) on
1986 deep groundwater circulation systems in Hungary with reference to paleoclimate,
1987 *Radiocarbon*, 31(3), 902–918, doi:10.1017/s0033822200012522, 1990.
- 1988
- 1989 Svenning, J., Normand, S. and Kageyama, M.: Glacial refugia of temperate trees in Europe :
1990 insights from species distribution modelling, , (Svenning 2003), 1117–1127,
1991 doi:10.1111/j.1365-2745.2008.01422.x, 2008.
- 1992
- 1993 Tarasov, P. E., Webb, T., Andreev, A. A., Afanas'eva, N. B., Berezina, N. A., Bezusko, L.
1994 G., Blyakharchuk, T. A., Bolikhovskaya, N. S., Cheddadi, R., Chernavskaya, M. M.,
1995 Chernova, G. M., Dorofeyuk, N. I., Dirksen, V. G., Elina, G. A., Filimonova, L. V., Glebov,
1996 F. Z., Guiot, J., Gunova, V. S., Harrison, S. P., Jolly, D., Khomutova, V. I., Kvavadze, E. V.,
1997 Osipova, I. M., Panova, N. K., Prentice, I. C., Saarse, L., Sevastyanov, D. V., Volkova, V. S.
1998 and Zernitskaya, V. P.: Present-day and mid-Holocene biomes reconstructed from pollen and
1999 plant macrofossil data from the former Soviet Union and Mongolia, *J. Biogeogr.*, 25(6),
2000 1029–1053, doi:10.1046/j.1365-2699.1998.00236.x, 1998.
- 2001
- 2002 Tarasov, P. E., Volkova, V. S., Webb, T., Guiot, J., Andreev, A. A., Bezusko, L. G.,
2003 Bezusko, T. V., Bykova, G. V., Dorofeyuk, N. I., Kvavadze, E. V., Osipova, I. M., Panova,
2004 N. K. and Sevastyanov, D. V.: Last glacial maximum biomes reconstructed from pollen and
2005 plant macrofossil data from northern Eurasia, *J. Biogeogr.*, 27(3), 609–620,
2006 doi:10.1046/j.1365-2699.2000.00429.x, 2000.
- 2007
- 2008 Tarasov, P.E., Andreev, A.A., Anderson, P.M., Lozhkin, A.V., Haltia-Hovi, E., Nowaczyk,
2009 N.R., Wennrich, V., Brigham-Grette, J., Melles, M.: A pollen-based biome reconstruction
2010 over the last 3.562 million years in the Far East Russian Arctic e new insights on climate-
2011 vegetation relationships at the regional scale. *Clim. Past* 9, 2759-2775, doi: 10.5194/cp-9-
2012 2759-2013, 2013.
- 2013

2014 Telford, R. J. and Birks, H. J. B.: Evaluation of transfer functions in spatially structured
2015 environments, *Quat. Sci. Rev.*, 28(13–14), 1309–1316, doi:10.1016/j.quascirev.2008.12.020,
2016 2009.

2017

2018 Turner, M. G., Wei, D., Prentice, I. C., & Harrison, S. P. The impact of methodological
2019 decisions on climate reconstructions using WA-PLS. *Quaternary Research*, 99, 341–356,
2020 2021.

2022 Valero-Garcés, B. L., González-Sampériz, P., Navas, A., Machin, J., Delgado-Huertas, A.,
2023 Pena-Monné, J. L., Sancho-Marcén, C., Stevenson, T. and Davis, B.: Paleohydrological
2024 fluctuations and steppe vegetation during the last glacial maximum in the central Ebro valley
2025 (NE Spain), *Quat. Int.*, 122(1 SPEC. ISS.), doi:10.1016/j.quaint.2004.01.030, 2004.

2026

2027 Valsecchi, V., Sanchez Goñi, M. F. and Londeix, L.: Vegetation dynamics in the
2028 Northeastern Mediterranean region during the past 23 000 yr: Insights from a new pollen
2029 record from the Sea of Marmara, *Clim. Past*, 8(5), 1941–1956, doi:10.5194/cp-8-1941-2012,
2030 2012.

2031

2032 Vandenberghe, J., French, H. M., Gorbunov, A., Marchenko, S., Velichko, A. A., Jin, H.,
2033 Cui, Z., Zhang, T. and Wan, X.: The Last Permafrost Maximum (LPM) map of the Northern
2034 Hemisphere: Permafrost extent and mean annual air temperatures, 25–17ka BP, *Boreas*,
2035 43(3), 652–666, doi:10.1111/bor.12070, 2014.

2036

2037 Varsányi, I., Palcsu, L. and Kovács, L. Ó.: Groundwater flow system as an archive of
2038 palaeotemperature: Noble gas, radiocarbon, stable isotope and geochemical study in the
2039 Pannonian Basin, Hungary, *Appl. Geochemistry*, 26(1), 91–104,
2040 doi:10.1016/j.apgeochem.2010.11.006, 2011.

2041

2042 Vegas-Vilarrúbia, T., González-Sampériz, P., Morellón, M., Gil-Romera, G., Pérez-Sanz, A.
2043 and Valero-Garcés, B.: Diatom and vegetation responses to late glacial and early holocene
2044 climate changes at lake estanya (southern pyrenees, NE spain), *Palaeogeogr. Palaeoclimatol.*
2045 *Palaeoecol.*, 392, 335–349, doi:10.1016/j.palaeo.2013.09.011, 2013.

2046

2047 Vegas, J., Ruiz-Zapata, B., Ortiz, J. E., Galán, L., Torres, T., García-Cortés, Á., Gil-García,
2048 M. J., Pérez-González, A. and Gallardo-Millán, J. L.: Identification of arid phases during the
2049 last 50 cal. ka BP from the Fuentillejo maar-lacustrine record (Campo de Calatrava Volcanic
2050 Field, Spain), *J. Quat. Sci.*, 25(7), 1051–1062, doi:10.1002/jqs.1262, 2010.

2051

2052 Velasquez, P., Kaplan, J. O., Messmer, M., Ludwig, P. and Raible, C. C.: The role of land
2053 cover in the climate of glacial Europe, *Clim. Past*, 17(3), 1161–1180, doi:10.5194/cp-17-
2054 1161-2021, 2021.

2055

2056 Vicente-Serrano, S. M., Trigo, R. M., López-Moreno, J. I., Liberato, M. L. R., Lorenzo-
2057 Lacruz, J., Beguería, S., Morán-Tejeda, E. and El Kenawy, A.: Extreme winter precipitation
2058 in the Iberian Peninsula in 2010: Anomalies, driving mechanisms and future projections,
2059 *Clim. Res.*, 46(1), 51–65, doi:10.3354/cr00977, 2011.

2060

2061 Williams, J.W., Grimm, E.G., Blois, J., Charles, D.F., Davis, E., Goring, S.J., Graham, R.,
2062 Smith, A.J., Anderson, M., Arroyo-Cabrales, J., Ashworth, A.C., Betancourt, J.L., Bills,
2063 B.W., Booth, R.K., Buckland, P., Curry, B., Giesecke, T., Hausmann, S., Jackson, S.T.,

2064 Latorre, C., Nichols, J., Purdum, T., Roth, R.E., Stryker, M., Takahara, H. :The Neotoma
2065 Paleocology Database: A multi-proxy, international community-curated data resource. *Quat.*
2066 *Res.* 89, 156-177, doi:10.1017/qua.2017.105, 2018.
2067
2068 Williams, J. W. and Jackson, S. T.: Palynological and AVHRR observations of modern
2069 vegetational gradients in eastern North America, , 4, 485–497, 2003.
2070
2071 Williams, J. W., Webb, T., Shurman, B. N. and Bartlein, P. J.: Do Low CO₂ Concentrations
2072 Affect Pollen-Based Reconstructions of LGM Climates? A Response to “Physiological
2073 Significance of Low Atmospheric CO₂ for Plant–Climate Interactions” by Cowling and
2074 Sykes, *Quat. Res.*, 53(3), 402–404, doi:10.1006/qres.2000.2131, 2000.
2075
2076 Willis, K. J. and Van Andel, T. H.: Trees or no trees? The environments of central and
2077 eastern Europe during the Last Glaciation, *Quat. Sci. Rev.*, 23(23–24), 2369–2387,
2078 doi:10.1016/j.quascirev.2004.06.002, 2004.
2079
2080 Wu, H., Guiot, J., Brewer, S. and Guo, Z.: Climatic changes in Eurasia and Africa at the last
2081 glacial maximum and mid-Holocene: Reconstruction from pollen data using inverse
2082 vegetation modelling, *Clim. Dyn.*, 29(2–3), 211–229, doi:10.1007/s00382-007-0231-3, 2007.
2083
2084 Yu, G. and Harrison, S. P.: Lake status records from Europe: data base documentation,
2085 NOAA Paleoclimatology Publications Series, Boulder, Colorado., 1995.
2086
2087 Zaarur, S., Affek, H. P. and Stein, M.: Last glacial-Holocene temperatures and hydrology of
2088 the Sea of Galilee and Hula Valley from clumped isotopes in *Melanopsis* shells, *Geochim.*
2089 *Cosmochim. Acta*, 179, 142–155, doi:10.1016/j.gca.2015.12.034, 2016.
2090
2091 Zanon, M., Davis, B. A. S., Marquer, L., Brewer, S. and Kaplan, J. O.: European forest cover
2092 during the past 12,000 years: A palynological reconstruction based on modern analogs and
2093 remote sensing, *Front. Plant Sci.*, 9, doi:10.3389/fpls.2018.00253, 2018.
2094
2095 Zech, M., Buggle, B., Leiber, K., Marković, S., Glaser, B., Hambach, U., Huwe, B., Stevens,
2096 T., Sümegi, P., Wiesenberg, G. and Zöller, L.: Reconstructing Quaternary vegetation history
2097 in the Carpathian Basin, SE-Europe, using n-alkane biomarkers as molecular fossils:
2098 Problems and possible solutions, potential and limitations, *Quat. Sci. J.*, 58(2), 148–155,
2099 doi:10.3285/eg.58.2.03, 2010.
2100
2101

2102
2103
2104

Tables

Site	Site Name	Country/Ocean	Latitude	Longitude	Elevation	Site Type	Data Type	Samples	Source	Reference
1	MD95-2039 (M)	Atlantic	40.578333	-10.348333	-3381	Marine	Raw Count	21	EPD (E#1472)	Roucoux et al. 2005
2	SU81-18 (M)	Atlantic	37.77	-9.82	-3135	Marine	Raw Count	10	ACER	Turon et al. 2003
3	MD99-2331 (M)	Atlantic	41.15	-9.68	-2110	Marine	Raw Count	41	ACER	Naughton et al. 2006
4	Carn Morval	United Kingdom	49.926111	-6.313889	5	Lake	Digitised	1	Publication	Scourse 1991
5	Gorham Cave	Spain	36.132826	-5.347358	0	Cave	Digitised	1	Publication	Carrion et al. 2008
6	Dozmary Pool	United Kingdom	50.5347222	-4.5358333	265	Lake	Raw Count	32	Author	Kelly et al. 2010
7	Bajondillo	Spain	36.619722	-4.496389	20	Cave	Raw Count	1	EPD (E#1570)	Cortes-Sanchez et al 2011
8	Laguna del maar de Fuentillejo	Spain	38.937996	-4.0539	637	Lake	Digitised	1	Publication	Ruiz-Zapata et al. 2009
9	Padul-1	Spain	37.016338	-3.608503	785	Peat Bog	Digitised	13	Publication	Pons & Reille 1988
10	Padul-2	Spain	37.010833	-3.603889	726	Peat Bog	Digitised	1	Publication	Camuera et al. 2019
11	Cova di Carihuela	Spain	37.4489	-3.4297	1020	Cave	Digitised	1	Publication	Carrion 1992
12	Ifri El Baroud	Morocco	34.75	-3.3	539	Cave	Digitised	1	Publication	Poti et al. 2019
13	MD95-2043 (M)	Mediterranean	36.14	-2.621	-1841	Marine	Raw Count	7	ACER	Fletcher et al. 2008
14	San Rafael	Spain	36.773611	-2.601389	0	Peat Bog	Raw Count	2	EPD (E#574)	Pantalón-Cano 1997
15	Siles	Spain	38.24	-2.3	1320	Lake	Digitised	1	Publication	Carrion 2002
16	Torreçilla de Valmadrid	Spain	41.4469444	-0.895	570	Colluvium	Digitised	1	Publication	Valero-Garcés et al. 2004
17	Navarrés-1	Spain	39.1	-0.683333	225	Peat Bog	Raw Count	1	EPD (E#469)	Carrion & Dupré-Olivier 1996
18	Navarrés-2	Spain	39.1	-0.683333	225	Peat Bog	Raw Count	1	EPD (E#470)	Carrion & Dupré-Olivier 1996
19	Tourbiere de l'Estarres	France	43.0933	-0.3792	356	Lake	Digitised	1	Publication	Jalut et al. 1988
20	Cova de les Malladetes	Spain	39.058	-0.321	20	Cave	Digitised	1	Publication	Dupré-Olivier 1988
21	Lourdes	France	43.033333	-0.075	430	Lake	Digitised	15	Publication	Reille & Andrieu 1995
22	Lake Estanya	Spain	42.0333333	0.53333333	670	Lake	Digitised	1	Publication	Vegas-Villarubia et al. 2013
23	Freychinède	France	42.7833	1.4333	1350	Lake	Digitised	1	Publication	Jalut et al. 1992
24	Banyoles	Spain	42.133333	2.75	173	Lake	Raw Count	13	EPD (E#931)	Pérez-Obiol & Julia 1994
25	Lac du Bouchet B5	France	44.916667	3.783333	1200	Lake	Digitised	14	Publication	Reille & de Beaulieu 1988
26	MD99-2348 (103) (M)	Mediterranean	42.692778	3.841667	-296	Marine	Raw Count	41	EPD (E#1474)	Beaudouin et al. 2007
27	Les Echets G	France	45.9	4.93	267	Peat Bog	Digitised	136	ACER	de Beaulieu & Reille 1984
28	La Grotte Walou	Belgium	50.585278	5.536389	252	Cave	Digitised	1	Publication	Damblon 2011
29	Bergsee	Germany	47.5722222	7.93638889	382	Lake	Digitised	1	Publication	Duprat-Oualid et al. 2017
30	Garaat El-Ouez	Algeria	36.818333	8.33333	45	Peat Bog	Raw Count	6	EPD (E#1501)	Benslama et al 2010
31	Pian del Lago	Italy	44.321561	9.485682	833	Lake	Digitised	1	Publication	Guido et al. 2020
32	Pilsensee	Germany	48.0267	11.1883	534	Lake	Digitised	1	Publication	Küster 1995
33	Orgiano	Italy	45.29	11.43	19	Peat Bog	Digitised	1	Publication	Paganelli 1996
34	Lago della Costa	Italy	45.2702778	11.7430556	7	Lake	Digitised	8	Publication	Kaltenrieder et al. 2009
35	Lagaccione	Italy	42.566667	11.85	355	Lake	Raw Count	7	ACER	Magri 1999
36	Lago Vico	Italy	42.3166667	12.1666667	510	Lake	Digitised	15	Publication	Magri & Sadori 1999
37	Stracciaccappa	Italy	42.13	12.32	220	Lake	Raw Count	2	ACER	Giardini 2007
38	Lago di Monterosi	Italy	42.2166667	12.4333333	237	Lake	Raw Count	1	Publication	Bonatti 1970
39	Venice	Italy	45.629523	12.654086	0	Peat Bog	Digitised	1	Publication	Miola et al. 2006
40	Azzano Decimo	Italy	45.8833	12.7165	10	Alluvial Fan	Raw Count	6	ACER	Pini et al. 2009
41	Valle di Castiglione	Italy	41.89	12.75	44	Lake	Raw Count	2	ACER	Follieri et al. 1989
42	Travesio	Italy	46.2	12.87	220	Lake	Digitised	1	Publication	Monegato et al. 2007
43	Orvenco	Italy	46.252088	13.169771	380	Alluvial Fan	Digitised	1	Publication	Monegato et al. 2007
44	Rio Doidis	Italy	46.12	13.19	152	Lake	Digitised	1	Publication	Monegato et al. 2007
45	Billerio	Italy	46.22	13.21	300	Lake	Digitised	1	Publication	Monegato et al. 2007
46	Kersdorf-Briesen	Germany	52.333704	14.269142	44	Lake	Digitised	1	Publication	Strahl 2005
47	Lago Grande di Monticchio	Italy	40.944444	15.6	1326	Lake	Raw Count	6	EPD (E#932)	Watts et al. 1996
48	Nagymohos	Hungary	48.326944	20.436389	297	Peat Bog	Raw Count	14	Publication	Magyari et al 1999
49	Safarka	Slovakia	48.8819444	20.575	600	Peat Bog	Digitised	1	Publication	Jankovska 2008
50	Feher Lake	Hungary	46.45	20.65	86	Lake	Raw Count	10	Publication	Magyari et al. 2014
51	Ioannina	Greece	39.75	20.85	470	Peat Bog	Raw Count	20	ACER	Tzedakis et al. 2004
52	Kokad	Hungary	47.4027778	21.9286111	112	Peat Bog	Raw Count	2	Publication	Magyari et al. 2019
53	Lake Xinias	Greece	39.05	22.27	500	Lake	Raw Count	5	EPD (E#976)	Bottema 1979
54	Mickunai	Lithuania	54.722114	25.532218	143	Lake	Digitised	1	Publication	Satkunas & Grigiene 2012
55	Lake Sfanta Anna	Romania	46.1263889	25.8880556	946	Lake	Digitised	1	Publication	Magyari et al. 2014
56	Megali Limni	Greece	39.1	26.3	323	Lake	Digitised	1	Publication	Margari et al. 2009
57	Straldzha	Bulgaria	42.630278	26.77	138	Peat Bog	Raw Count	3	Publication	Connor et l. 2013
58	MD01-2430 (M)	Turkey	40.796833	27.725166	-580	Marine	Digitised	1	Publication	Valsecchi et al. 2012
59	Lake Iznik	Turkey	40.433889	29.533056	88	Lake	Raw Count	7	EPD (E#714)	Miebach et al 2016
60	M72/5 628-1 (M)	Black Sea	42.1035	36.62383	-418	Marine	Raw Count	6	Pangaea (833387)	Shumilovskikh et al. 2014
61	Dziguta	Georgia	42.99	41.07	35	Peat Bog	Digitised	1	Publication	Arslanov et al. 2007
62	Lake Van LG	Turkey	38.667	42.669	1649	Lake	Raw Count	10	Pangaea (853779)	Pickarski et al. 2015
63	Lake Zeribar	Iran	35.533333	46.116667	1286	Lake	Raw Count	17	EPD (E#714)	van Zeist & Bottema 1977

Table 1. List of selected sites

2105
2106
2107
2108
2109
2110

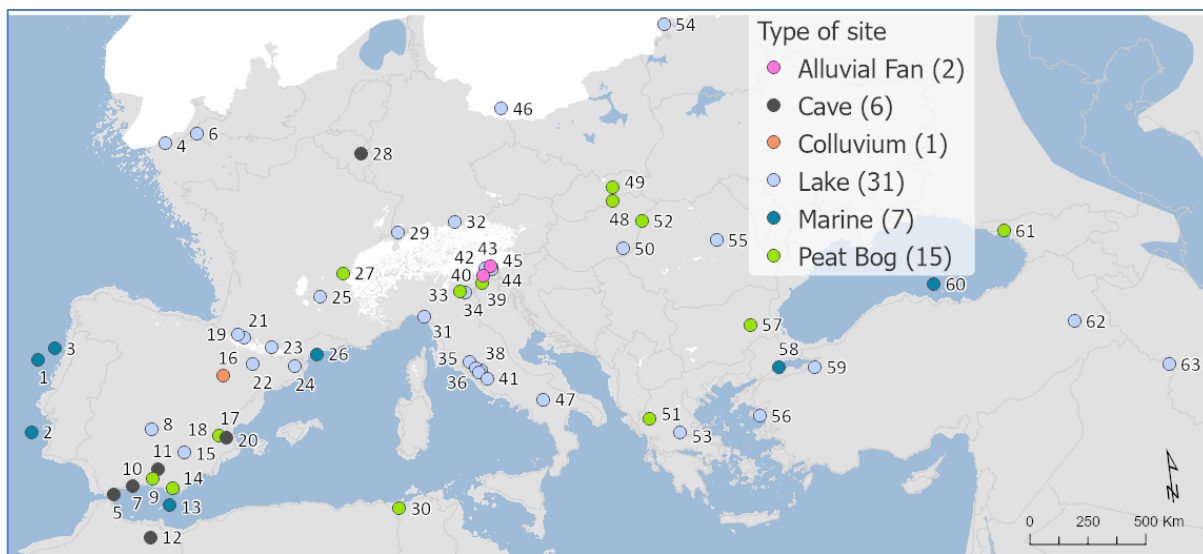
2111
2112
2113
2114
2115

	RMSE	R2
TANN	2.28	0.9
TDJF	3.35	0.91
TJJA	2.21	0.81
PANN	224.94	0.69
PDJF	78.51	0.69
PJJA	52.49	0.75
Tree Cover	21.03	0.52

2116
2117
2118
2119
2120
2121
2122
2123
2124
2125

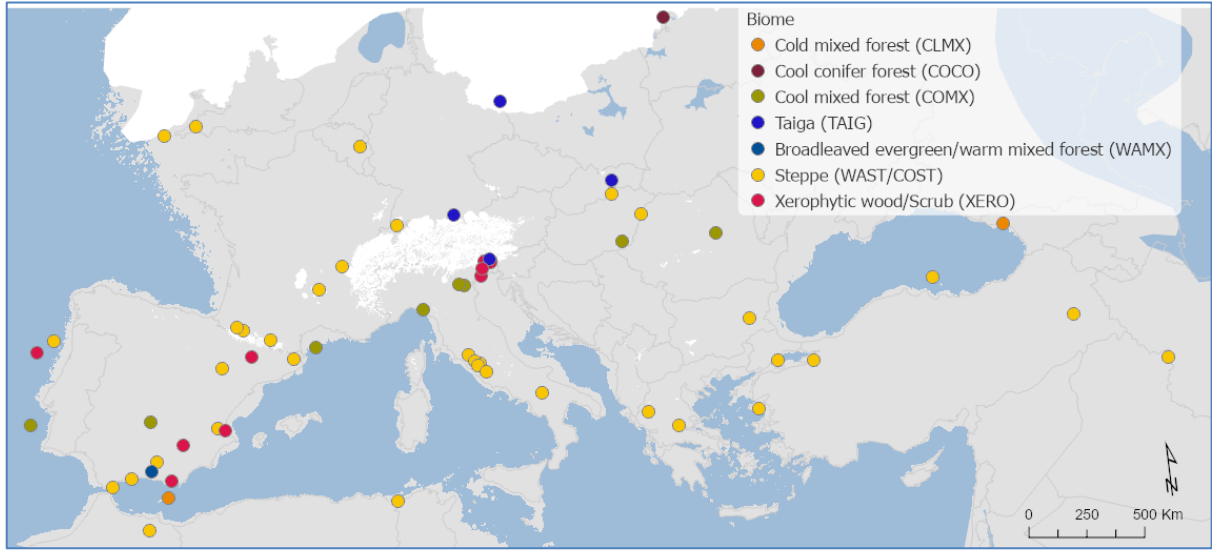
Table 2. MAT performance statistics based on the modern pollen sample training set. This includes Mean Annual Temperature and Precipitation (TANN and PANN), Mean Winter Temperature and Precipitation (TDJF and PDJF) and Mean Summer Temperature and Precipitation (TJJA and PJJA).

2126 **Figures**
2127
2128
2129



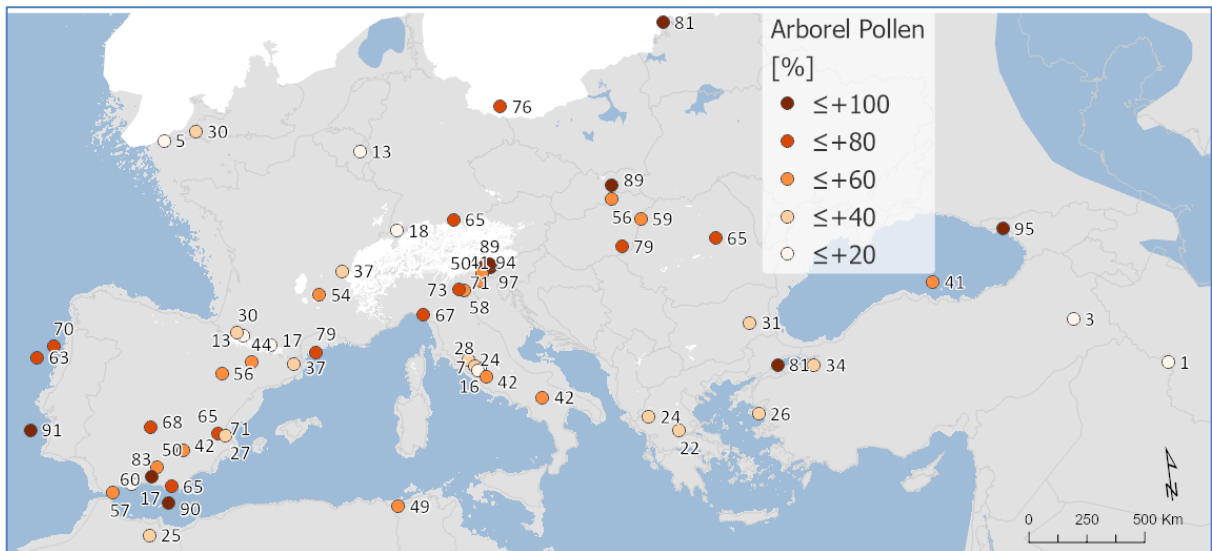
2130
2131
2132 **Figure 1. Site locations and archives (Site numbers are as shown in Table 1)**
2133
2134
2135

2136



2137
2138
2139
2140
2141

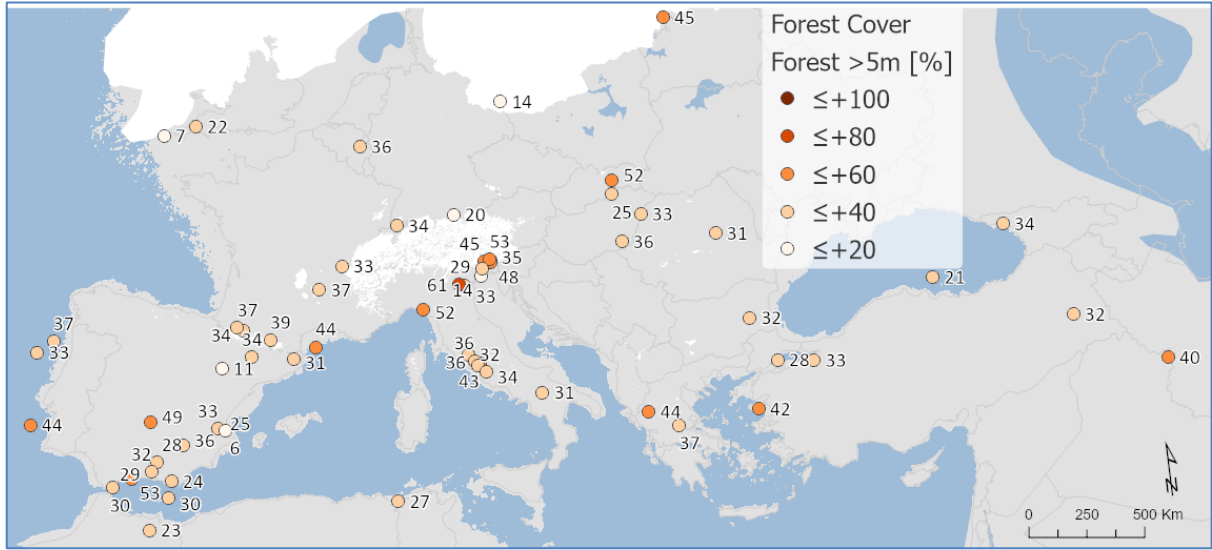
Figure 2. Pollen biomes



2142
2143
2144
2145
2146

Figure 3. Arboreal Pollen (AP) % forest cover

2147



2148

2149

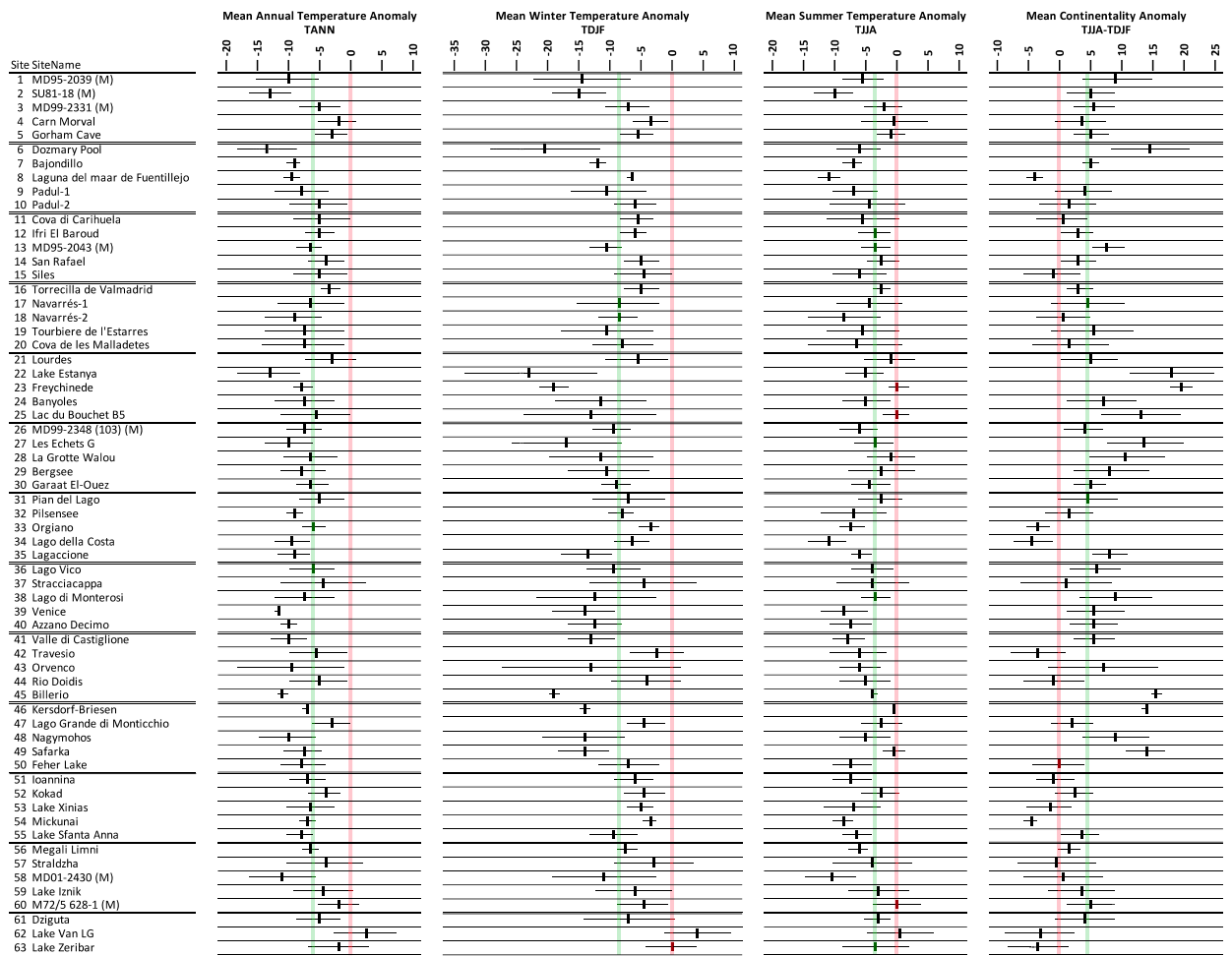
2150

2151

2152

Figure 4. Modern Analogue Technique (MAT) % forest cover

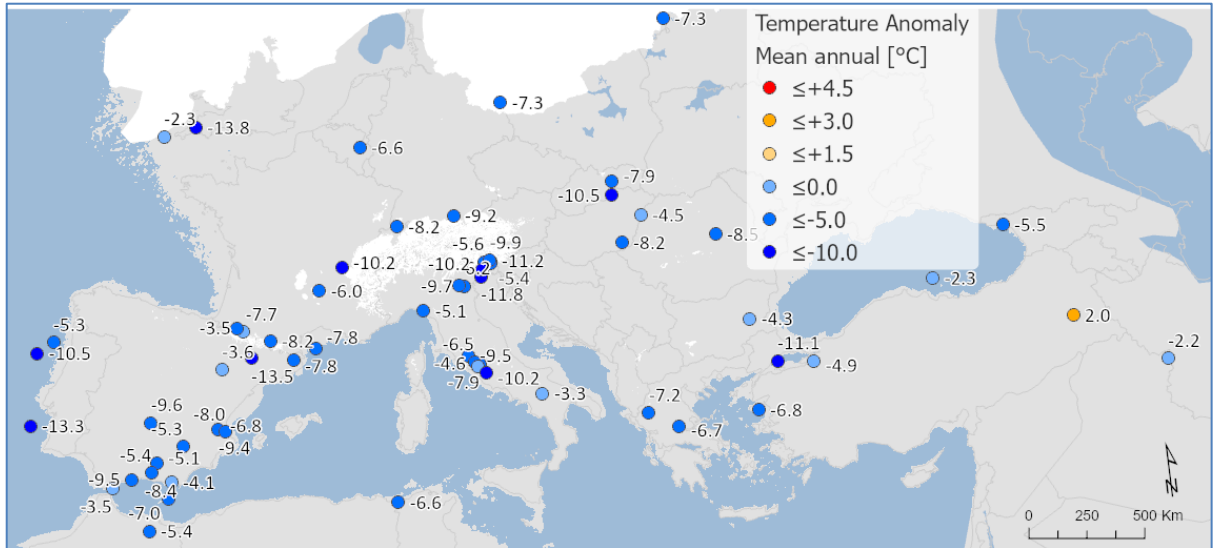
2153
2154



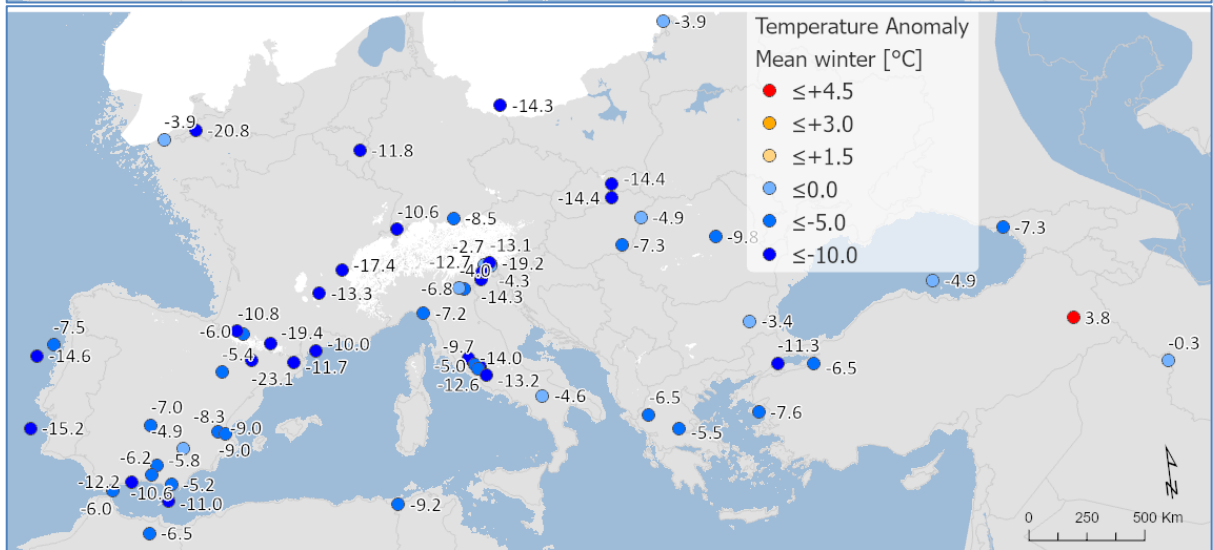
2155
2156
2157
2158
2159
2160
2161
2162
2163
2164

Figure 5. Pollen-based MAT reconstructions for LGM annual, winter and summer temperature anomalies (uncertainties represent one standard deviation). Continentality represents the difference in temperature between summer and winter, with positive anomalies indicating an increase in the temperature difference between summer and winter. All values are expressed as anomalies compared with the present day. The green line indicates the mean for all the sites.

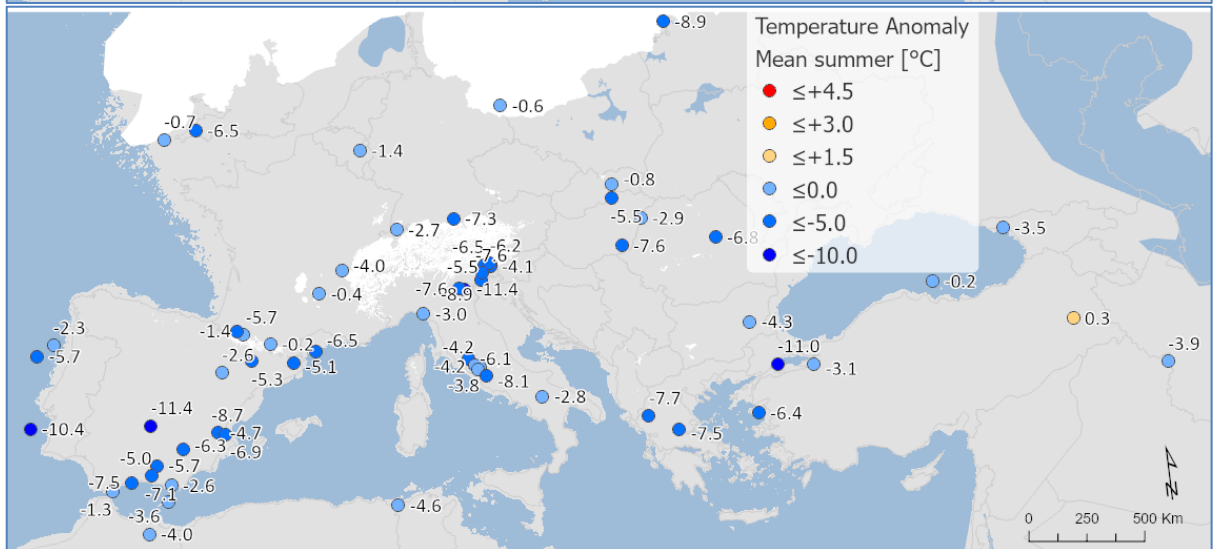
2165

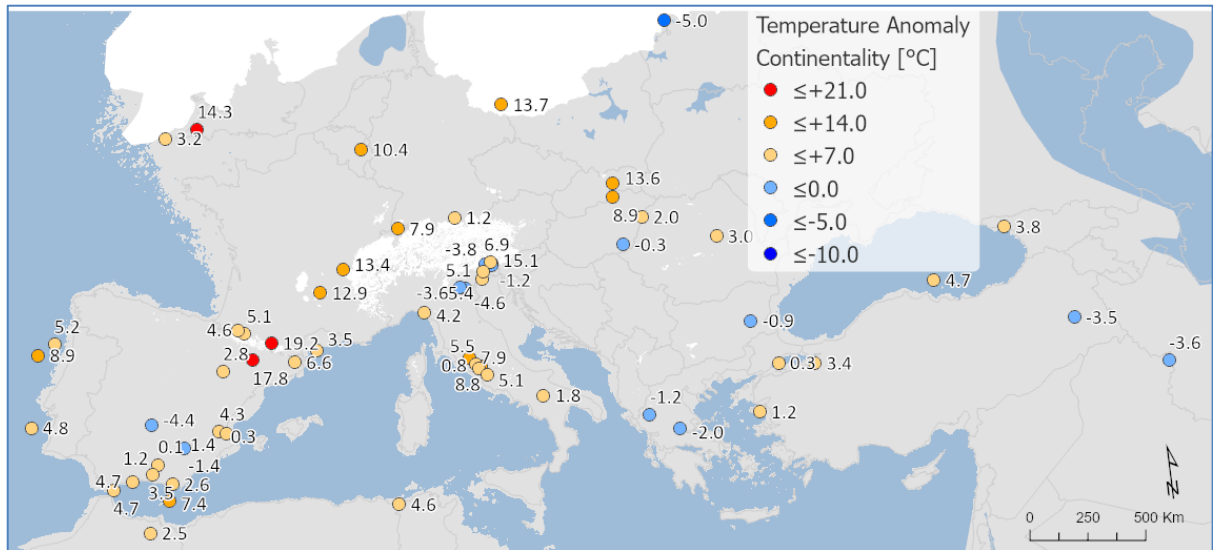


2166



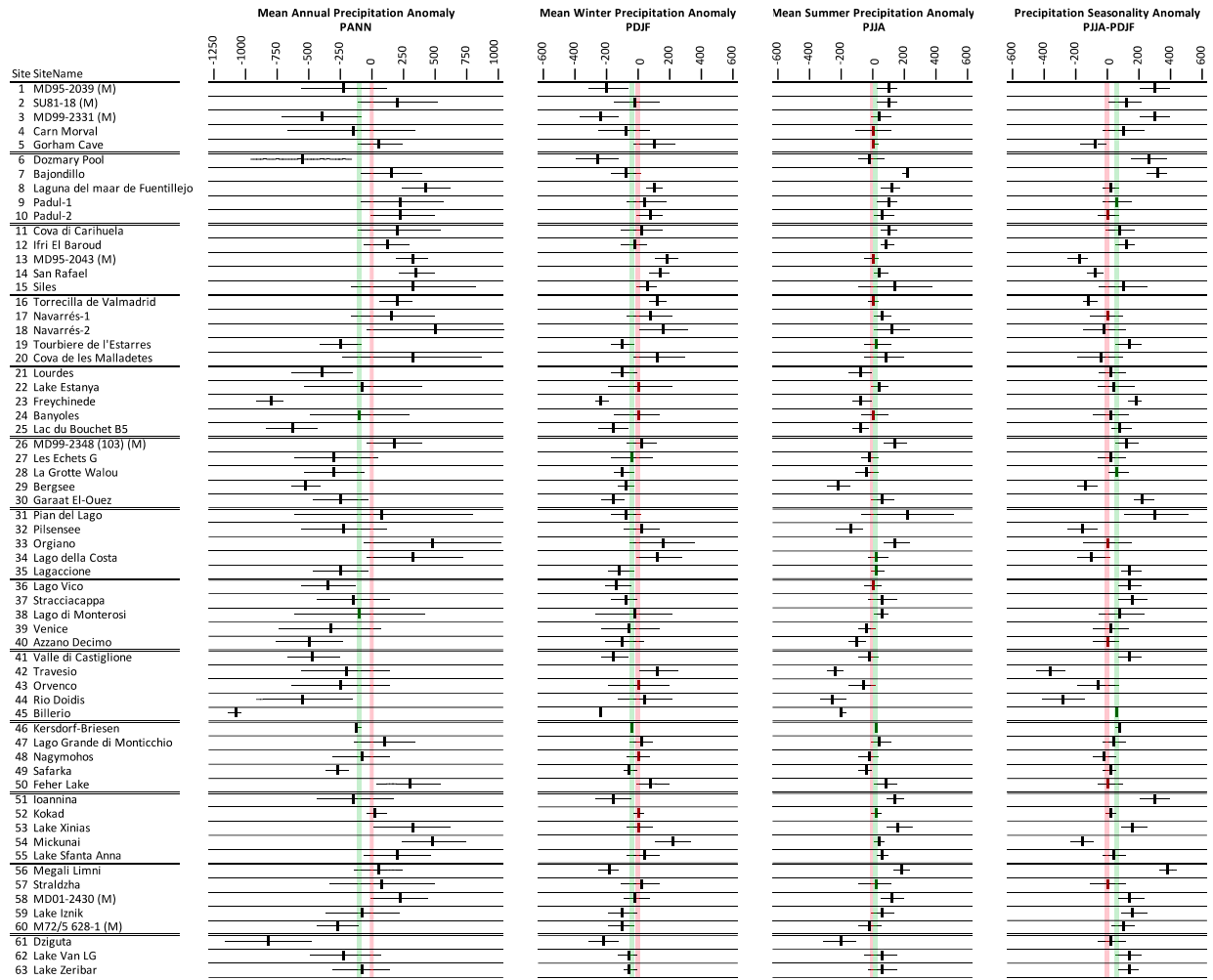
2167





2168
 2169
 2170
 2171
 2172
 2173
 2174
 2175

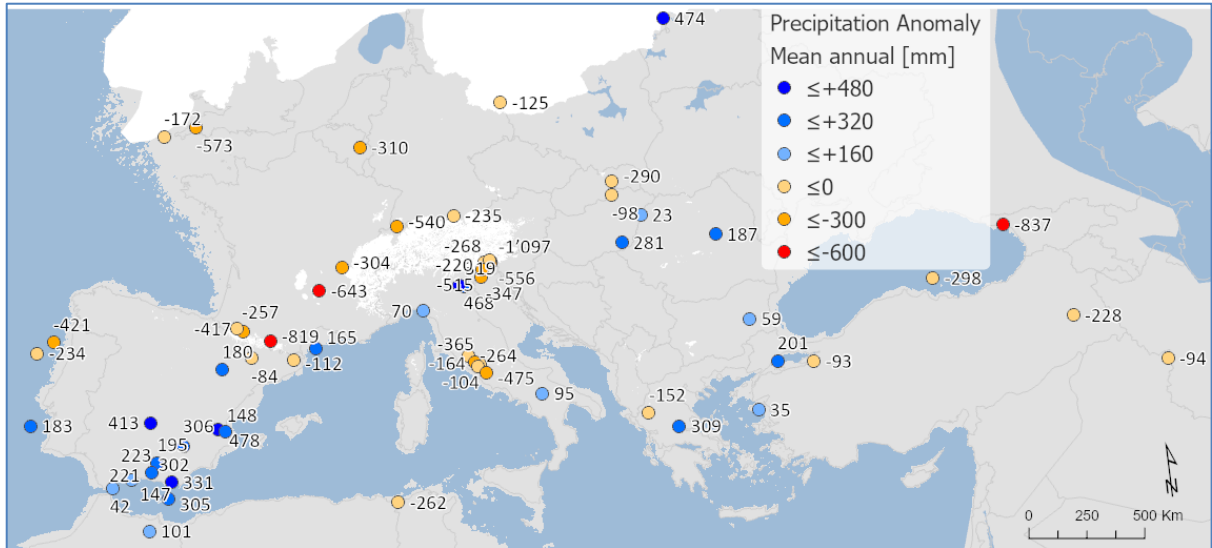
Figure 6. Maps of pollen-based MAT reconstructions for LGM annual, winter and summer temperature anomalies (as shown in figure 9). Continentality represents the difference in temperature between summer and winter, with positive anomalies indicating an increase in the temperature difference between summer and winter. All values are expressed as anomalies compared with the present day.



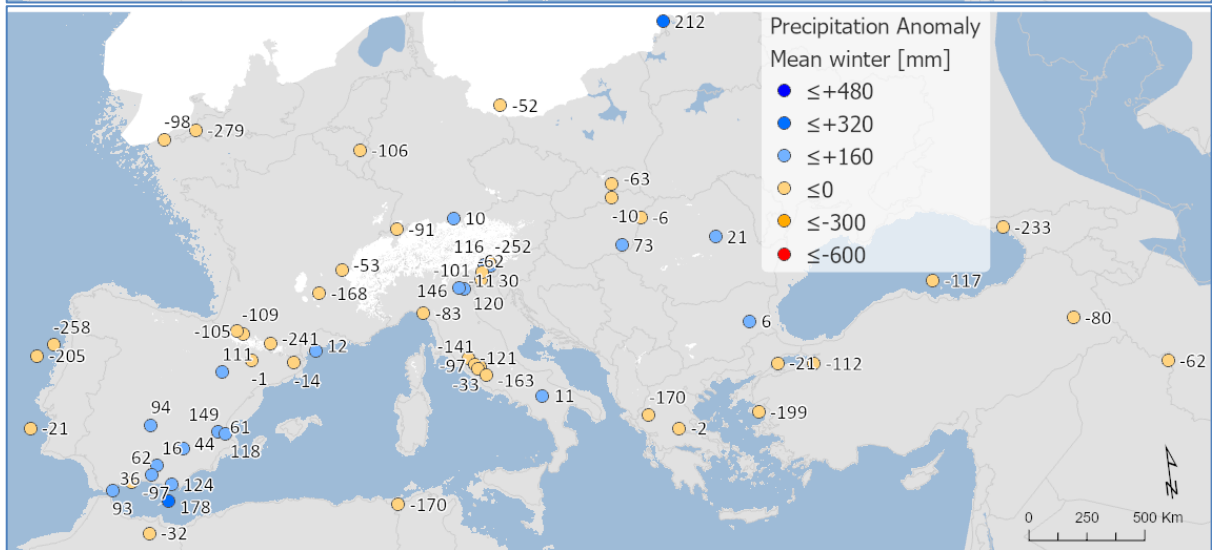
2177
 2178
 2179
 2180
 2181
 2182
 2183
 2184

Figure 7. Pollen-based MAT reconstructions for LGM annual, winter and summer precipitation anomalies (uncertainties represent one standard deviation). Seasonality represents the difference in precipitation between summer and winter, with positive anomalies indicating an increase in summer precipitation compared to winter. All values are expressed as anomalies compared with the present day. The green line indicates the mean for all the sites.

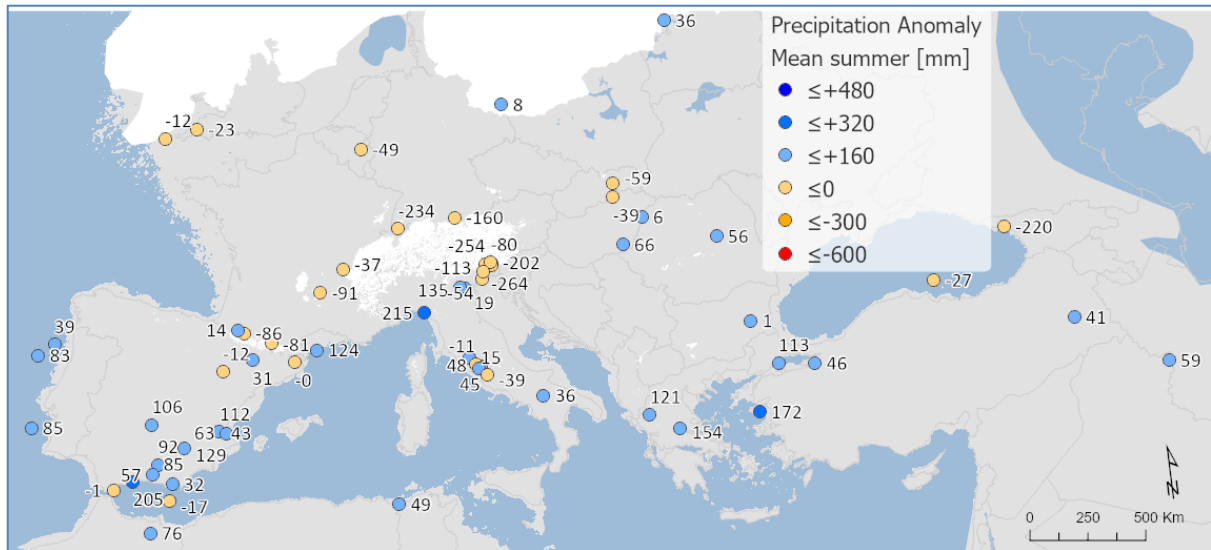
2185



2186

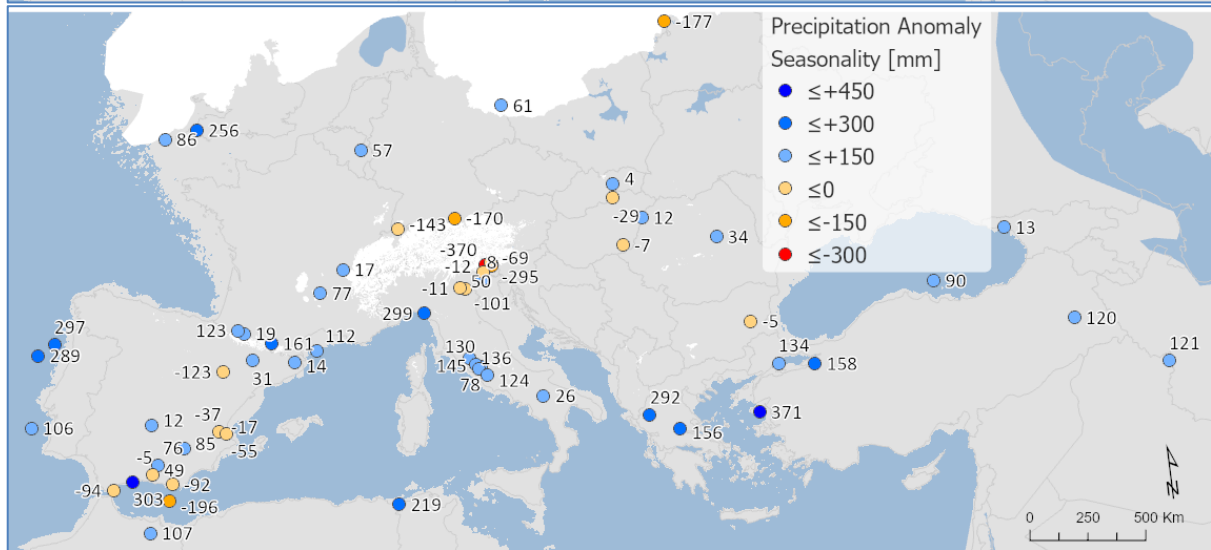


2187



2188

2189



2190

2191

2192

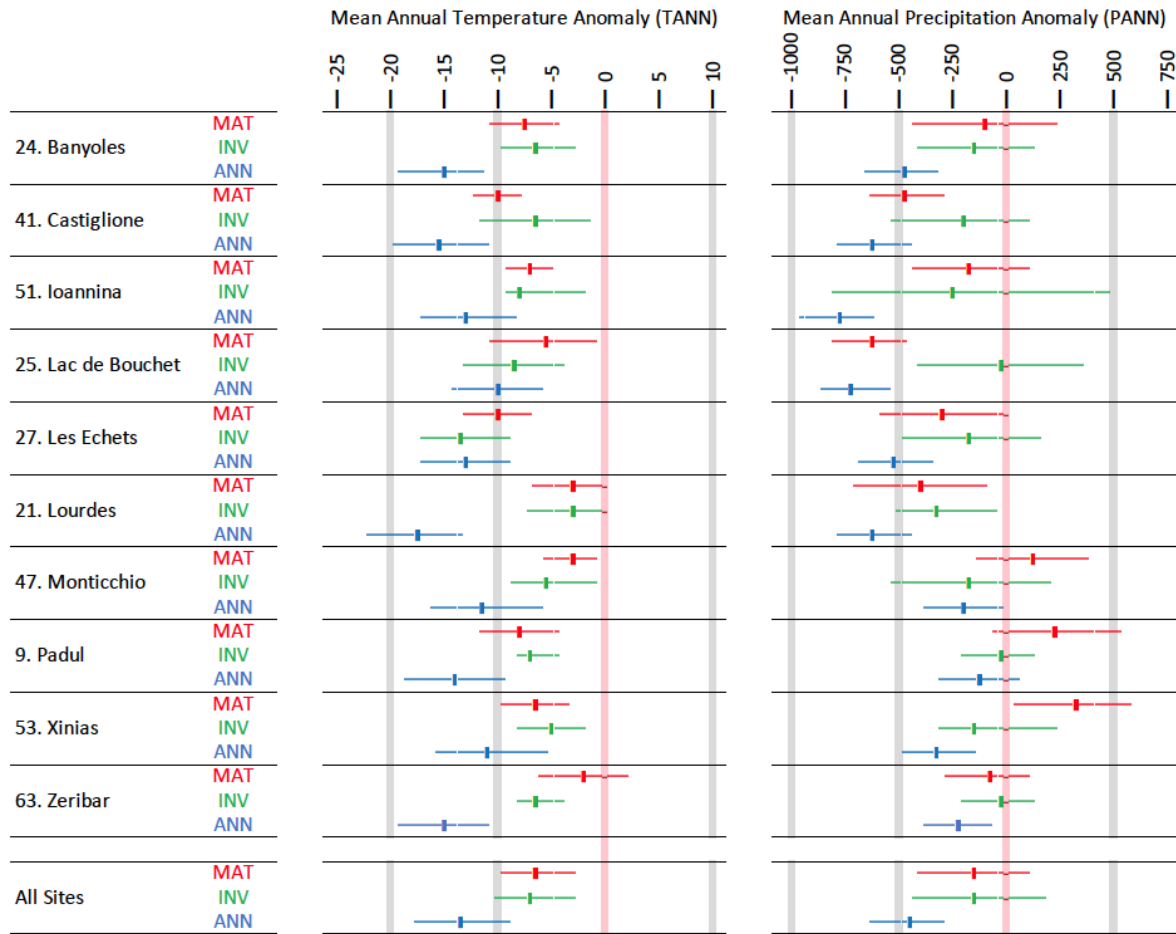
2193

2194

2195

2196

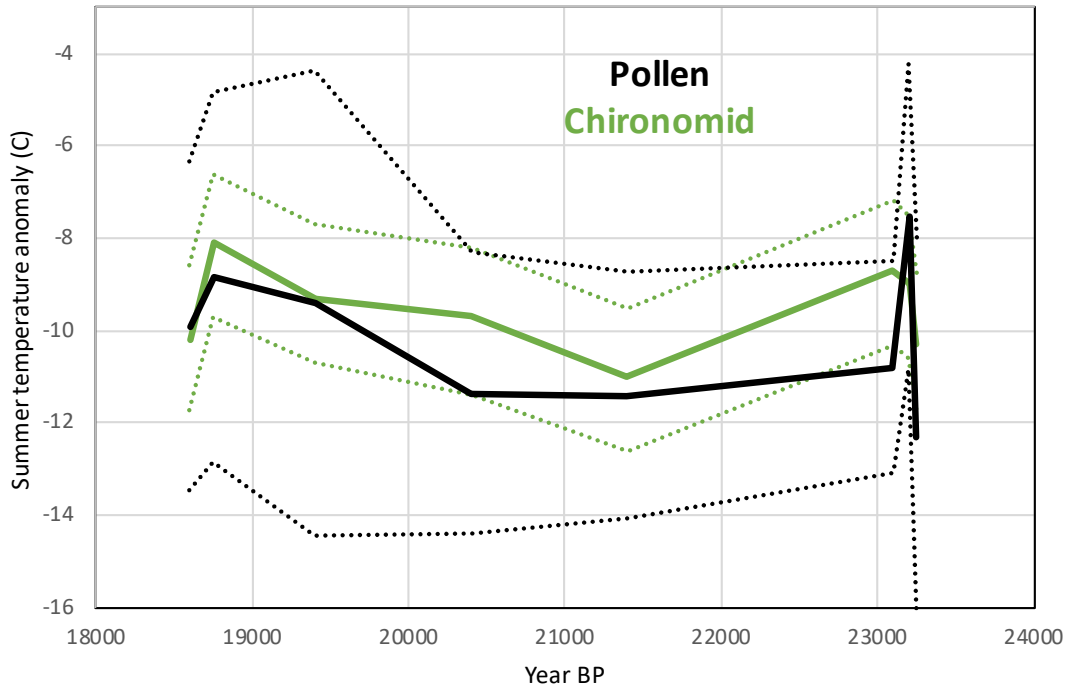
Figure 8. Maps of pollen-based MAT reconstructions for LGM annual, winter and summer precipitation anomalies (as shown in figure 11). Seasonality represents the difference in precipitation between summer and winter, with positive anomalies indicating an increase in summer precipitation compared to winter. All values are expressed as anomalies compared with the present day.



2198
 2199
 2200
 2201
 2202
 2203
 2204
 2205

Figure 9. A site-by-site comparison between LGM pollen-climate reconstructions based on Modern Analogue Technique MAT (this study), neural-networks ANN (Peyron et al., 1998), and Inverse Modelling INV (Wu et al., 2007). The results show that MAT and INV give similar climate reconstructions, but ANN is significantly cooler/drier.

2206
2207
2208



2209
2210
2211
2212
2213
2214
2215

Figure 10. Comparison between LGM pollen-climate MAT and chironomid summer temperature reconstructions at Lago della Costa, Italy (chironomid reconstruction and pollen data from Samartin et al., 2016). Dash lines show uncertainties.

2216
2217
2218

Appendix

Site	Site Name	COHMAP Quality	COHMAP							Upper 14C	Upper Cal. BP	Lower 14C	Lower Cal. BP
			< 17k	18k	19k	20k	21k	22k	23k				
1	MD95-2039 (M)	3C								14830±80	18166±269	19950±210	23883±374
2	SU81-18 (M)	2C								17510±270	20952±404	21250±280	25420±441
3	MD99-2331 (M)	2C								16170±130	19325±303	19770±170	23682±336
4	Carn Morval	4C									18600±3700	21500±890/800	25867±1127
5	Gorham Cave	4D										18440±160	22055±341
6	Dozmary Pool	2C								14568±129	17569±523	18325±216	21769±602
7	Bajondillo	1C									18701±2154		
8	Laguna del maar de Fuentillejo	5D								16540±90	19847±308		
9	Padul-1	3D								18300±300	21821±412	19100±160	22922±308
10	Padul-2	1D										17450±539	21082±539
11	Cova di Carihuela	2C								15700±220	18958±280	21430±130	25659±226
12	Ifri El Baroud	2D								17296±87	20761±293		
13	MD95-2043 (M)	2C								15440±90	18533±294	18260±120	21951±335
14	San Rafael	3D								9980±60	11464±133	16860±120	20083±292
15	Siles	2D								17030±80	20345±351		
16	Torreçilla de Valmadrid	2D								17100±85	20456±366		
17	Navarrés-1	4D								18360±195	22001±353	20700±295	24664±411
18	Navarrés-2	5D								5150±50	5881±85	16000±	19144±
19	Tourbiere de l'Estarres	1C								17150±250	20522±470	18970±160	22847±317
20	Cova de les Malladetes	5D								16300±1500	19686±1723		
21	Lourdes	4D								18510±130	22112±130	20025±175	23952±355
22	Lake Estanya	5D									9498±50		19184±251
23	Freychinède	3C								14800±800	17912±856	21300±760	25615±1030
24	Banyoles	2C									19878±100		27862±3000
25	Lac du Bouchet B5	4C								15350±350	18513±435	19200±300	23006±384
26	MD99-2348 (103) (M)	1D								17660±60	21065±310	19350±90	23111±271
27	Les Echets G	1C								17530±270	20970±407	18030±250	21704±473
28	La Grotte Walou	1D											21200±700
29	Bergsee	2D										17780±90	21244±306
30	Garaat El-Ouez	2C								16010±320	19200±801		
31	Pian del Lago	2D											21260±320
32	Pilsensee	6D								15860±250	19073±290		
33	Orgiano	2D								17760±160	21221±373	19290±520	23141±621
34	Lago della Costa	2C								15400±150	18484±330	19285±160	23052±302
35	Lagacione	2C								16080±450	19369±527	20615±940	24746±1201
36	Lago Vico	3C								14385±140	17541±272	20500±230	24430±376
37	Stracciaccappa	4C								12060±130	14093±281	19745±820	22675±955
38	Lago di Monterosi	2D								17040±350	20398±544		
39	Venice	5D										18640±100	22277±336
40	Azzano Decimo	2D								18000±300	21637±529	21025±245	25179±449
41	Valle di Castiglione	3C								14220±145	17443±270	20300±700	24266±842
42	Travesio	5D										18780±200	22483±406
43	Orvenco	2D								17760±160	21221±373	19290±520	23141±621
44	Rio Doidis	5D										18860±190	22390±373
45	Billerio	3D										18165±200	21872±382
46	Kersdorf-Briesen	1D										17622±94	21183±356
47	Lago Grande di Monticchio	2C									20204±		24014±
48	Nagymohos	2C								14246±144	17361±425	18159±247	21735±622
49	Safarka	3D										18287±1512	21912±1781
50	Feher Lake	1D								17715±250	21190±463	19911±81	23841±313
51	Ioannina	3C								15330±140	18420±312	20760±230	24748±330
52	Kokad	5D								14326±63	17433±443	16280±90	19685±538
53	Lake Xinias	6C								11150±130	13049±160	21390±430	25671±648
54	Mickunai	1D									21000±2200		
55	Lake Sfanta Anna	1D								17626±96	20955±432		
56	Megali Limni	6D								19072±237	22906±340		
57	Straldzha	6C								14696±65	18022±364	23653±114	28580±390
58	MD01-2430 (M)	4C								12050±75	14904±324	18310±380	21746±968
59	Lake Iznik	7D								16910±100	19515±115		
60	M72/5 628-1 (M)	2C								16835±85	18490±	19495±90	21280±
61	Dziguta	4C								12990±160	15839±483	20560±880	24666±1126
62	Lake Van LG	2C									18590±62		23290±596
63	Lake Zeribar	4C								13650±160	16610±399	22000±500	26462±880

COHMAP chronological quality classification:
 1C: Bracketing dates within 2000 14C (2360 Cal.) yr interval about the time being assessed
 2C: Bracketing dates, one within 2000 14C (2360 Cal.) yr and the second within 4000 14C (4682 Cal.) yr of the time being assessed
 3C: Bracketing dates within 4000 14C (4682 Cal.) yr interval about the time being assessed
 4C: Bracketing dates, one being within 4000 14C (4682 Cal.) yr and the second being within 6000 14C (7490 Cal.) yr of the time being assessed
 5C: Bracketing dates within 6000 14C (7490 Cal.) yr interval about the time being assessed
 6C: Bracketing dates, one within 6000 14C (7490 Cal.) yr and the second within 8000 14C (9681 Cal.) yr of the time being assessed
 7C: Poorly dated
 1D: Date within 250 14C (206 Cal.) yr of the time being assessed
 2D: Date within 500 14C (684 Cal.) yr of the time being assessed
 3D: Date within 750 14C (975 Cal.) yr of the time being assessed
 4D: Date within 1000 14C (1123 Cal.) yr of the time being assessed
 5D: Date within 1500 14C (1881 Cal.) yr of the time being assessed
 6D: Date within 2000 14C (2360 Cal.) yr of the time being assessed
 7D: Poorly dated

2210
2211
2212
2213
2214
2215
2216
2217
2218
2219
2220
2221
2222
2223
2224
2225
2226
2227
2228
2229
2230
2231
2232
2233
2234
2235
2236
2237
2238

Table A1. Chronological control

2239
2240

Site Number	Site Name	Site Type	TANN	TDJF	TJJA	PANN	PDJF	PJJA
1	MD95-2039 (M)	Marine	15.7	10.7	20.8	1047	427	70
2	SU81-18 (M)	Marine	20.8	15.3	26.5	629	282	25
3	MD99-2331 (M)	Marine	14.6	9.8	19.4	1239	507	88
4	Carn Morval	Lake	12.5	8.7	16.9	1183	392	206
5	Gorham Cave	Cave	18.3	13.4	23.7	740	336	25
6	Dozmary Pool	Lake	10.3	6.0	15.2	1271	422	236
7	Bajondillo	Cave	16.6	10.5	23.4	542	223	27
8	Laguna del maar de Fuentillejo	Lake	16.1	8.1	25.4	474	156	47
9	Padul-1	Peat Bog	16.6	9.6	24.9	417	157	23
10	Padul-2	Peat Bog	16.6	9.6	24.9	417	157	23
11	Cova di Carihuela	Cave	15.7	8.1	25.1	551	187	57
12	Ifri El Baroud	Cave	16.9	10.7	24.0	457	184	22
13	MD95-2043 (M)	Marine	17.9	12.4	24.0	214.2	37	72
14	San Rafael	Peat Bog	18.1	11.9	24.9	243	87	14
15	Siles	Lake	14.4	6.8	23.4	658	195	92
16	Torrecilla de Valmadrid	Colluvium	14.2	6.6	22.5	390	75	82
17	Navarrés-1	Peat Bog	17.0	10.9	23.8	421	96	51
18	Navarrés-2	Peat Bog	17.0	10.9	23.8	421	96	51
19	Tourbiere de l'Estalles	Lake	13.0	6.1	20.4	1045	272	217
20	Cova de les Malladetes	Cave	18.1	12.1	24.8	478	117	60
21	Lourdes	Lake	12.6	5.5	20.1	1002	256	212
22	Lake Estanya	Lake	12.8	5.1	21.0	641	125	152
23	Freychinede	Lake	10.8	3.9	19.0	1128	257	277
24	Banyoles	Lake	14.3	7.7	21.9	698	157	139
25	Lac du Bouchet B5	Lake	8.2	1.3	15.9	1070	251	221
26	MD99-2348 (103) (M)	Marine	14.6	8.0	21.9	618	158	95
27	Les Echets G	Peat Bog	11.4	3.6	19.6	876	175	215
28	La Grotte Walou	Cave	10.3	3.2	17.0	903	215	249
29	Bergsee	Lake	9.6	1.4	17.6	1048	189	387
30	Garaat El-Ouez	Peat Bog	17.3	11.0	24.3	830	360	33
31	Pian del Lago	Lake	12.4	5.1	20.0	995	266	149
32	Pilsensee	Lake	9.3	0.6	17.7	947	151	374
33	Orgiano	Peat Bog	13.0	3.3	22.3	907	200	228
34	Lago della Costa	Lake	12.9	3.3	22.1	888	196	224
35	Lagaccione	Lake	14.2	7.2	21.7	705	203	109
36	Lago Vico	Lake	13.7	6.4	21.5	870	258	132
37	Stracciaccappa	Lake	14.6	7.3	22.4	867	266	115
38	Lago di Monterosi	Lake	15.0	7.7	22.9	837	248	115
39	Venice	Peat Bog	13.4	4.5	22.1	1050	221	277
40	Azzano Decimo	Alluvial Fan	13.3	4.4	22.1	1170	241	311
41	Valle di Castiglione	Lake	16.3	9.1	24.0	988	294	144
42	Travesio	Lake	12.6	3.7	21.3	1415	281	375
43	Orvenco	Alluvial Fan	13.0	3.3	22.3	907	200	228
44	Rio Doidis	Lake	12.8	4.1	21.2	1529	315	392
45	Billerio	Lake	12.8	4.1	21.2	1529	315	392
46	Kersdorf-Briesen	Lake	8.8	-1.0	17.9	538	110	175
47	Lago Grande di Monticchio	Lake	11.5	4.1	19.8	518	154	76
48	Nagymohos	Peat Bog	9.5	-1.5	19.1	616	103	230
49	Safarka	Peat Bog	7.0	-3.2	16.0	755	119	280
50	Feher Lake	Lake	11.0	-0.1	20.7	546	112	185
51	Ioannina	Peat Bog	14.7	6.5	23.3	1000	364	98
52	Kokad	Peat Bog	10.2	-0.9	19.8	601	130	204
53	Lake Xiniás	Lake	15.6	7.5	24.1	563	211	47
54	Mickunai	Lake	6.0	-5.0	16.3	682	131	230
55	Lake Sfanta Anna	Lake	11.6	5.2	18.4	867	253	172
56	Megali Limni	Lake	15.5	8.2	23.4	684	357	28
57	Straldzha	Peat Bog	12.5	2.6	21.8	591	158	135
58	MD01-2430 (M)	Marine	18.0	8.7	27.5	595	219	75
59	Lake Iznik	Lake	13.9	6.1	21.8	677	250	85
60	M72/5 628-1 (M)	Marine	14.5	8.0	21.6	857	251	156
61	Dziguta	Peat Bog	14.1	6.6	21.7	1549	409	373
62	Lake Van LG	Lake	12.0	0.9	23.1	635	201	34
63	Lake Zeribar	Lake	17.1	5.0	29.0	427	167	6

2241
2242
2243
2244
2245

Table A2. Modern climate values for each site used in the calculation of anomalies (taken from WorldClim 2, Fick & Hijmans 2017)

2246
2247
2248
2249

	All surface samples		Steppe only	
	RMSE	R2	RMSE	R2
TANN	2.28	0.9	2.51	0.87
TDJF	3.35	0.91	3.26	0.88
TJJA	2.21	0.81	2.49	0.82
PANN	224.94	0.69	185.7	0.71
PDJF	78.51	0.69	66.5	0.66
PJJA	52.49	0.75	43.8	0.79

2250
2251
2252
2253
2254
2255
2256
2257
2258
2259
2260

Table A3. A comparison of MAT performance statistics based on the modern pollen sample training set using all surface samples from the EMPD2 used in the LGM reconstruction (as shown in Table 3), and a subset of 1588 samples from the EMPD2 that were classified as steppe. The results show little difference between the two different types of samples. The table includes Mean Annual Temperature and Precipitation (TANN and PANN), Mean Winter Temperature and Precipitation (TDJF and PDJF) and Mean Summer Temperature and Precipitation (TJJA and PJJA).

Site Name	Site#	Pollen Biome	Modern Analogue Biome	Modern Analogue Ecoregion
MD95-2039	1	XERO	Mediterranean Forests, woodlands and scrubs	Iberian conifer forests
SU81-18	2	COMX	Mediterranean Forests, woodlands and scrubs	Iberian conifer forests
MD99-2331	3	STEP	Mediterranean Forests, woodlands and scrubs	Alps conifer and mixed forests
Carn Morval	4	STEP	Temperate broadleaf and mixed forests	North Atlantic moist mixed forests
Gorham Cave	5	STEP	Mediterranean Forests, woodlands and scrubs	Cyprus Mediterranean forests
Dozmary Pool	6	STEP	Temperate Coniferous Forest	Alps conifer and mixed forests
Bajondillo	7	STEP	Temperate broadleaf and mixed forests	Central European mixed forests
Laguna del maar de Fuentillejo	8	COMX	Mediterranean Forests, woodlands and scrubs	Northwest Iberian montane forests
Padul	9	STEP	Mediterranean Forests, woodlands and scrubs	Central Anatolian steppe
Padul-15-05	10	WAMX	Mediterranean Forests, woodlands and scrubs	Iberian sclerophyllous and semi-deciduous forests
Cova di Carhuela	11	STEP	Deserts and xeric shrublands	Azerbaijan shrub desert and steppe
Ifri El Baroud	12	STEP	Mediterranean Forests, woodlands and scrubs	Iberian sclerophyllous and semi-deciduous forests
MD95-2043	13	CLMX	Mediterranean Forests, woodlands and scrubs	Southern Anatolian montane conifer and deciduous forests
San Rafael	14	XERO	Mediterranean Forests, woodlands and scrubs	Tyrrhenian-Adriatic Sclerophyllous and mixed forests
Siles	15	XERO	Mediterranean Forests, woodlands and scrubs	Northwest Iberian montane forests
Torreçilla de Valmadrid	16	STEP	Mediterranean Forests, woodlands and scrubs	Southern Anatolian montane conifer and deciduous forests
Navarres	17	XERO	Mediterranean Forests, woodlands and scrubs	Iberian sclerophyllous and semi-deciduous forests
Navarres	18	STEP	Temperate broadleaf and mixed forests	Pyrenees conifer and mixed forests
Tourbiere de IEstarres	19	STEP	Temperate grasslands, savannas and shrublands	Eastern Anatolian montane steppe
Cova de les Malladetes	20	XERO	Mediterranean Forests, woodlands and scrubs	Pyrenees conifer and mixed forests
Lourdes	21	STEP	Temperate broadleaf and mixed forests	Gissaro-Alai open woodlands
Estanya	22	XERO	Temperate broadleaf and mixed forests	Western Siberian hemiboreal forests
Freychinede	23	STEP	Temperate grasslands, savannas and shrublands	Mongolian-Manchurian grassland
Lake Banyoles	24	STEP	Temperate grasslands, savannas and shrublands	Gissaro-Alai open woodlands
Lac du Bouchet B5	25	STEP	Temperate grasslands, savannas and shrublands	Gissaro-Alai open woodlands
MD99-2348-103	26	COMX	Temperate broadleaf and mixed forests	Rodope montane mixed forests
Les Echets G - DIGI	27	STEP	Temperate broadleaf and mixed forests	Western Siberian hemiboreal forests
La Grotte Walou	28	STEP	Temperate broadleaf and mixed forests	Kazakh forest steppe
Bergsee	29	STEP	Temperate broadleaf and mixed forests	Kazakh forest steppe
Garaat El-Ouez	30	STEP	Mediterranean Forests, woodlands and scrubs	Anatolian conifer and deciduous mixed forests
Pian del Lago	31	COMX	Temperate broadleaf and mixed forests	Western European broadleaf forests
Pilsensee	32	TAIG	Tundra	Kola Peninsula tundra
Orgiano	33	COMX	Temperate broadleaf and mixed forests	Western European broadleaf forests
Lago della Costa	34	COMX	Temperate Coniferous Forest	Alps conifer and mixed forests
Lagaccione	35	STEP	Temperate grasslands, savannas and shrublands	Gissaro-Alai open woodlands
Lago Vico	36	STEP	Temperate grasslands, savannas and shrublands	Gissaro-Alai open woodlands
Stracciaccappa	37	STEP	Mediterranean Forests, woodlands and scrubs	Western European broadleaf forests
Lago di Monterosi	38	STEP	Temperate grasslands, savannas and shrublands	Northwest Iberian montane forests
Venice	39	XERO	Tundra	Scandinavian Montane Birch forest and grasslands
Azzano Decimo	40	XERO	Temperate broadleaf and mixed forests	Scandinavian Montane Birch forest and grasslands
Valle di Castiglione	41	STEP	Temperate broadleaf and mixed forests	Tian Shan montane steppe and meadows
Travesio	42	XERO	Mediterranean Forests, woodlands and scrubs	Iberian conifer forests
Orvenco	43	TAIG	Temperate broadleaf and mixed forests	Western Siberian hemiboreal forests
Rio Doidis	44	XERO	Mediterranean Forests, woodlands and scrubs	Cyprus Mediterranean forests
Billerio	45	TAIG	Temperate broadleaf and mixed forests	Western Siberian hemiboreal forests
Kersdorf-Briesen	46	TAIG	Temperate broadleaf and mixed forests	Western Siberian hemiboreal forests
Lago Grande di Monticchio	47	STEP	Temperate broadleaf and mixed forests	Tian Shan montane steppe and meadows
Nagymohos Pleistocene	48	STEP	Tundra	Sarmatic mixed forests
Safarka	49	TAIG	Boreal forests / Taiga	Ural montane forests and tundra
Fehertó	50	COMX	Temperate Coniferous Forest	Alps conifer and mixed forests
Ioannina	51	STEP	Temperate broadleaf and mixed forests	Central European mixed forests
Kokad	52	STEP	Temperate broadleaf and mixed forests	East European forest steppe
Lake Xiniás	53	STEP	Temperate broadleaf and mixed forests	Western European broadleaf forests
Mickunai	54	COCO	Tundra	Scandinavian Montane Birch forest and grasslands
Lake Sfanta Anna	55	COMX	Temperate Coniferous Forest	Alps conifer and mixed forests
Lesvos ML01 Megali Limni	56	STEP	Temperate broadleaf and mixed forests	Rodope montane mixed forests
Straldzha	57	STEP	Temperate broadleaf and mixed forests	Aegean and Western Turkey sclerophyllous and mixed forests
MD01-2430	58	STEP	Temperate broadleaf and mixed forests	Euxine-Colchic broadleaf forests
Lake Iznik	59	STEP	Temperate broadleaf and mixed forests	Tian Shan montane steppe and meadows
M72/5 628-1	60	STEP	Deserts and xeric shrublands	Azerbaijan shrub desert and steppe
Dziguta Core 1	61	CLMX	Temperate broadleaf and mixed forests	Northeastern Spain and Southern France Mediterranean forests
Lake Van LG	62	STEP	Mediterranean Forests, woodlands and scrubs	Aegean and Western Turkey sclerophyllous and mixed forests
Lake Zeribar	63	STEP	Temperate grasslands, savannas and shrublands	Pontic steppe

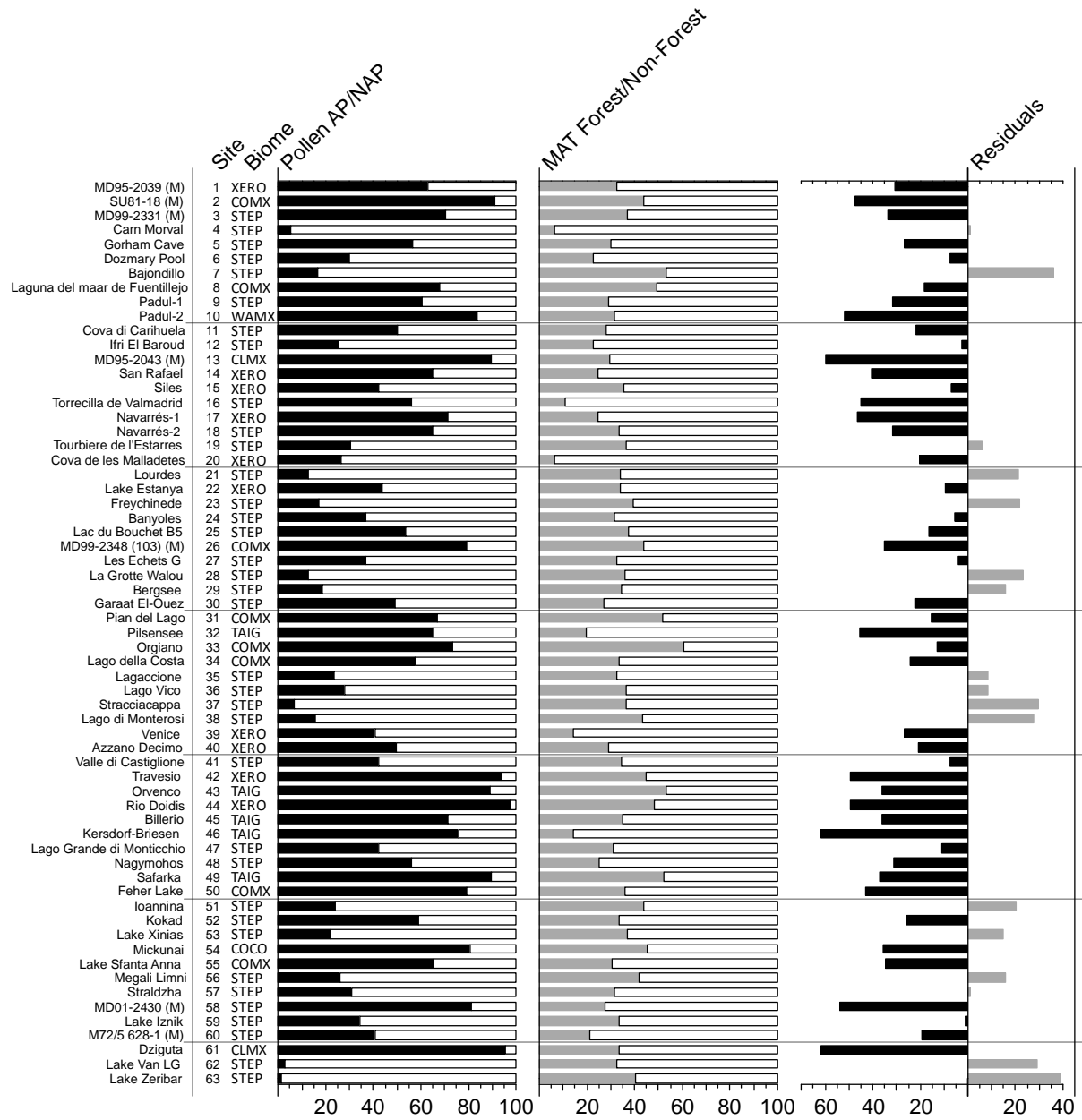
Notes: Modern analogue Biomes and Ecoregions were calculated as the most commonly occurring amongst all 6 best modern analogue pollen samples in all LGM samples for each pollen site/record. These are taken from the EMPD2 (Davis et al 2020), using the classification of Olsen et al 2001.

2261
2262
2263
2264
2265
2266
2267
2268

Table A4. The biome and ecoregion of the modern surface samples used as analogues in the pollen-climate reconstructions.

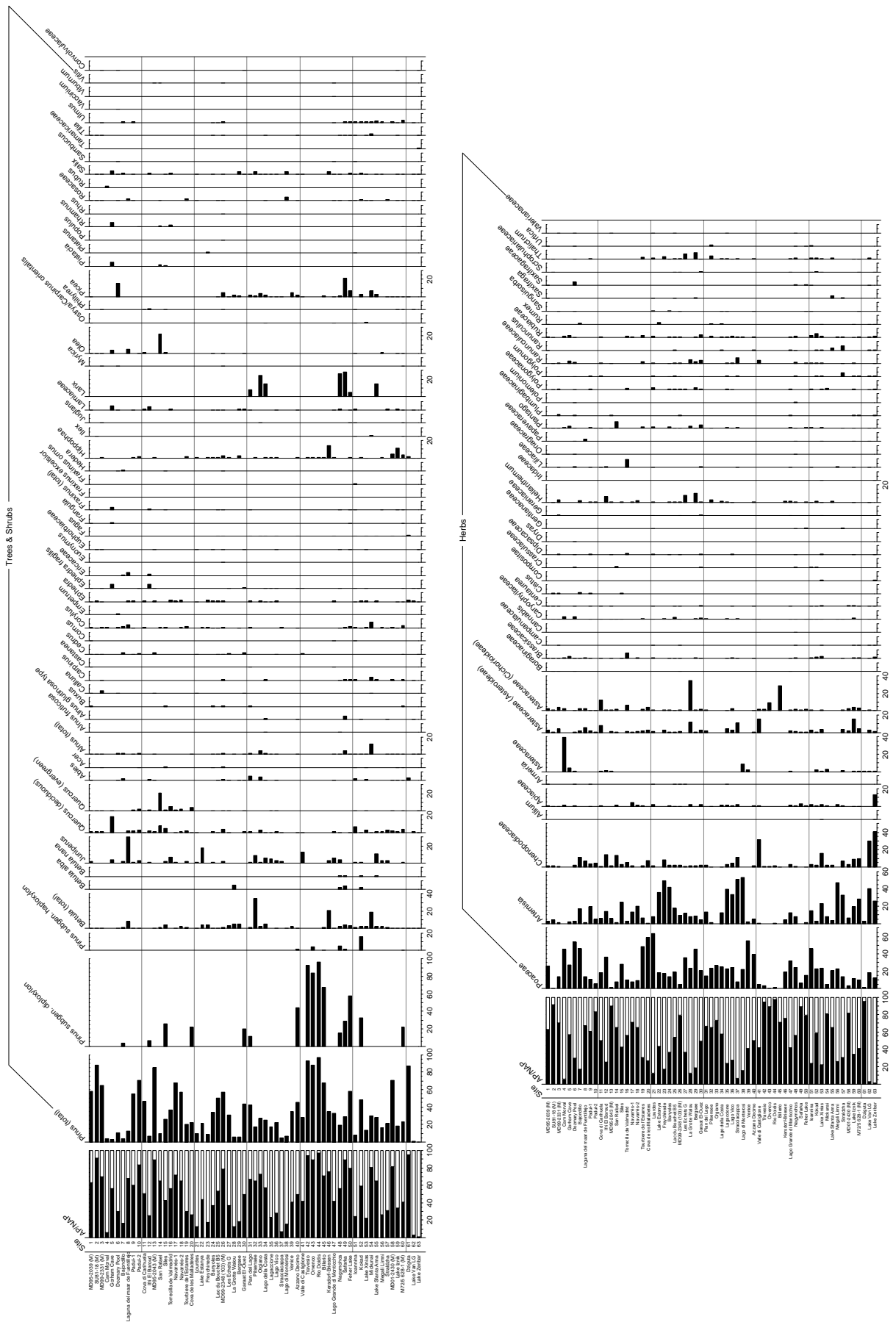
2269
 2270
 2271
 2272
 2273

Figures



2274
 2275
 2276
 2277
 2278

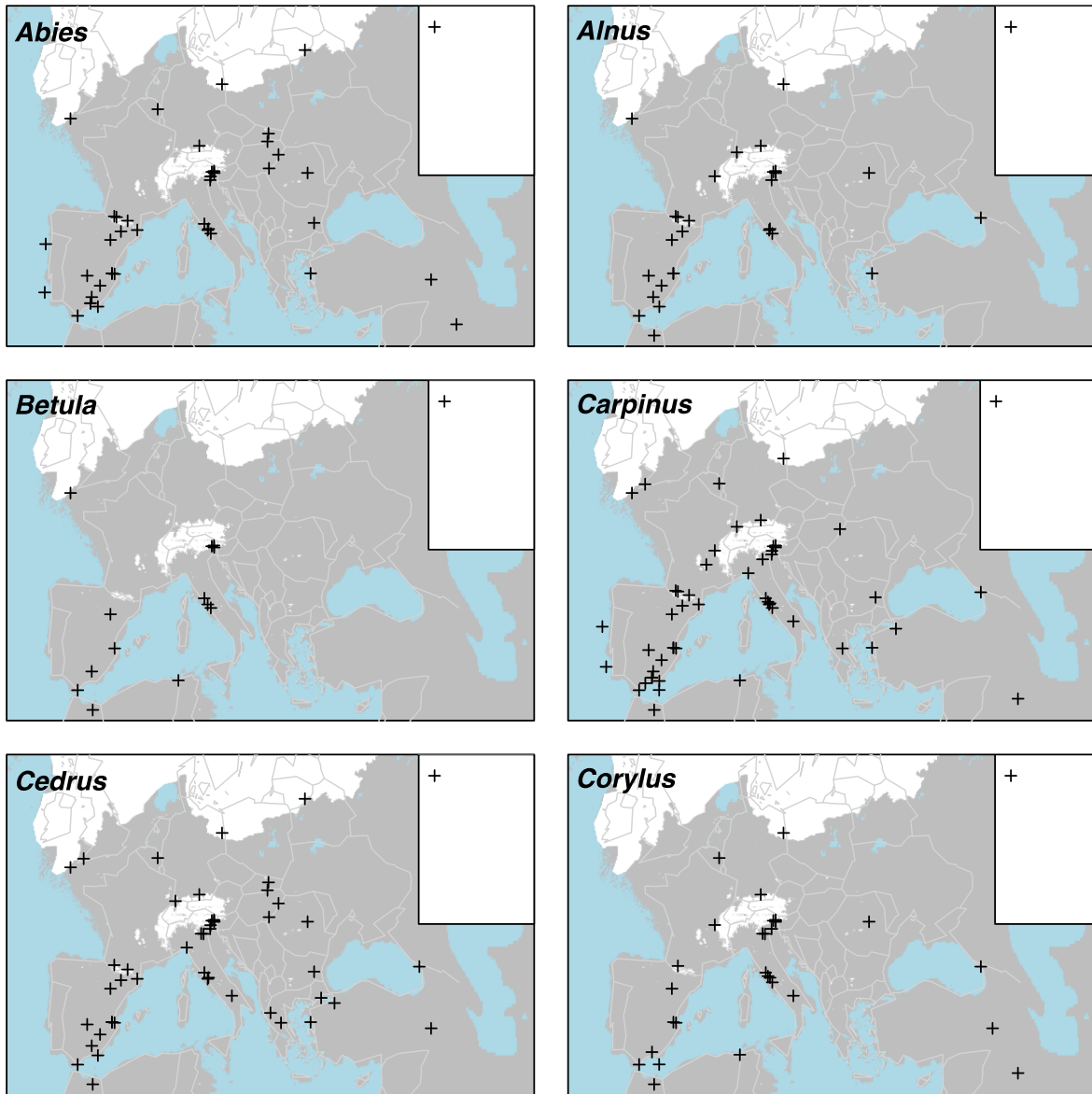
Figure A1. Pollen biomes (see figure 2 for key), Arboreal Pollen (AP) % forest cover, MAT % forest cover and residuals (AP % compared to MAT Forest %)



2279
2280

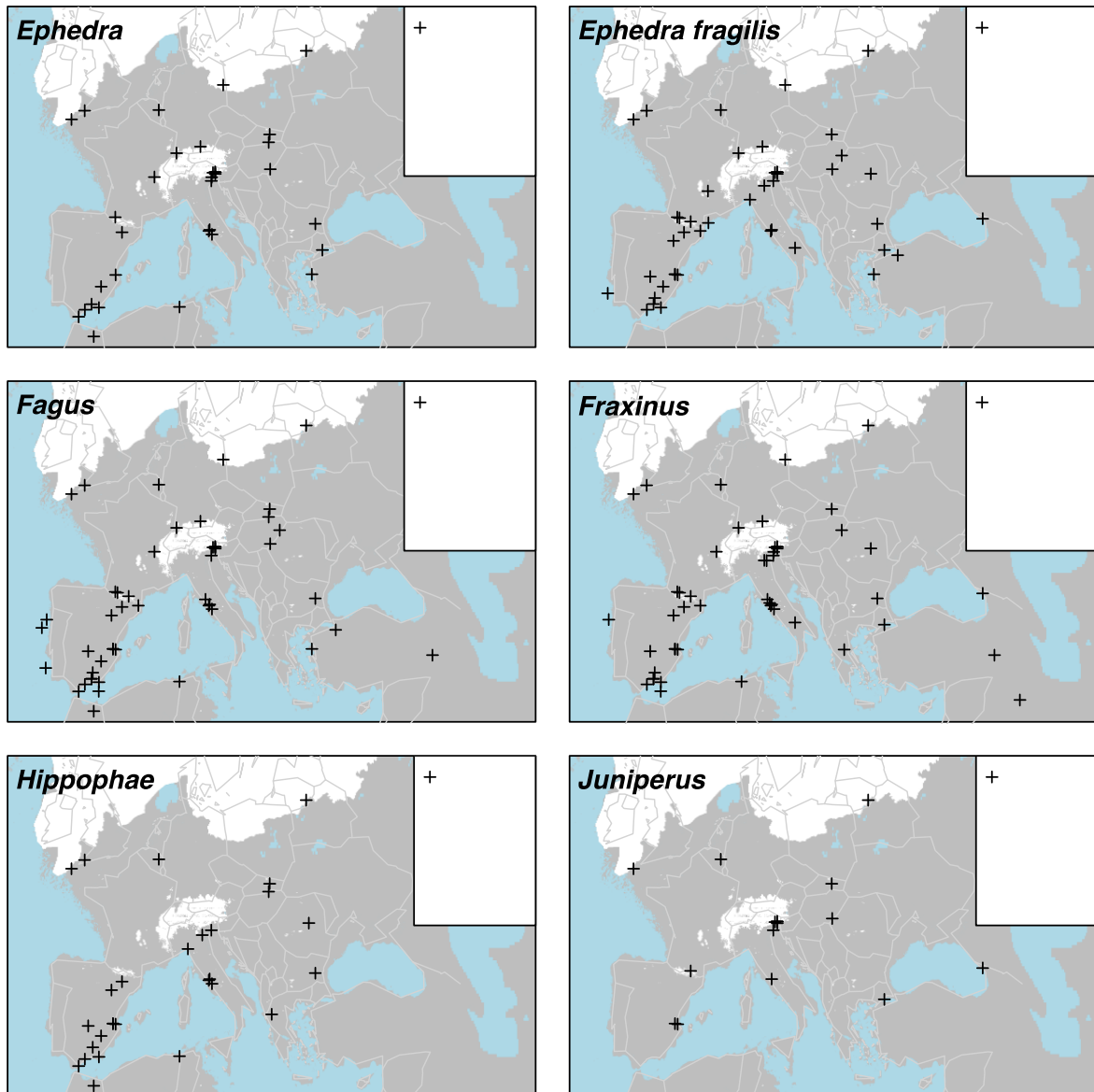
Figure A2. Pollen taxa percentages for all LGM sites/records

2281
2282
2283
2284



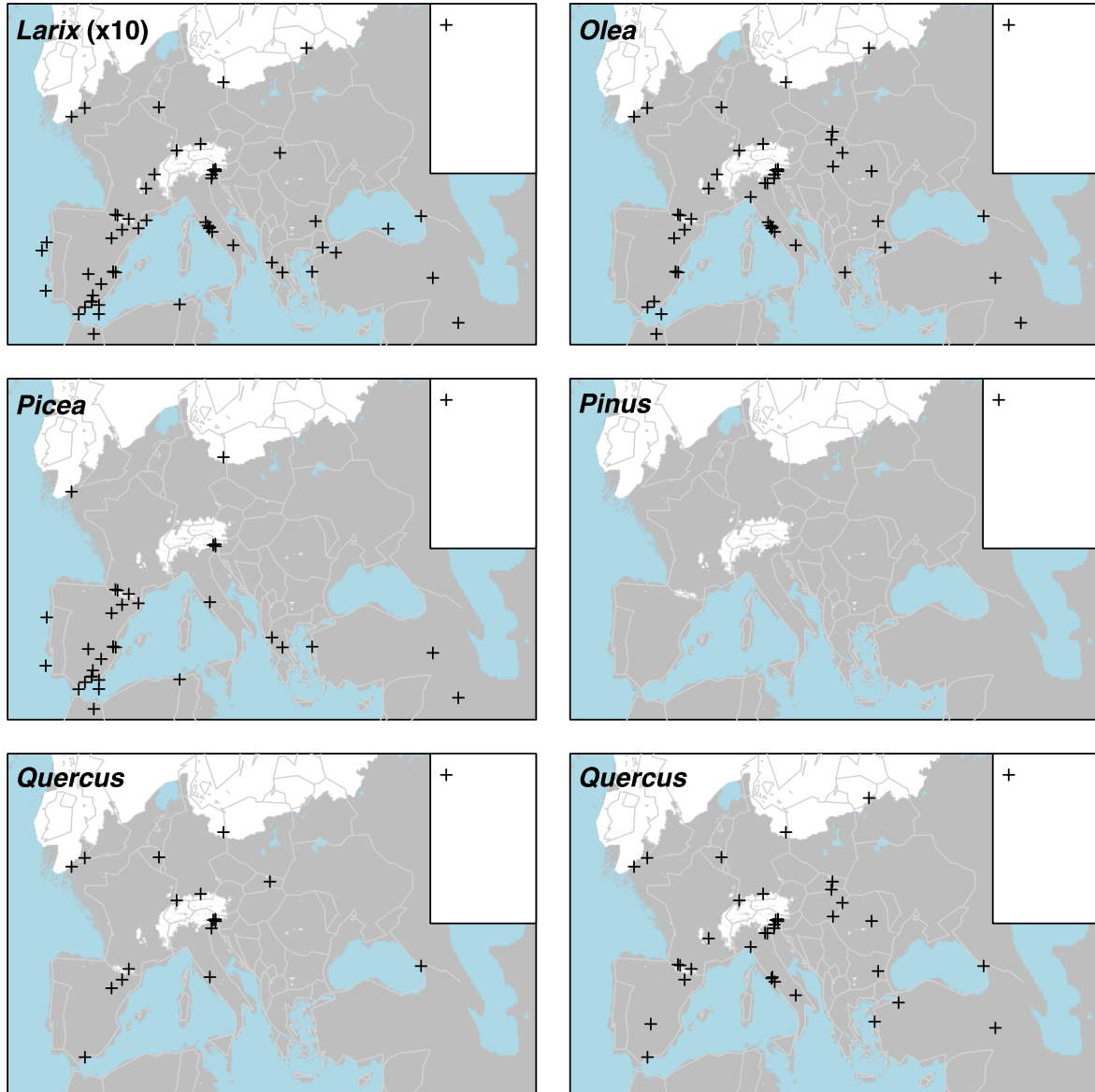
2285
2286
2287
2288

Figure A3a. Percentage maps of *Abies*, *Alnus*, *Betula*, *CarPinus*, *Cedrus* and *Corylus*



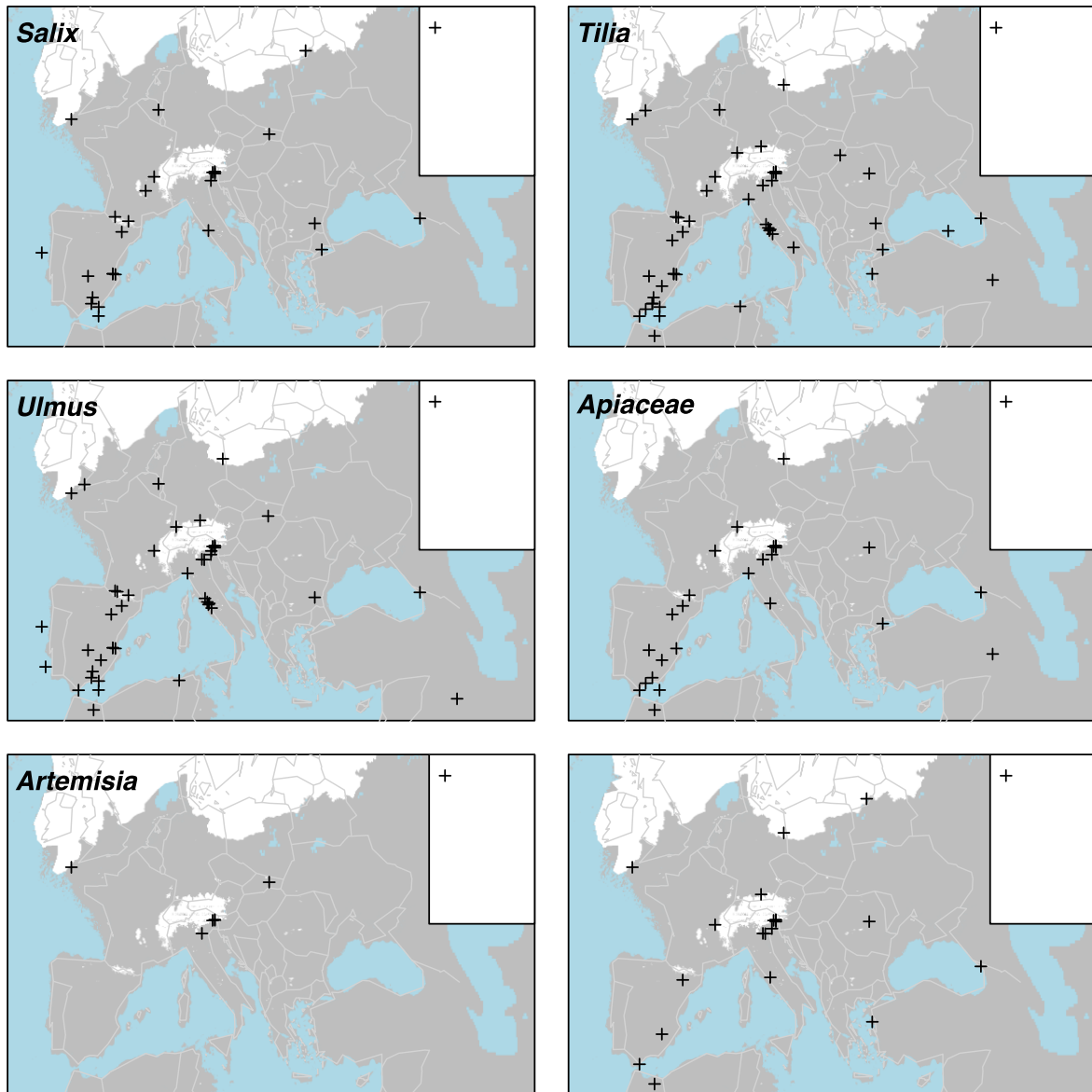
2289
 2290
 2291
 2292
 2293

Figure A3b. Percentage maps of *Ephedra*, *Ephedra fragilis*, *Fagus*, *Fraxinus*, *Hippophae* and *Juniperus*



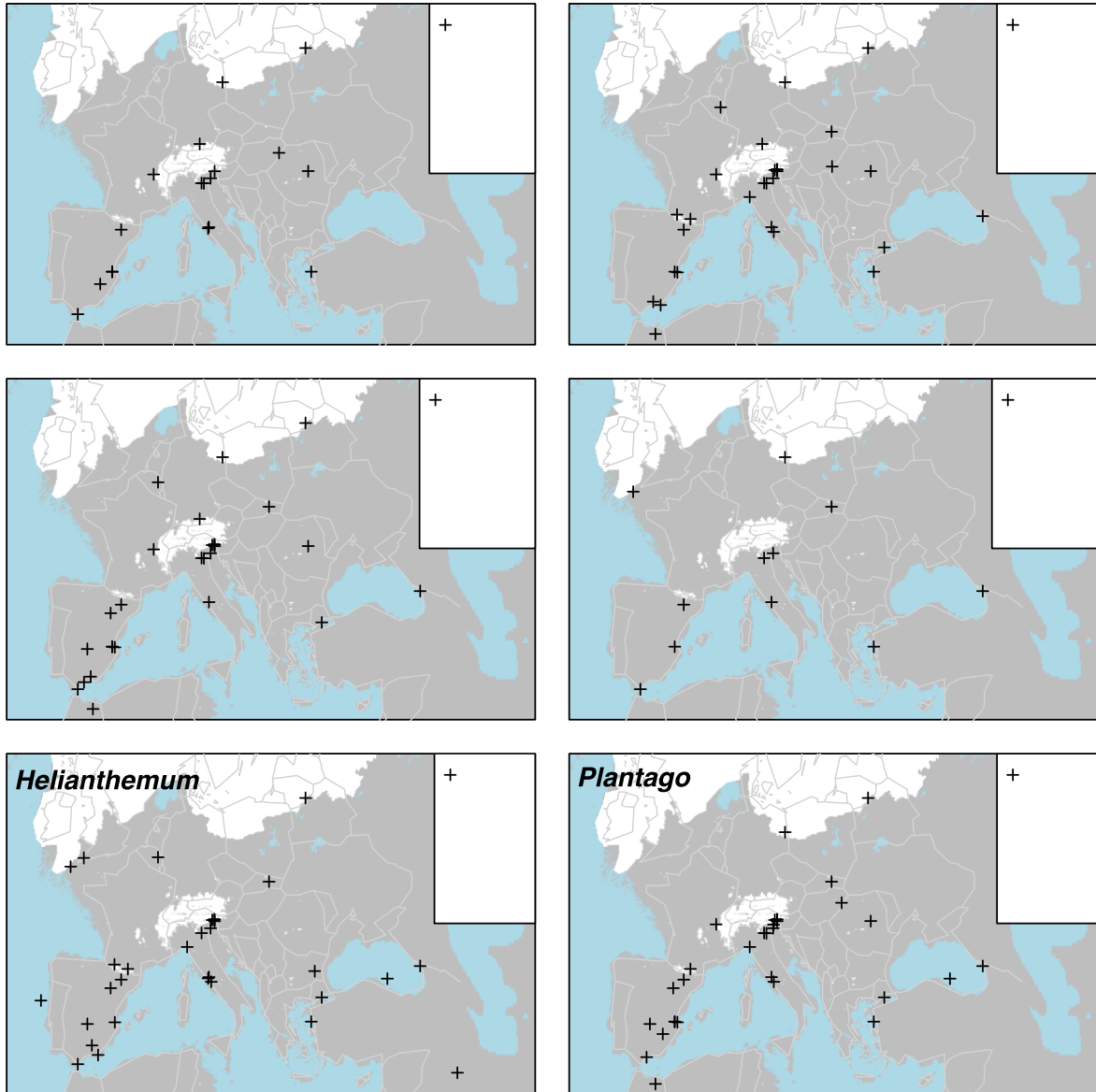
2294
 2295
 2296
 2297
 2298

Figure A3c. Percentage maps of *Larix* (x10 exaggeration), *Olea*, *Picea*, *Pinus*, *Quercus* (deciduous) and *Quercus* (evergreen)



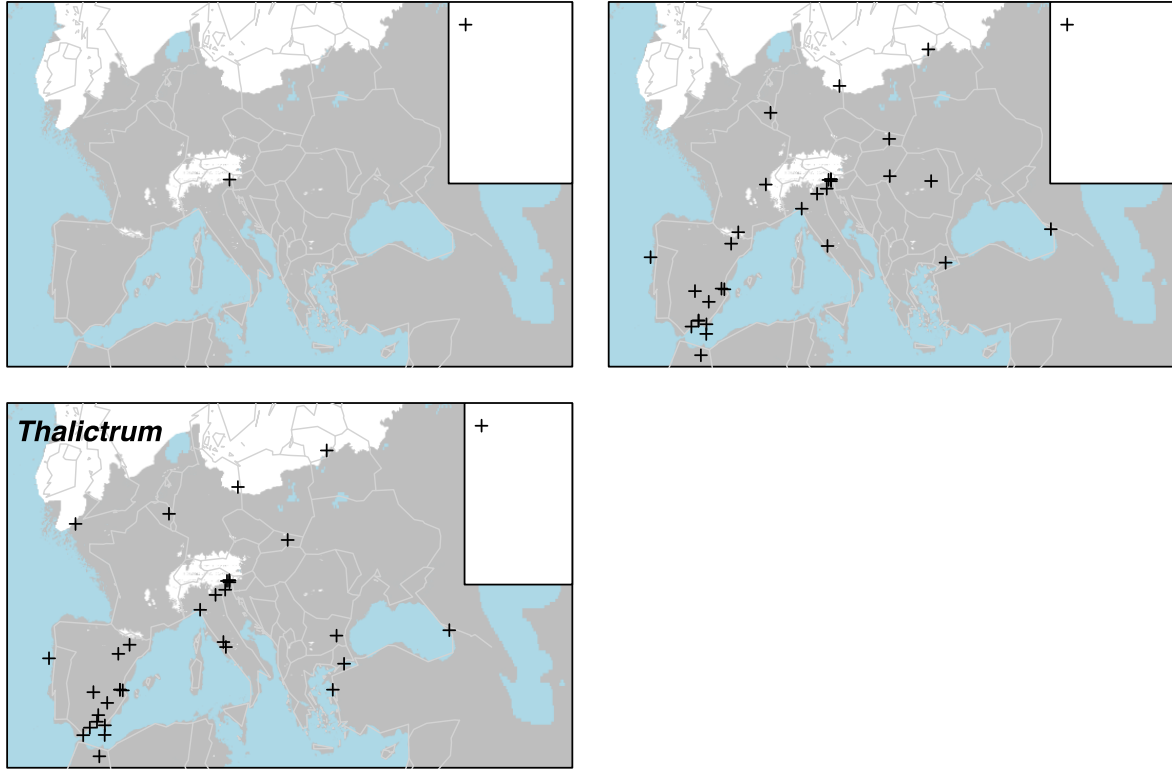
2299
 2300
 2301
 2302

Figure A3d. Percentage maps of *Salix*, *Tilia*, *Ulmus*, *Apiaceae*, *Artemisia* and *Asteraceae* (*Asteroideae*)



2303
 2304
 2305
 2306
 2307

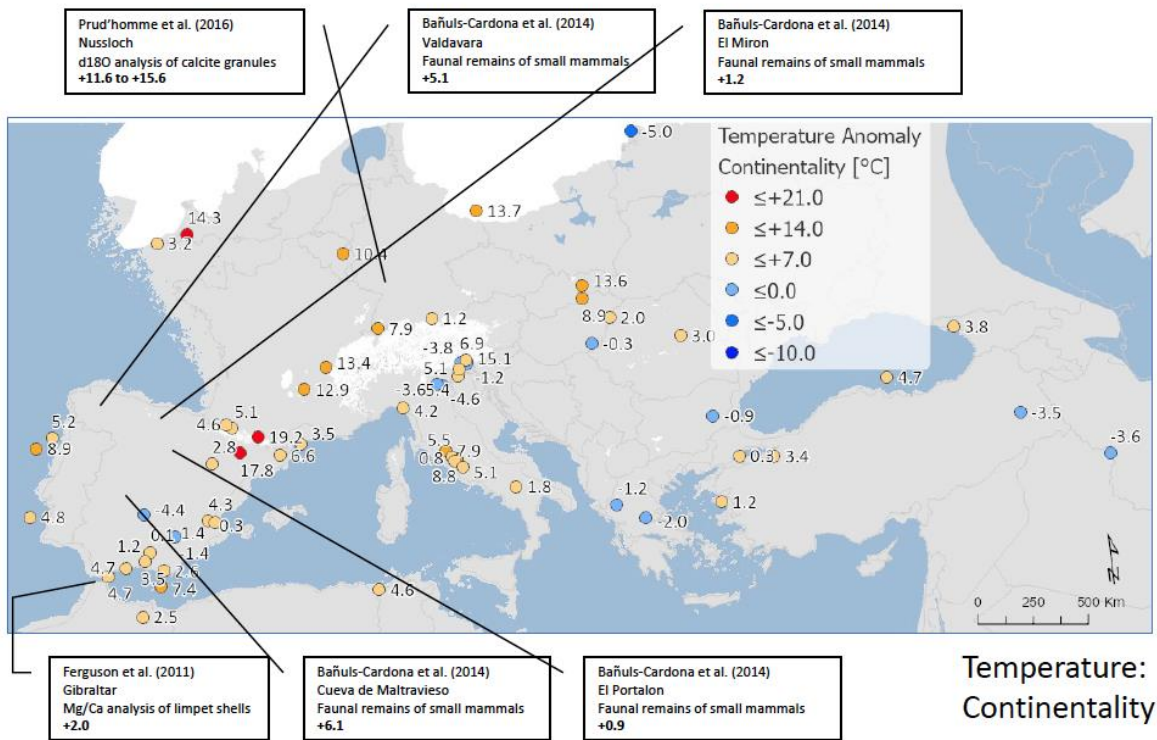
Figure A3e. Percentage maps of Asteraceae (Cichorioideae), Brassicaceae, Caryophyllaceae, Chenopodiaceae, *Helianthemum* and *Plantago*



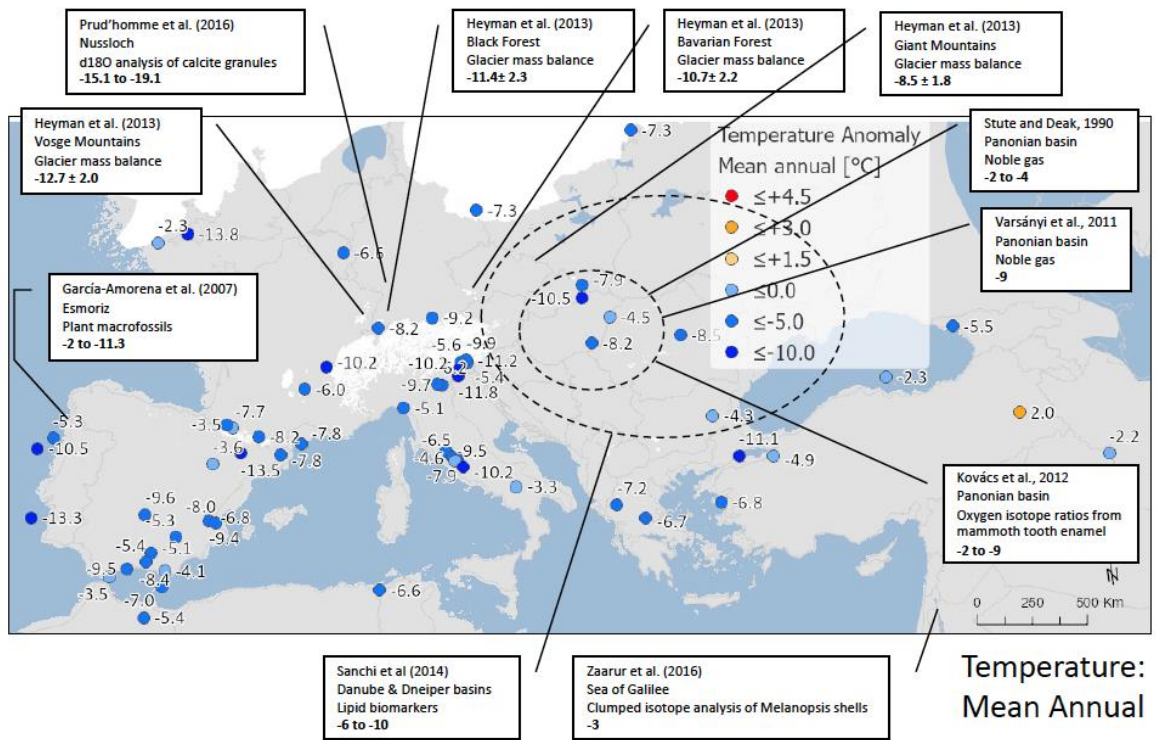
2308
 2309
 2310
 2311
 2312
 2313
 2314
 2315
 2316

Figure A3f. Percentage maps of Poaceae, Rubiaceae and *Thalictrum*

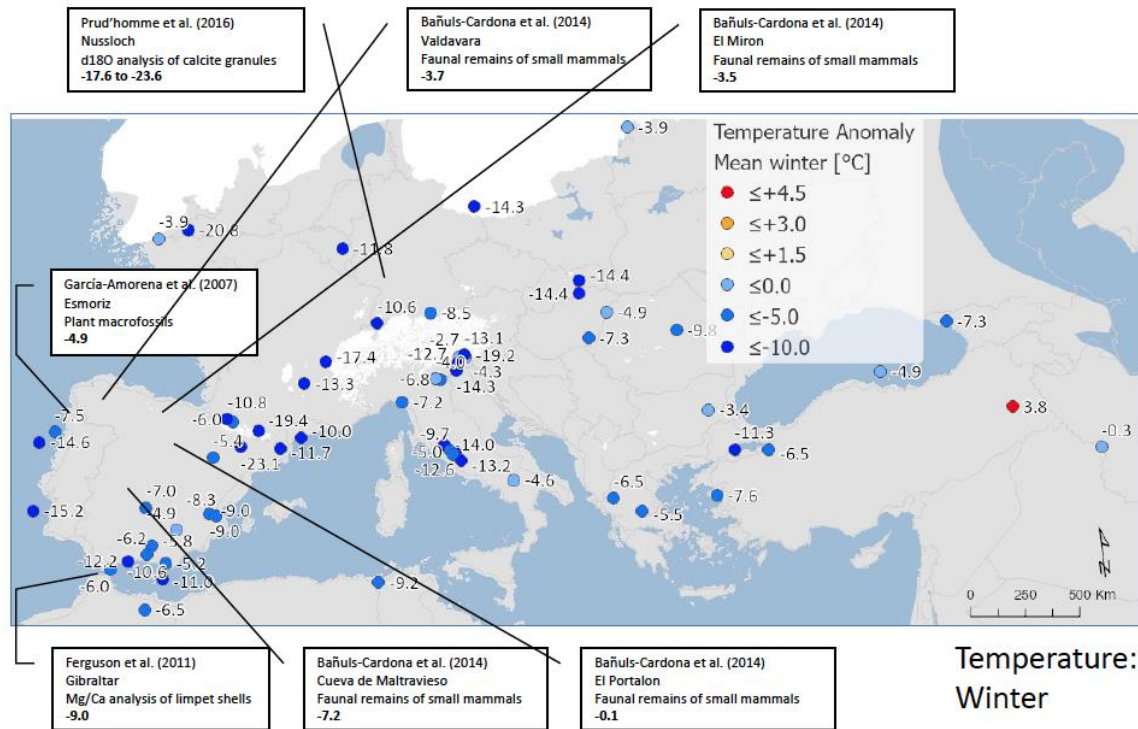
2317



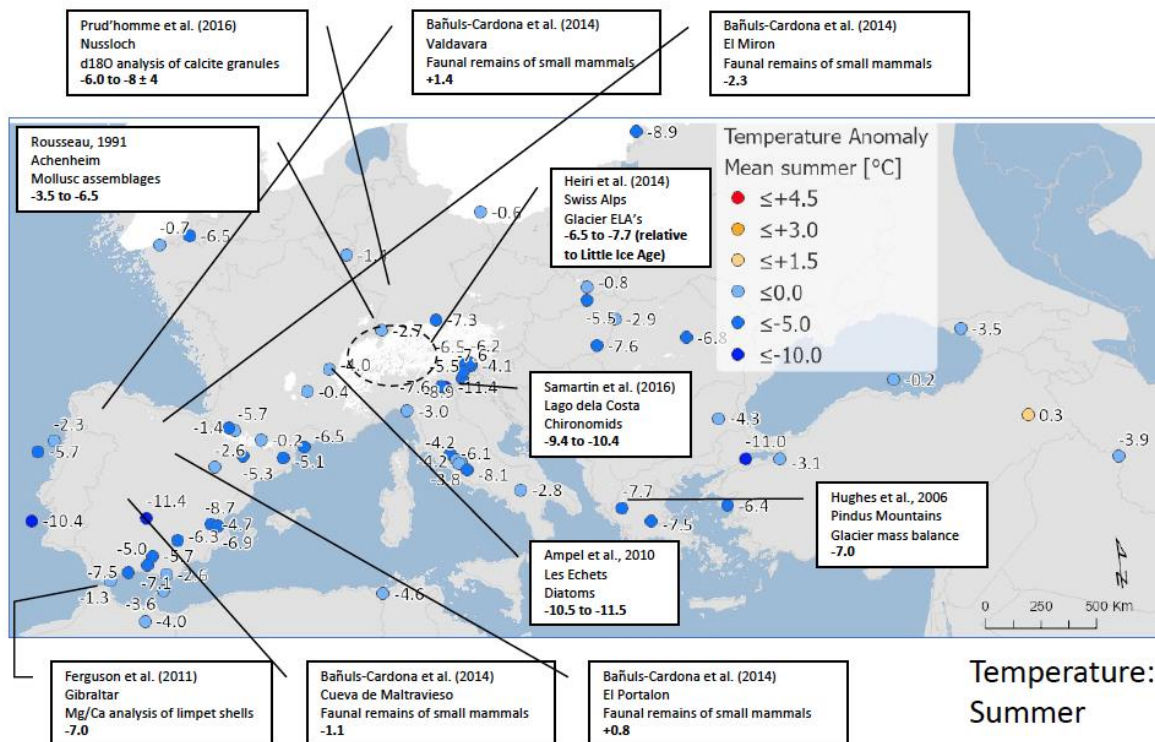
2318
2319



2320
2321
2322



Temperature:
Winter



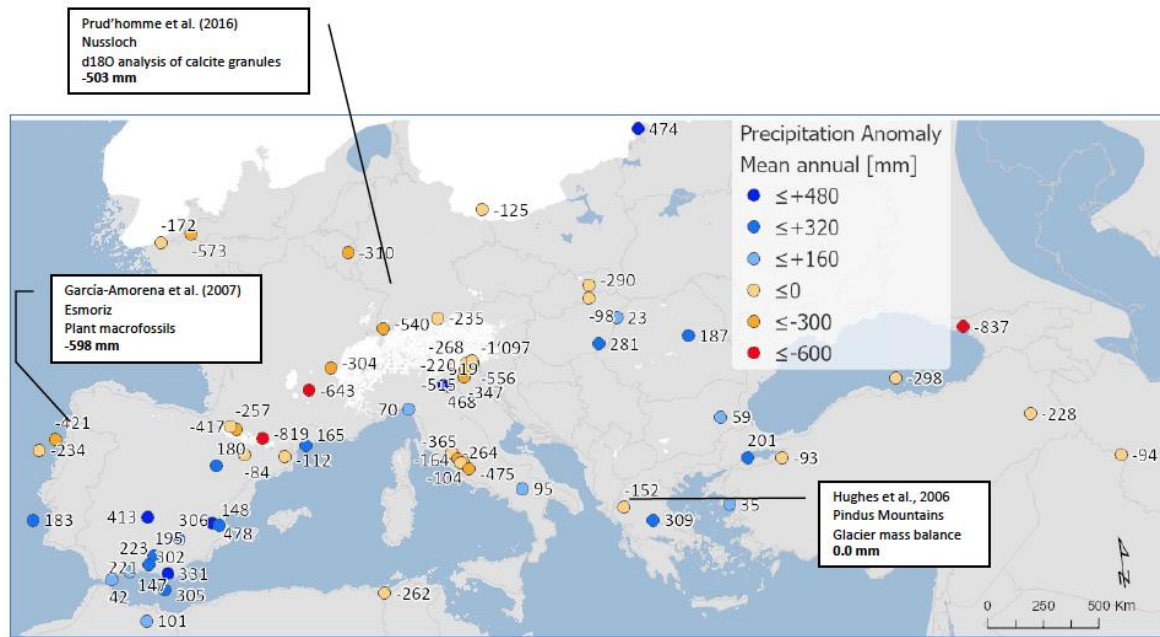
Temperature:
Summer

2323
2324

2325
2326

2327 Figure A4. Maps of pollen-based MAT reconstructions for LGM annual, winter and summer
2328 temperature anomalies (as shown in figure 10), shown together with the results of other
2329 published studies. Continentality represents the difference in temperature between summer
2330 and winter, with positive anomalies indicating an increase in the temperature difference
2331 between summer and winter. All values are expressed as anomalies compared with the
2332 present day unless otherwise indicated.

2333



Precipitation:
Mean Annual

2334
2335
2336
2337
2338
2339

Figure A5. Maps of pollen-based MAT reconstructions for LGM annual precipitation anomalies (as shown in figure 12), shown together with the results of other published studies. All values are expressed as anomalies compared with the present day.

2340
2341